U.S. Department
of Transportation
Federal Railroad
Administration

Office of Research,
Development and Technology
Washington, DC 20590

Wheel Failure Investigation Program: Phase 3

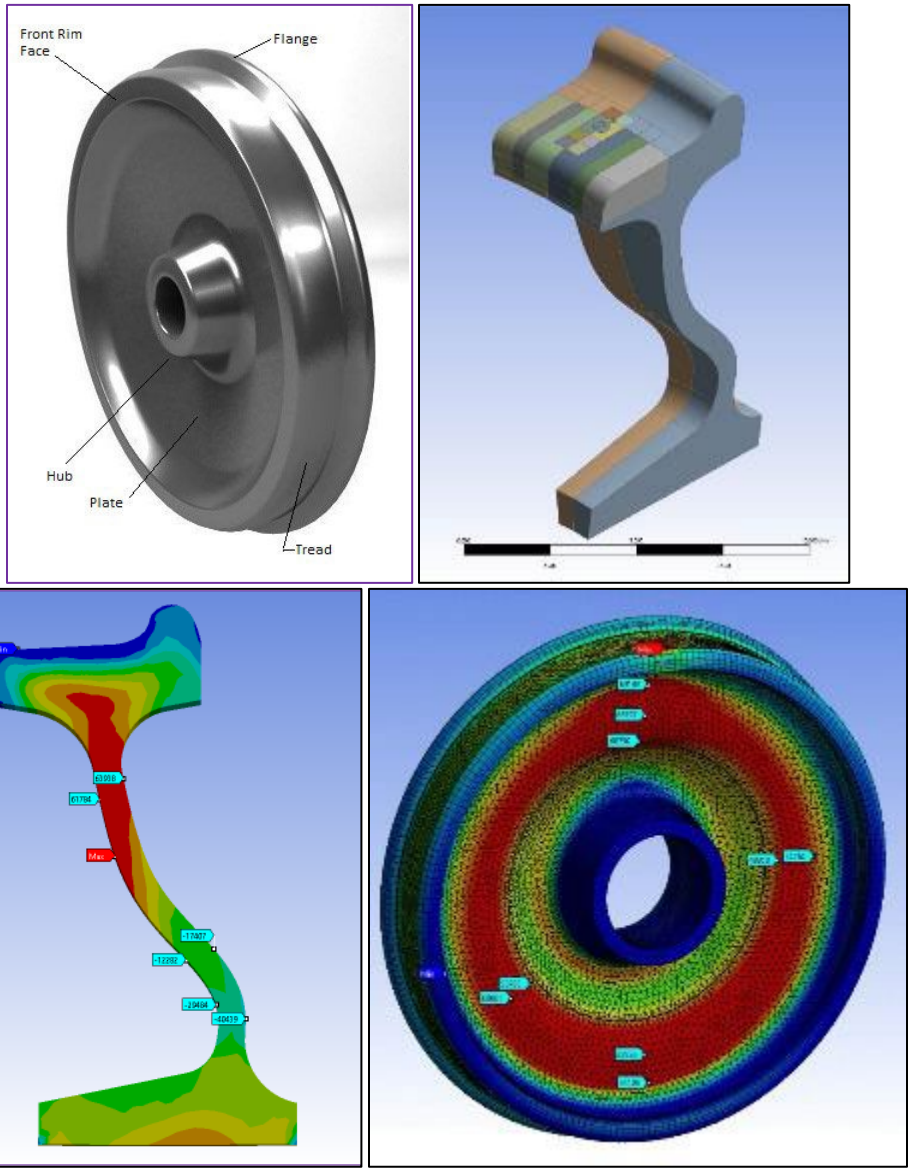

REPORT DOCUMENTATION PAGE

Form Approved
OMB No. 0704-0188

1. REPORT DATE *(DD-MM-YYYY)*	**2. REPORT TYPE**	**3. DATES COVERED** *(From - To)*
12/12/2024	Technical Report	September 2020–December 2023

4. TITLE AND SUBTITLE

Wheel Failure Investigation Program: Phase 3

5a. CONTRACT NUMBER
693JJ6-18-D-000005

5b. GRANT NUMBER

5c. PROGRAM ELEMENT NUMBER

6. AUTHOR(S)

Eric Sherrock, ORCID: 0000-0001-6004-7490

Ron Gagnon, ORCID: 0009-0004-5104-2486

Steven L. Dedmon, ORCID: 0009-0004-6608-8233

Alejandro Alvarez-Reyes, ORCID: 0000-0002-5631-0660

5d. PROJECT NUMBER

5e. TASK NUMBER
693JJ619F000103

5f. WORK UNIT NUMBER

7. PERFORMING ORGANIZATION NAME(S) AND ADDRESS(ES)
ENSCO, Inc.
5400 Port Royal Road
Springfield, VA 22151

8. PERFORMING ORGANIZATION REPORT NUMBER
SERV-REPT-0003169

9. SPONSORING/MONITORING AGENCY NAME(S) AND ADDRESS(ES)
U.S. Department of Transportation
Federal Railroad Administration
Office of Research, Development, and Technology
1200 New Jersey Avenue, SE
Washington, DC 20590

10. SPONSOR/MONITOR'S ACRONYM(S)

11. SPONSOR/MONITOR'S REPORT NUMBER(S)
DOT/FRA/ORD-24/44

12. DISTRIBUTION/AVAILABILITY STATEMENT
This document is available to the public through the FRA website.

13. SUPPLEMENTARY NOTES
COR: Monique Ferguson Stewart, Jeffrey Gordon

14. ABSTRACT
Vertical Split Rims (VSRs) are one of the leading causes for wheel removals in North American freight rail service. The Federal Railroad Administration funded a research effort in which a group of researchers and subject matter experts explored a better understanding of VSRs using finite element analysis (FEA). The analysis was intended to identify the relative contributions of factors that can lead to VSR failures with a goal of establishing approaches to minimizing derailments associated with these wheel failures. In February 2016, researchers established a multi-phase research program to comprehensively understand various wheel failure mechanisms, identify major contributing factors, arrive at potential strategies to mitigate the failures, and consequently improve the safety of rail network operations. Since the beginning of this effort, research has been conducted under the guidance of a stakeholder working group made up of members of the Association of American Railroads, North American wheel manufacturers, and researchers.

15. SUBJECT TERMS
Wheel failure, vertical split rims, VSR, shattered rims, broken flange, thermal cracking in flange, plate cracking, thin rim overload, rolling stock

16. SECURITY CLASSIFICATION OF:			**17. LIMITATION OF ABSTRACT**	**18. NUMBER OF PAGES**	**19a. NAME OF RESPONSIBLE PERSON**
a. REPORT	**b. ABSTRACT**	**c. THIS PAGE**		88	David C. Brabb
					19b. TELEPHONE NUMBER *(Include area code)* (719) 500-9400

Standard Form 298 (Rev. 8/98)
Prescribed by ANSI Std. Z39.18

METRIC/ENGLISH CONVERSION FACTORS

ENGLISH TO METRIC	METRIC TO ENGLISH
LENGTH (APPROXIMATE)	**LENGTH (APPROXIMATE)**
1 inch (in) = 2.5 centimeters (cm)	1 millimeter (mm) = 0.04 inch (in)
1 foot (ft) = 30 centimeters (cm)	1 centimeter (cm) = 0.4 inch (in)
1 yard (yd) = 0.9 meter (m)	1 meter (m) = 3.3 feet (ft)
1 mile (mi) = 1.6 kilometers (km)	1 meter (m) = 1.1 yards (yd)
	1 kilometer (km) = 0.6 mile (mi)
AREA (APPROXIMATE)	**AREA (APPROXIMATE)**
1 square inch (sq in, in^2) = 6.5 square centimeters (cm^2)	1 square centimeter (cm^2) = 0.16 square inch (sq in, in^2)
1 square foot (sq ft, ft^2) = 0.09 square meter (m^2)	1 square meter (m^2) = 1.2 square yards (sq yd, yd^2)
1 square yard (sq yd, yd^2) = 0.8 square meter (m^2)	1 square kilometer (km^2) = 0.4 square mile (sq mi, mi^2)
1 square mile (sq mi, mi^2) = 2.6 square kilometers (km^2)	10,000 square meters (m^2) = 1 hectare (ha) = 2.5 acres
1 acre = 0.4 hectare (he) = 4,000 square meters (m^2)	
MASS - WEIGHT (APPROXIMATE)	**MASS - WEIGHT (APPROXIMATE)**
1 ounce (oz) = 28 grams (gm)	1 gram (gm) = 0.036 ounce (oz)
1 pound (lb) = 0.45 kilogram (kg)	1 kilogram (kg) = 2.2 pounds (lb)
1 short ton = 2,000 pounds (lb) = 0.9 tonne (t)	1 tonne (t) = 1,000 kilograms (kg) = 1.1 short tons
VOLUME (APPROXIMATE)	**VOLUME (APPROXIMATE)**
1 teaspoon (tsp) = 5 milliliters (ml)	1 milliliter (ml) = 0.03 fluid ounce (fl oz)
1 tablespoon (tbsp) = 15 milliliters (ml)	1 liter (l) = 2.1 pints (pt)
1 fluid ounce (fl oz) = 30 milliliters (ml)	1 liter (l) = 1.06 quarts (qt)
1 cup (c) = 0.24 liter (l)	1 liter (l) = 0.26 gallon (gal)
1 pint (pt) = 0.47 liter (l)	
1 quart (qt) = 0.96 liter (l)	
1 gallon (gal) = 3.8 liters (l)	
1 cubic foot (cu ft, ft^3) = 0.03 cubic meter (m^3)	1 cubic meter (m^3) = 36 cubic feet (cu ft, ft^3)
1 cubic yard (cu yd, yd^3) = 0.76 cubic meter (m^3)	1 cubic meter (m^3) = 1.3 cubic yards (cu yd, yd^3)
TEMPERATURE (EXACT)	**TEMPERATURE (EXACT)**
[(x-32) (5/9)] °F = y °C	[(9/5) y + 32] °C = x °F

QUICK INCH - CENTIMETER LENGTH CONVERSION

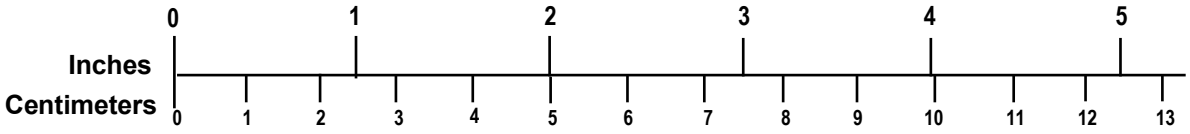

QUICK FAHRENHEIT - CELSIUS TEMPERATURE CONVERSIO

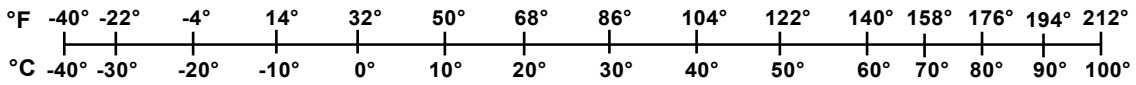

For more exact and or other conversion factors, see NIST Miscellaneous Publication 286, Units of Weights and Measures. Price $2.50 SD Catalog No. C13 10286

Updated 6/17/98

Contents

Illustrations

Tables

Executive Summary

This report summarizes the results of the third phase of a multi-phase study to determine the underlying mechanism(s) for catastrophic wheel failures, such as shattered rims and vertical split rims (VSRs), and potential solutions and strategies to minimize derailments due to these types of failures. The Federal Railroad Administration (FRA) sponsored ENSCO, Inc., to lead the study, with significant contributions made by Steven Dedmon and SimuTech Group, as well as members of the Association of American Railroads (AAR), car owners, and wheel suppliers.

Between 2013 and 2015, accidents associated with wheel failures represented 11 percent of all equipment-caused accidents.[1] Although rare, broken wheel derailments tend to be more catastrophic than other derailment types due to sudden fracture, which can occur at revenue train speeds. Coupled with increased movement of hazardous material (including crude oil), this scenario poses an increasing risk to public and railroad safety. In response to this increased risk, FRA's Administrator tasked the FRA Office of Railroad Safety (RRS) with arriving at a better understanding of VSRs and other wheel failure modes. RRS's objectives include improved insight into failure causes, the development of detection and prevention methods, and establishment of approaches to minimize wheel failure-related derailments.

Past studies and research supported by FRA have focused on developing an understanding of wheel failures from various perspectives. A definitive study to determine the underlying mechanism(s) for wheel failures, such as shattered and vertical split rims, and potential solution(s) and strategies to minimize derailments due to these types of wheel failures was needed. In response to a request from RRS, FRA's Office of Research, Development, and Technology established a multi-phase research program in February 2016 to develop a comprehensive understanding of various wheel failure mechanisms, identify major contributing factors to these failures, arrive at potential strategies to mitigate them, and consequently improve safety of rail network operations. The initial vision of this FRA program includes the following phases:

- Phase 1: Problem Definition and Size Analysis
- Phase 2: Review and Analysis of Tests and Analytic Studies on Investigation of Wheel Failure Mechanisms
- Phase 3: Modeling and Analysis of Underlying Wheel Failure Mechanisms and Failure Prevention and Mitigation Strategies

A key element of FRA's approach is its creation of an industry stakeholder working group (SWG) made up of members of the AAR, car owners, and researchers as active participants. Researchers working with FRA and the SWG identified the following wheel failures to consider under this program: VSR, shattered rims, broken flange, plate cracking, thermal cracking in flanges, and thin rim overloads. Based on the prevalence of VSR and shattered rim failures as causes of accidents due to broken wheels, much of the Phase 1 and Phase 2 efforts were focused on these failure modes.

[1] Based on equipment-caused accident data available from FRA's Office of Railroad Safety, November 2016.

Due to the complicated nature and multi-cause origin of VSR failures, Phase 3 focused on the investigation of its contributing factors through Finite Element Analysis (FEA). This included analysis of wheel failure mechanisms, recommendations for improvements to industry data collection efforts, and identification of potential strategies to mitigate the failures, consequently improving rail network operations safety and reducing risks.

The research team drew the following conclusions from Phase 3 and prior research activities:

- The likelihood of a VSR increases with increased brake heating. Without brake heating the probability of a VSR is diminished.
- In order of importance, the contributing factors to the development of a VSR are brake heating, subsurface crack size, and distance from the tread contact point with the rail to the subsurface crack tip.
- A large percentage of subsurface cracks will break out to the tread, creating an out-of-round condition and high impact readings from wayside detectors. Those which turn away from the tread (and generate a VSR) need high thermal gradients to generate the thermal stresses necessary to drive crack growth.
- Manufacturing residual compressive stresses prevents the subsurface crack from breaking out to the front rim face, instead forcing a crack path to the rim inner diameter.
- Wheel-rail contact loads cause crack initiation (likely in the presence of a material anomaly) and propagation. The larger the crack gets, the less important wheel-rail contact becomes, since the distance to the crack tip gets larger and stresses decrease.
- Unstable crack growth occurs when the crack tip progresses away from the tread surface and into a tensile residual axial stress pool resulting from heat treatment.

1. Introduction

This report summarizes the results of the third phase of a multi-phase study initiated in February 2016. This study was conducted to determine the underlying mechanism(s) for catastrophic wheel failures, such as shattered rims and vertical split rims (VSRs), and potential strategies and recommendations to minimize derailments due to these types of failures.

1.1 Background

The Federal Railroad Administration (FRA) continuously evaluates derailment causes to identify trends in the industry that merit additional research to improve the safety and efficiency of railroad operations. Accidents resulting from in-service failure of freight rail vehicle wheels is one such area in which additional efforts are required.

Between 2013 and 2015, accidents associated with wheel failures represented 11 percent of all equipment-caused accidents.[2] Broken wheel derailments tend to be more catastrophic than other derailment types due to the sudden fracture and ensuing derailment which can occur at high train speeds. Coupled with movements of hazardous materials, including crude oil, this scenario poses a risk to public and railroad safety. In response to this increased risk, the FRA Administrator tasked FRA's Office of Railroad Safety (RRS) with developing a better understanding of VSRs and other wheel failure modes. RRS's objectives include improved insight into failure causes, the development of detection and prevention methods, and establishment of approaches to minimize wheel failure-related derailments.

Broken wheel derailments occur when a wheel experiences a fracture that removes a significant portion of the wheel or causes the wheel to become loose on the axle. The FRA Derailment Cause Codes[3] and Rule 41 in the Association of American Railroads' (AAR) Field Manual of Interchange Rules detail the different types of broken wheels which can cause derailments. Wheel failures that have historically been the most problematic are illustrated in Figure 1:

- **VSR**: A VSR occurs when subsurface tread cracking reaches a critical location within the rim. A tread subsurface horizontal crack is initiated and grows. These horizontal cracks can be surface initiated (i.e., shelling, spalling, rolling contact fatigue, thermal cracking) or subsurface initiated (delamination) [1]. This crack then turns in a vertical direction and propagates towards the wheel tread, resulting in a loss of wheel material. Current research has not completely identified the root cause of or proper mitigation actions for VSR failures. Although some railroads have noted a decrease in VSR failures over the past several years, this wheel failure mode continues to represent a derailment risk.
- **Shattered Rim**: Shattered rim failures are due to contact stress creating subsurface fatigue cracking initiated at voids or inclusions. Thin rim thickness and impact loads can increase the contact stresses in proximity to subsurface voids and inclusions. Bending

[2] Based on equipment-caused accident data available from FRA's Office of Railroad Safety, November 2016.

[3] Train Accident Cause Codes (Appendix C of FRA Guide for Preparing Accident/Incident Reports), namely: Broken Flange (E60C, E60L), Broken Hub (E63C, E63L), Broken Plate (E62C, E62L), Broken Rim (E61C, E61L), Other Wheel Defects (E69C, E69L), Thermal Crack (flange or tread) (E6AC, E6AL)

stresses cause the subsurface fatigue crack to grow to be quite large before fracture, eventually causing an extensive loss of wheel rim material.

- **Thermal Crack Extended into Plate**: A thermal crack is a transverse fatigue crack initiated at the surface of the tread or flange that occurs when the rim hoop residual stress is transformed from the beneficial compressive stress that exists following manufacture to the detrimental tensile stress. This stress reversal occurs due to significant tread braking. If the fatigue crack grows during repeated heating cycles to eventually reach the critical size, a large transverse overload fracture will propagate into the plate and can turn to remove a large portion of the rim and plate, or progress to the hub and cause the wheel to become loose on the axle.

Figure 1. Example of Vertical Split Rim (left), Shattered Rim (center), and Thermal Crack (right) Failed Wheels [1]

Past studies and research supported by FRA focused on developing an understanding of wheel performance from various perspectives, including material properties (i.e., metallurgy, strength, and toughness), manufacturing processes (i.e., casting, forging, heat treatment, surface treatment, and residual stresses), design parameters (i.e., wheel diameter, rim thickness, and plate type), and the operating environment (e.g., axle load, maximum operating speed, tread braking capacity, wheel-rail interaction under curving and traction conditions, and track perturbations). However, a definitive study to determine the underlying mechanism(s) for catastrophic wheel failures such as shattered rims, VSRs, and potential solution(s) and strategies to minimize derailments due to these types of failures remains to be completed.

In response to this need, FRA's Office of Research, Development, and Technology, cooperated with RRS to establish a multi-phase research program to gain a comprehensive understanding of the various wheel failure mechanisms, identify major contributing factors to these failures, arrive at potential strategies to mitigate them, and consequently improve rail network operations safety. The initial vision of this FRA program includes the following phases:

- Phase 1: Problem Definition and Scope Analysis
- Phase 2: Review and Analysis of Tests and Analytic Studies on Investigation of Wheel Failure Mechanisms
- Phase 3: Modeling and Analysis of Underlying Wheel Failure Mechanisms and Failure Prevention and Mitigation Strategies

A key element of FRA's approach is its creation of an industry stakeholder working group (SWG) made up of railroads, car owners, and researchers as active participants in the research program. Membership in the SWG included personnel from:

- AAR
- BNSF Railway
- CN
- CP
- CSX
- GATX Corporation
- Greenbrier Companies
- Griffin Wheel, an Amsted Rail Company
- Norfolk Southern Corporation
- ORX Rail
- Standard Steel
- Transportation Technology Center, Inc.
- UTLX
- Union Pacific Railroad
- Volpe National Transportation Systems Center

Results of Phase 1 were documented in late 2017 [1]. Based on the lack of definitive understanding of the formation of VSR failures, Phase 2 activities focused on VSR failures and were documented in late 2021 [2].

1.2 Objectives

The objective of Phase 3 of this wheel failure research focused on comprehensive finite element analysis (FEA) of wheel failure mechanisms, emphasizing VSR contributing factors and recommendations for improvements to industry data collection efforts, and identification of potential strategies to mitigate the failures and consequently improve rail network operations safety and reduce risks.

1.3 Overall Approach

Phase 3 of the investigation focused on several FEA-based scenarios designed to further explore aspects identified during the first two phases of the study. Models were created to simulate wheel heat treatment, cold work from rolling contact between the wheel tread, and rail and on-tread brake heating. Then, seven cracks were individually introduced to the wheel model to evaluate the effect of various operating conditions on crack growth. These analyses were initially performed on a model of a new wheel with a full rim and then on a model of a wheel with worn rim. Both the cracks and wheel profiles are shown in Figure 2.

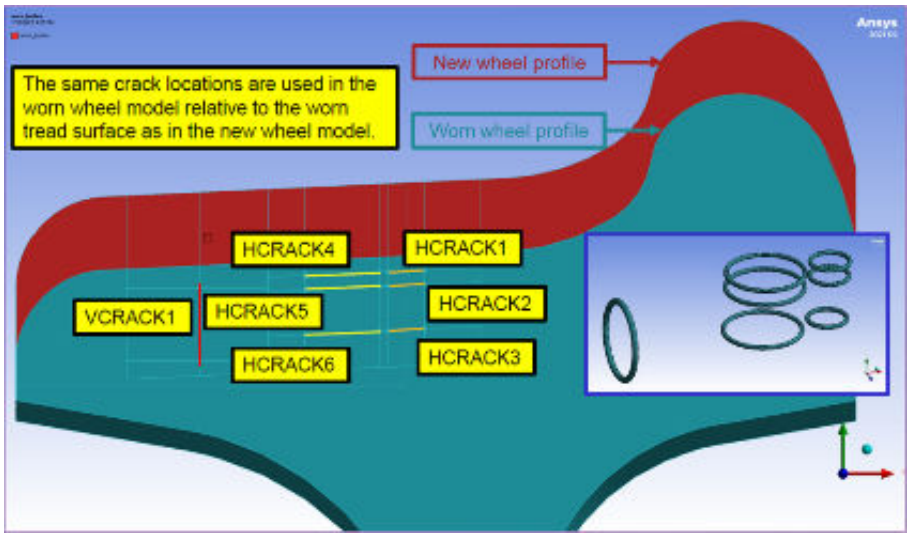

Figure 2. Wheel profiles, crack locations, and sizes

The research team produced a model of the process of VSR development with the data produced from the simulations. Most VSRs begin with a subsurface crack that propagates parallel to the tread surface of the wheel. Eventually this crack turns into the rim and away from the tread. The crack tip propagates into an area with high axial residual tensile stress. Unstable crack growth in both the radial and tangential directions eventually lead to wheel failure. The research team aims to answer several fundamental questions including:

- What causes the crack to "turn in"?
- What are the influences of thermal heating from brakes?
- What causes some subsurface cracks to propagate toward the tread producing a shell, and others to turn inward resulting in a VSR?

Answers from these questions could lead to feasible, cost-effective ways to mitigate VSRs.

1.4 Scope

The scope of Phase 3 of FRA's Wheel Failure Program was:

- Conduct a thorough analysis of the wheel failure problem using an FEA-based approach to identify the driving factors behind VSR failures and recommended approaches to identify wheels at risk for VSR prior to failure to minimize the impact and implications to freight railroads' operational safety and the risk posed by such failures to the public at large.
- The research effort builds upon reviews of industry and academic research efforts conducted under Phases I and II that have focused on wheel failure incidences, underlying causes and mechanisms, failure data and analysis, information on wheel inspection and shop practices, wheel manufacturing processes, and the impact of current wheel research. Further, contemporary research efforts were examined in relation to underlying causes that were identified but not fully investigated to determine their contribution to the wheel failures.

- Members of the SWG that participated in Phases I and II continued to be involved in Phase III efforts. The SWG created a smaller working group (the FEA Working Group) to focus on specific aspects of this phase of the research program.

1.5 Organization of the Report

This report summarizes the results of the efforts conducted by research team through early summer of 2023. The report is organized as follows:

- Section 2 summarizes the lessons learned from previous phases.
- Section 3 presents the finite element modeling methodology and development conducted during this effort.
- Section 4 provides an overview of the analyses performed with the results of the FEA modelling process.
- Section 5 summarizes the conclusions reached at this stage of the effort and provides recommendations.

2. Lessons Learned from Previous Phases

This section summarizes the current understanding of VSR failures determined through data analysis, a review of existing literature, and SWG discussions.

2.1 Phase 1

Past research efforts focused on three categories: the role of axial stresses, the role of subsurface cracks, and the role of geometry.

Tensile axial stresses and high stress gradients can create Mode I forces, which would result in a crack on the circumferential/radial plane typically found with VSR cracks. Axial stresses are produced during heat treatment, cold work from rolling contact, and mechanical loads, including impact loading and brake heating from on-tread brake systems. Compressive axial stresses are protective in that cracks must overcome the magnitude of compressive stresses plus the critical stress required to propagate a crack. The protective nature of residual compressive stresses at the field side of the wheel rim may be the reason VSR cracks are often very long in the circumferential (hoop) direction. An attempt to induce a VSR through repeated high load impacts on the field side of the tread was not successful [3]. Surface and near surface residual stresses tend to be compressive in both the axial and hoop directions but become increasingly tensile at deeper positions in the wheel rim. The axial tensile stress pool at deeper positions may be a key in VSR development [4].

Subsurface cracks propagated by rolling contact were noted by researchers on failed VSR wheels. Some researchers called these cracks “delaminations.” [5] From limited research, they posited that the cause of initiation of the subsurface cracks was either non-metallic inclusions or porosity. The role subsurface cracks play in VSR formation is essential to understand the initiation, propagation, unstable crack growth, subsurface crack “turn-in”, and development of a vertical crack and its propagation.

Subsurface crack propagation occurs parallel to the tread surface due to protective residual compressive stresses imparted by cold work during rolling contact. The crack does not penetrate to the rim interior because rolling contact forces attenuate quickly at greater depths. Thus, the subsurface crack propagates within a narrow band parallel to the tread surface. Initially, the crack is roughly equiaxed in the tangential (hoop) and axial directions. As the crack grows, it becomes increasingly oval shaped with the long axis in the hoop direction. The increased ovality is due to two factors: there is more room for growth in the hoop direction, and stresses at the crack tips decrease in the axial direction but increase in the hoop direction, revealed by the distance between fatigue beach marks in either direction.

The crack turning inward was evident on almost all failed VSR wheels examined in this study. Despite the decreasing stresses in the axial direction, especially to the field side of the rim, a small, wedge-shaped crack forms and extends at an angle to the subsurface crack. The driving force for the turning-in of these cracks appears to be a singular event with the apex of the crack occurring at a point or small area on the edge of the horizontal subsurface crack. The singular event cannot be the result of normal rolling contact, as these stresses have attenuated due to longer axial distance of the crack tip from the contact patch.

The angle that the turn-in crack surface makes with the plane of the horizontal subsurface crack appears to be less than 45 degrees and is usually much less. The cause of the crack turning

inward appears to be either impact or thermal related, resulting from on-tread brake heating. From the turn-in crack, unstable crack growth occurs with rotations of the wheel, becoming larger until rim material is dislodged by a contact/impact with a switch or other track feature. The crack extends through the rim, breaks out to the rim fillet, and continues to grow circumferentially. As is typical of VSR failures, the outer portion of the wheel rim, which might contain invaluable information, is often missing when the failure is discovered.

Additional research deemed that the presence of a false flange had contributed to high lateral loads, specifically near the horizontal crack tip, and was a possible cause of crack growth. Other researchers posited that hydrodynamic forces from water entrapment at the crack tip may have led to crack growth. However, other researchers have noted that it is difficult for water to get into a subsurface crack. [1]

2.2 Phase 2

Three smaller teams performed phase 2 of the investigation. [2] They conducted destructive testing on failed VSR wheels and investigated the high impact load history of VSR wheel failures using data from wayside Wheel Impact Load Detectors (WILDs) to determine the feasibility of early detection and removal of an incipient failure. They also performed a demographic study on VSR failed wheels to determine the role of location, weather conditions, and manufacturing methods; if this had been successful, there would have been no need for further investigations.

Destructive testing was performed and confirmed that the mode of failure was consistent with the subsurface crack scenario. Additionally, the investigations confirmed significant thermal brake heating had occurred (as seen in Figure 3). The team found little evidence of false flanges. Fatigue evidence was seen in all subsurface cracks and most turn-in cracks. Some evidence of fatigue was noted in the unstable crack growth area, but in most cases the cracks features found in the region just prior to failure were either shear lips or depicted quasi-cleavage (a non-brittle fracture mode).

Figure 3. A VSR failure with deformed steel and purple coloration exhibiting high temperature exposure

The researchers created an algorithm to confirm the detection of high-impact loads (from WILD data) for about half of the wheels investigated; detecting more than that half was difficult because some cracks were outboard of the taping line, and the WILD is best suited to detect flat spots on tangent track. These impacts would be better confirmed if the measurements were made on curved track, though in this case, half of the wheelsets riding near the flange would still be missed. Additionally, there was insufficient time to detect, report, and take appropriate action before the failure was likely to occur. One investigator reported less than 1,000 miles would be required to fail a VSR wheel after the subsurface crack turned inward [6].

The demographic study did not reveal any significant location-, weather-, or manufacturing-related correlations beyond that which is already known (i.e., cold weather is related to increased brake system failures and therefore blocked wheels). [7]

3. Finite Element Modeling Methodology and Development

This section describes the methodology and approach used to develop the model, including references, configurations, and processes.

3.1 Modeling Methodology and Strategy

The methodology used in this project established representative FEA models of the items defined in Section 3.2. The modeling began simply and added complexity by defining two different analysis stages. The modeling also used a mix of two-dimensional (2D) and three-dimensional (3D) element formulations.

The first analysis undertaken represents a simple 3D geometry and crack configuration, which was verified by a closed-form solution. Next, the transition was made to representative railroad wheel geometry in 2D form. The 2D model simulated the heat treatment process to establish the temperature field over time, and the process was adjusted until satisfactory thermal behavior was achieved. Temperature field results were transferred to a coupled structural analysis model to determine the residual stresses generated by the heat treatment.

Completion of 2D model analyses was followed by extruding the 2D geometry into a 15° 3D sector model of the wheel. The sector model was the basis for most of the computational work. Various circular, embedded crack features were inserted into the 3D FEA model and were initially set to be inactive. The sector model was then subjected to the same heat treatment process as the 2D model, and the residual stress field was calculated using a coupled thermal-structural analysis process, as completed in the previous step.

Following the 3D sector model heat treatment simulation, a subsequent static structural analysis was conducted to simulate the cold work process on the new wheel. This consisted of applying a normal load of 71,500 lbf (using an elliptical pressure distribution function to represent wheel-rail contact) to the taping line at seven different sequential circumferential positions. This sequential loading was repeated four more times and established a modified residual stress field when compared to heat treatment alone.

After the cold work process was completed, crack 1 was activated, and the model was solved to establish the deformation, stress, strain, and J-integral results around the crack. The temperature field associated with the appropriate braking heat load was then applied, the structural model was solved, and the results were extracted. Lastly, a series of elliptical pressure loads were applied along the taping line at designated positions 1–7 and the results were retrieved. The magnitude of the elliptical pressure load was the same as that used for the cold work process. This sequence was repeated for cracks 2–7. The details of each step in the process are provided in the following sections.

3.2 Model Configurations

Two stages of analysis were specified, each requiring a different FEA model. The objective of each stage is explained in the following sections.

3.2.1 Simple Geometric Shape (Stage I)

The purpose of the simple geometric shape analysis is as follows:

To establish the proper methodologies and mesh sizing, the analysis should initially focus on a

simple geometric shape (e.g., a cylinder) with an embedded circular crack in it. The goal of the mesh convergence study is to determine that the individual contours and modeling results around the crack tip are producing the same stress intensity factor (SIF), since in theory the SIFs are independent of path. The simplified model should have dimensions, material properties and loadings similar to the rim of a railroad wheel.

Figure 4 illustrates the Stage I model concept and boundary conditions.

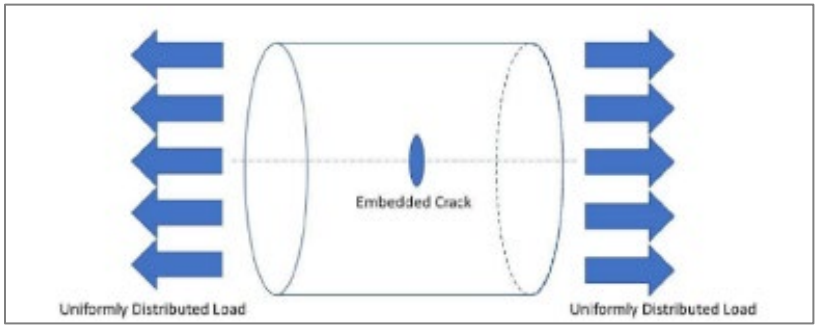

Figure 4. Simple Geometric Shape (Stage I): Model Concept

Figure 5 shows a round bar with circular internal cracks under uniform tension. The implementation of the relevant equations is shown in Figure 6. The closed-form solution calculates the Mode I energy release rate G_I and stress intensity factor K_I. For the conditions present in the FEA model (material is linear elastic and isotropic, thus, plane strain applies), the Mode I J-integral and energy release rate are equivalent ($J_I = G_I$).

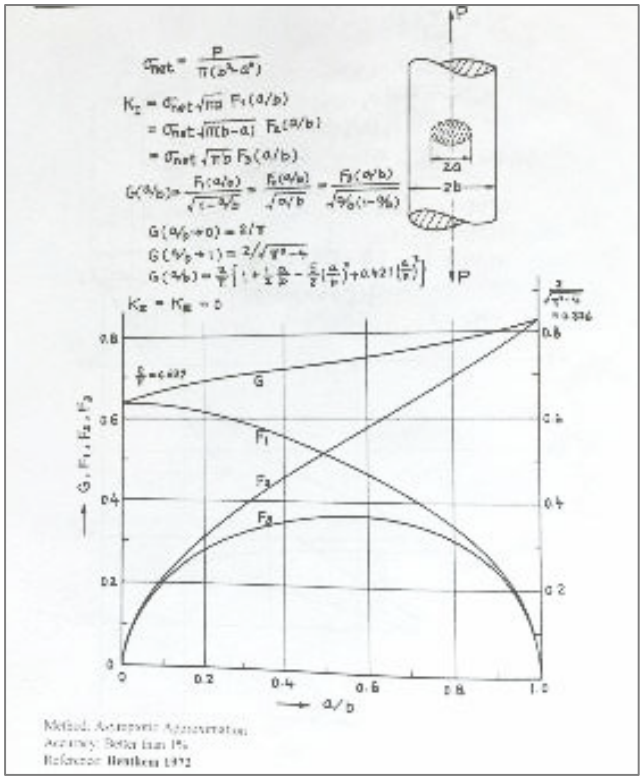

Figure 5. Stage I Model: Closed-Form Solution [8]

An Internal Circular Crack in a Round Bar, p. 396			
E =	3.00E+07	psi	elastic modulus, steel
ν =	0.30		Poisson's ratio, steel
$E' = \frac{E}{1-\nu^2}$	3.30E+07	psi	elastic constant, plane strain
P =	1000	lbf	applied remote load
a =	0.5	in	radius of circular crack
b =	6	in	radius of round bar
π =	3.141592654		pi
$\sigma_{net} = \frac{P}{\pi(b^2-a^2)}$	8.904	psi	round bar net section stress
$G\left(a/b\right) = \frac{2}{\pi}\left\{1+\frac{1}{2}\frac{a}{b}-\frac{5}{8}\left(\frac{a}{b}\right)^2+0.421\left(\frac{a}{b}\right)^3\right\}$	0.6605		alternate form of configuration correction factor
$F_1\left(a/b\right) = G\left(a/b\right)\sqrt{1-a/b}$	0.6324		configuration correction factor 1
$F_2\left(a/b\right) = G\left(a/b\right)\sqrt{a/b}$	0.1907		configuration correction factor 2
$F_3\left(a/b\right) = G\left(a/b\right)\sqrt{a/b\left(1-a/b\right)}$	0.1826		configuration correction factor 3
$K_I = \sigma_{net}\sqrt{\pi a}F_1\left(a/b\right)$	7.057	psi-in$^{1/2}$	mode I stress intensity factor using configuration correction factor 1
$K_I = \sigma_{net}\sqrt{\pi(b-a)}F_2\left(a/b\right)$	7.057	psi-in$^{1/2}$	mode I stress intensity factor using configuration correction factor 2
$K_I = \sigma_{net}\sqrt{\pi b}F_3\left(a/b\right)$	7.057	psi-in$^{1/2}$	mode I stress intensity factor using configuration correction factor 3
$G_I = \frac{K_I^2}{E'}$	1.511E-06	psi-in	mode I energy release rate for plane strain

Figure 6. Stage I Model: Closed-Form Solution

The Stage I ANSYS Mechanical FEA model geometry (Figure 7) is a cylinder with outside diameter 2b = 12 inches, height h = 24 inches, and embedded center circular crack diameter 2a = 1 inch.

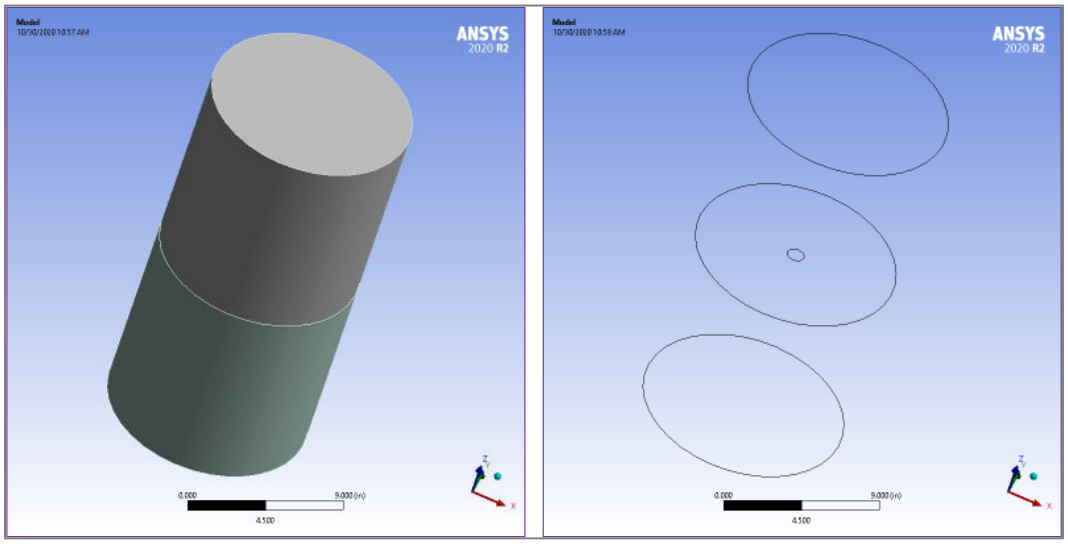

Figure 7. Stage I Model: FEA Geometry

Figure 8 indicates that a fixed boundary condition is applied to the bottom face of the cylinder, with a uniform remote force of 1,000 lbf normally applied to the top face of the cylinder.

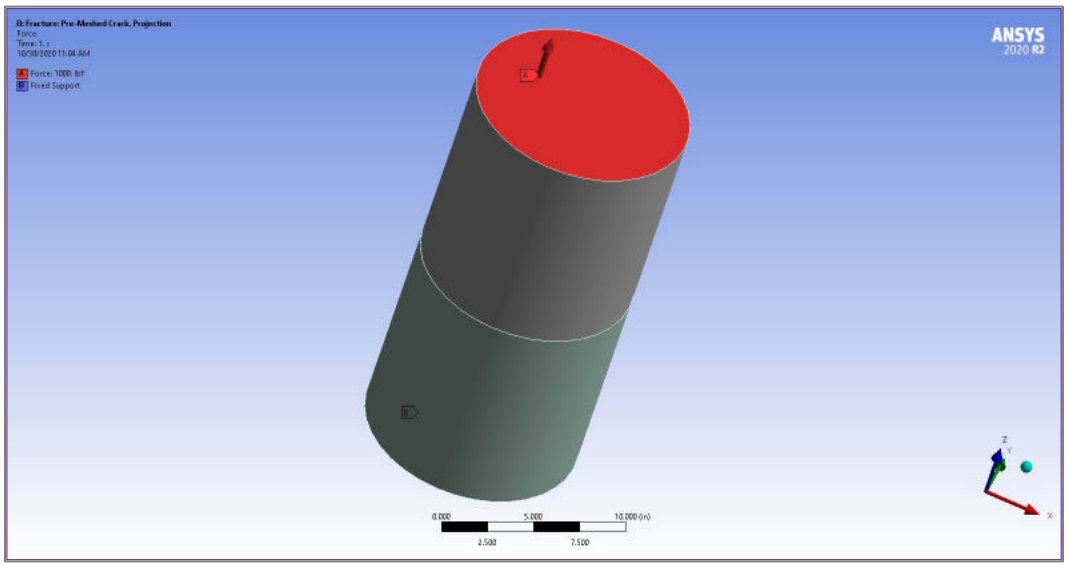

Figure 8. Stage I Model: FEA Loads and Boundary Conditions

The computational mesh in the vicinity of the circular internal crack is shown in Figure 9. A global mesh size of 0.5 inches was specified over most of the cylinder, but the crack front itself was assigned 128 element divisions and is identified in the figure by the discernable ring. This results in a computational mesh of about 620,000 nodes and 456,000 ANSYS SOLID187 quadratic (10 node) tetrahedron elements.

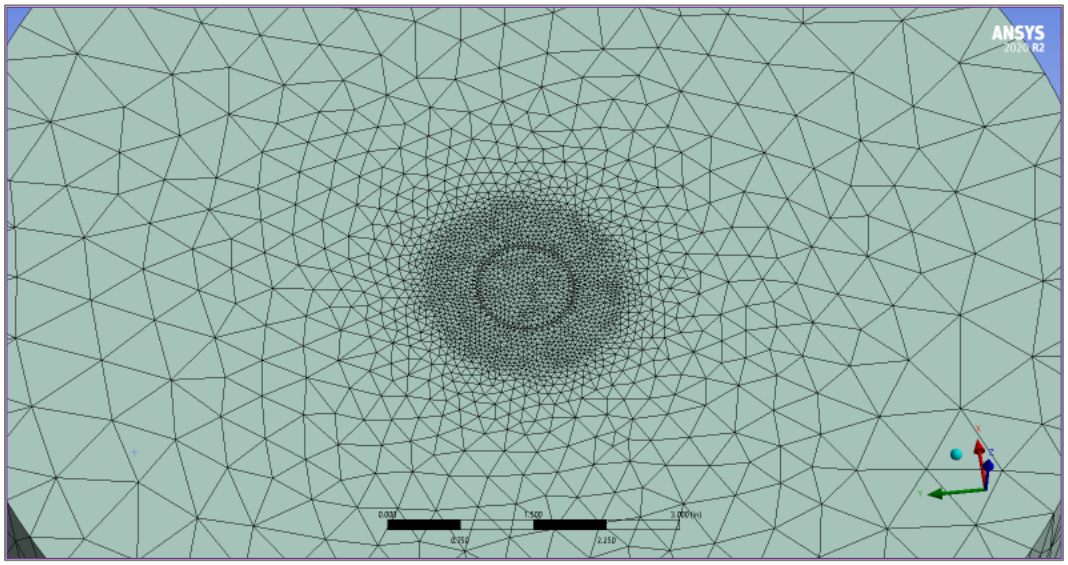

Figure 9. Stage I Model: FEA Computational Mesh

Results from the fracture mechanics analysis reveal an average J-integral value around the crack front of 1.664E-10 BTU/in^2 (1.554E-6 psi-in; see Figure 10). This is within 3 percent of the closed-form value of 1.511E-6 psi-in for plane strain conditions. The researchers conducted additional studies using coarser and finer meshes. Regardless of the mesh size, all computational

fracture mechanics results were within 5 percent of the closed-form solution when employing 10-noded tetrahedral elements. Using 20-noded ANSYS SOLID186 hexahedral elements produced even better results, within about 0.5 percent of the closed-form solution. The inset figure shows the basic contour integral path which is evaluated to determine the results.

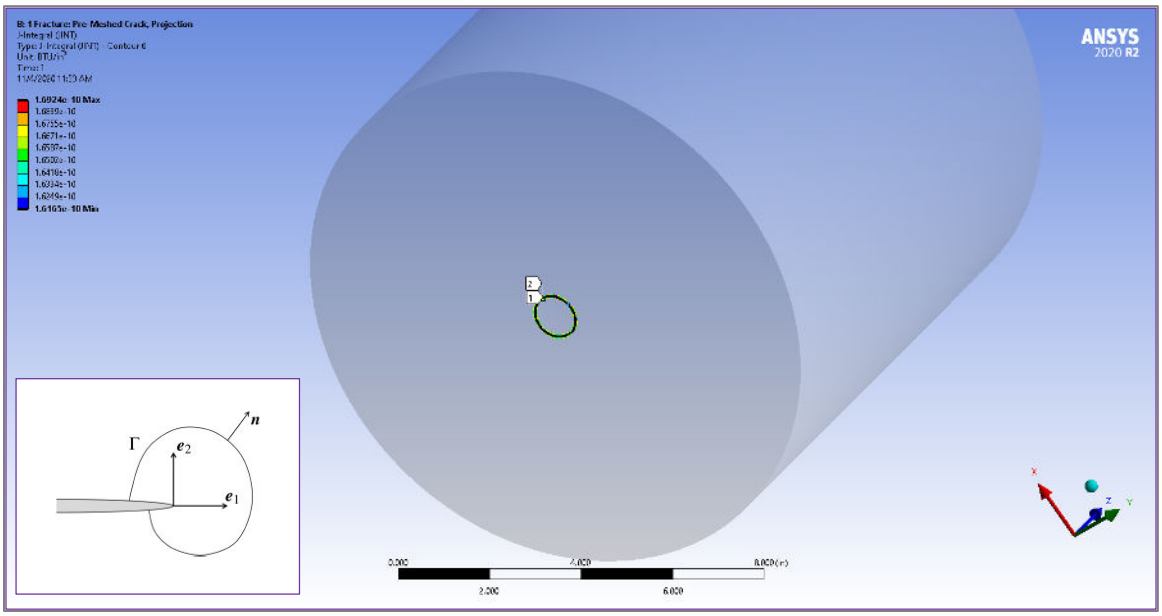

Figure 10. Stage I Model: FEA Crack Front J-Integral Results

Table 1 lists a set of Mode I J-integral and SIF results using 20-noded hexahedral elements. Six sets of contour results were requested from ANSYS. Results at Contour 1, which is closest to the crack front, tended to be variable and were usually discounted. Results for Contours 2–6 show only a small variance, which proves the path independence of the solution.

Table 1. Stage I Model: Comparative Results, Crack Contours 1–6

Mesh Iteration	Result	Contour Number					
		1	2	3	4	5	6
1 – Initial	K_I (psi-in$^{1/2}$)	6.591	7.081	7.083	7.083	7.083	7.083
	J (psi-in)	1.460E-6	1.517E-6	1.518E-6	1.518E-6	1.518E-6	1.518E-6
2 – Coarser	K_I	6.613	7.086	7.088	7.089	7.087	7.085
	J	1.461E-6	1.516E-6	1.517E-6	1.517E-6	1.516E-6	1.516E-6
3 – Finer	K_I	6.586	7.082	7.084	7.084	7.084	7.084
	J	1.460E-6	1.519E-6	1.519E-6	1.519E-6	1.519E-6	1.519E-6

3.2.2 Railroad Wheel (Stage II)

The purpose of the Stage II railroad wheel analysis was to conduct a detailed analysis for a section of railroad wheel, following the establishment of meshing and calculation methods required to capture the behavior of a crack. The terminology associated with a typical railroad wheel is shown in Figure 11. The subject of the detailed analysis should be a forged Grade C, 36-inch diameter, single wear railroad wheel. The analysis will consider new and worn wheels. Rim

thicknesses to be considered in the analysis to be 1.5 inches, representing a new wheel, and 1 inch to represent a worn wheel.

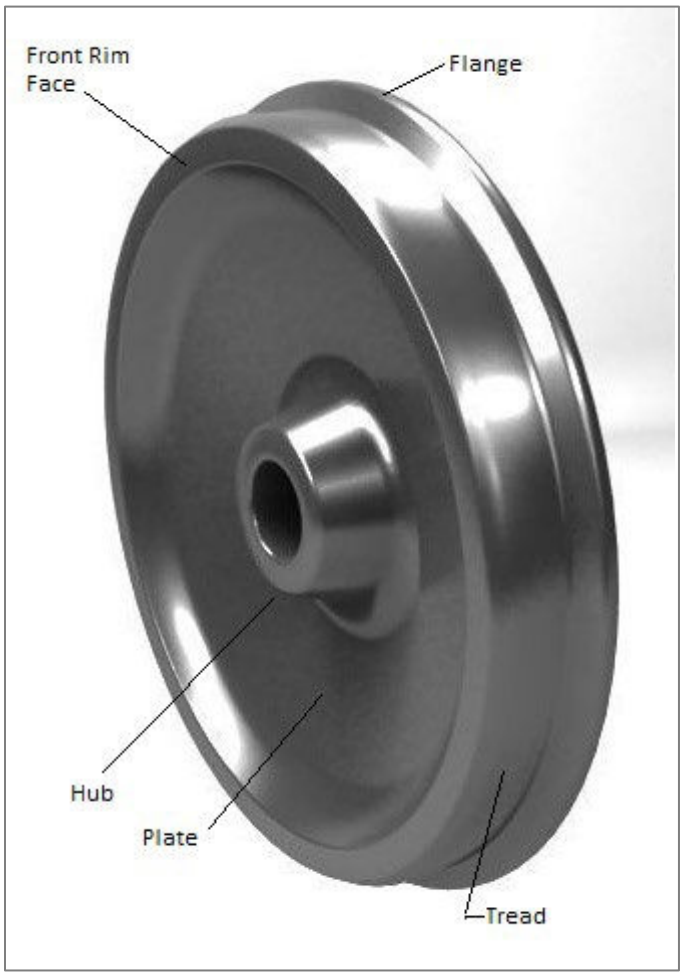

Figure 11. Railroad Wheel Terminology

Figure 12 and Figure 13 illustrate details of the cracks inserted into both new and worn wheels. For a new wheel with a rim thickness of 1.5 inches, there were a total of seven cracks at varying depths and positions relative to the taping line. The three cracks directly under the taping line were 0.25 inch in diameter. The remaining four cracks were 0.5 inch in diameter. Six of the seven cracks were horizontal, while the final crack was vertically oriented and located relatively close to the front rim face.

For a worn wheel with a rim thickness of 1 inch, only four of seven cracks were required. However, in practice, the same seven cracks in the new wheel were available in the worn wheel. Note that the depth of the cracks in either wheel were relative to the respective tread surface.

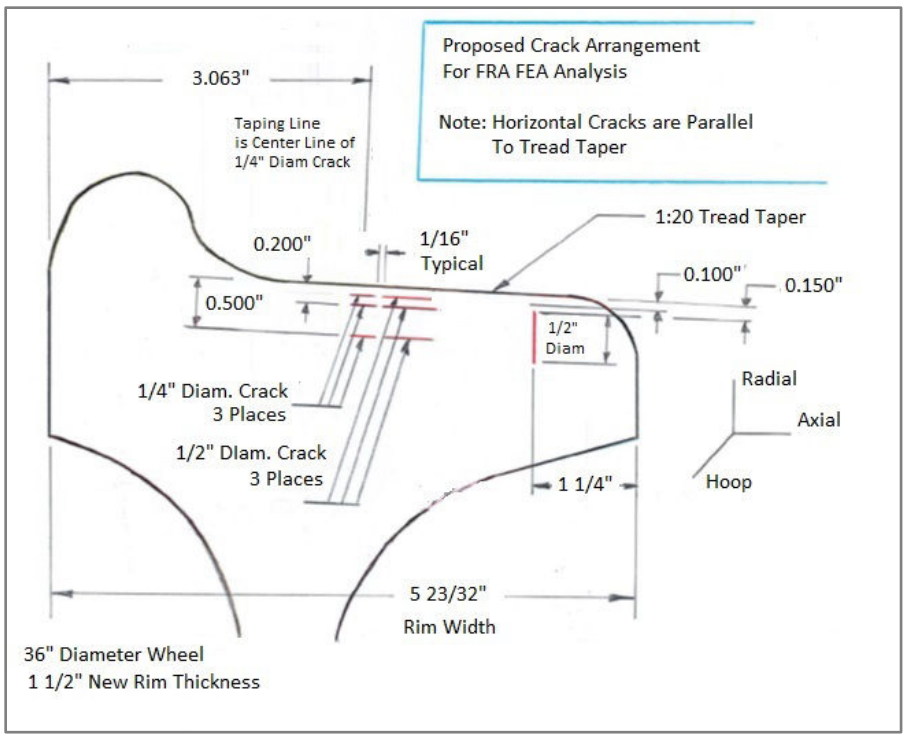

Figure 12. Recommended Introduction of Axial and Circumferential Cracks into Mechanical Model of Wheel with 1 1/2-inch Rim Thickness

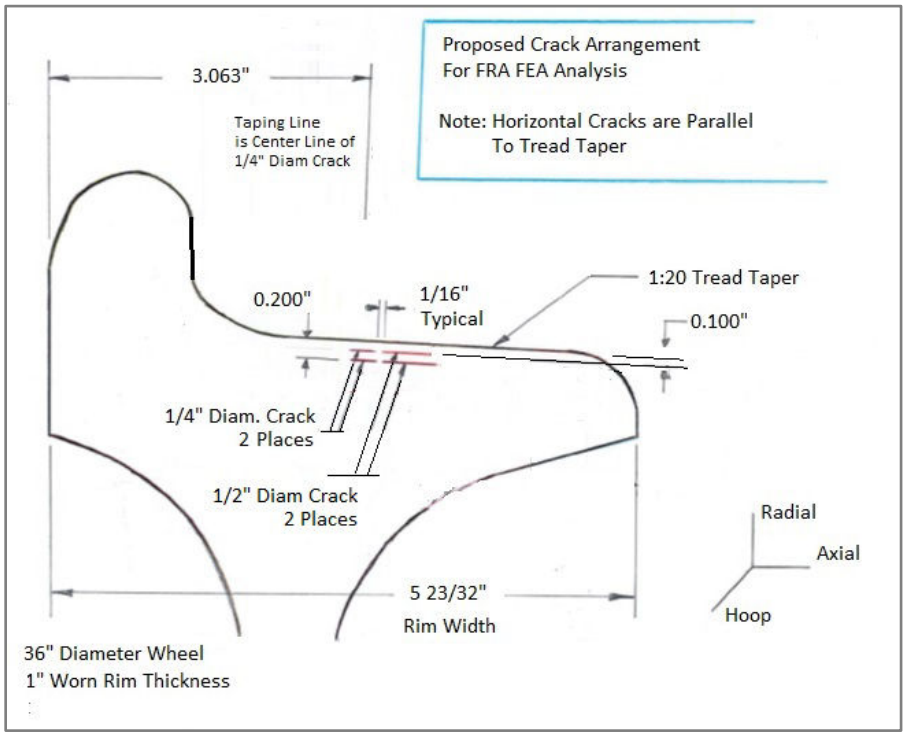

Figure 13. Recommended Introduction of Axial and Circumferential Cracks into Mechanical Model of Wheel with 1 inch Rim Thickness. Note: in the actual simulation of the worn wheel, the seven cracks shown in Figure 12 were introduced to the model.

3.3 Analysis Process Overview

The Stage II analysis process was outlined as follows:

- Create a new 1.5-inch rim thickness 2D wheel cross-section geometry.
- Create a new 1.5-inch rim thickness 2D FEA model.
- Perform 2D transient thermal heat treatment and coupled thermal stress analyses; optimize the heat treatment process until desired results are achieved.
- Expand 2D wheel model into full 360° 3D FEA model; perform braking heat and mechanical load stress checks per MSRP S-660.
- Expand 2D FEA model to 15° sector 3D FEA model.
- Generate 3D FEA geometry for seven discrete embedded cracks, define contact elements, determine initial and final computational mesh, and apply symmetry boundary conditions.
- Create hybrid analysis process using both ANSYS Mechanical and ANSYS APDL scripting to facilitate the required heat treatment, braking, cold work, and wheel load scenarios workflow (see solution process details in Figures 14–16).
- Create equivalent worn 1-inch rim thickness 3D FEA model with embedded cracks.
- Perform various other model check analyses on 3D FEA model.
- Complete multiple solves for wheel scenarios WS1, WS2, WS3, WS4 (1.5-inch rim) and WS8, WS9, WS10, WS11 (1-inch rim); extract results data including normal, shear, and principal stresses, J-integral, stress intensity factors, T-stress, and general crack behavior; predict crack turn-in directions.

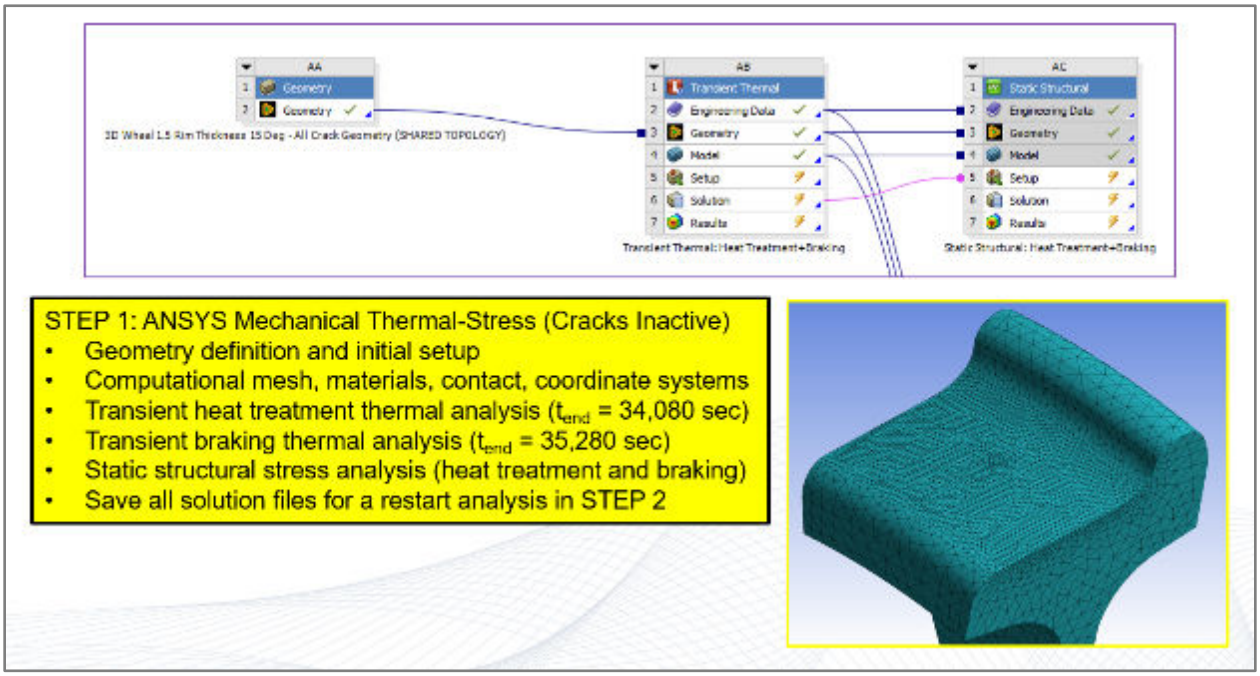

Figure 14. Solution Process Details: Step 1

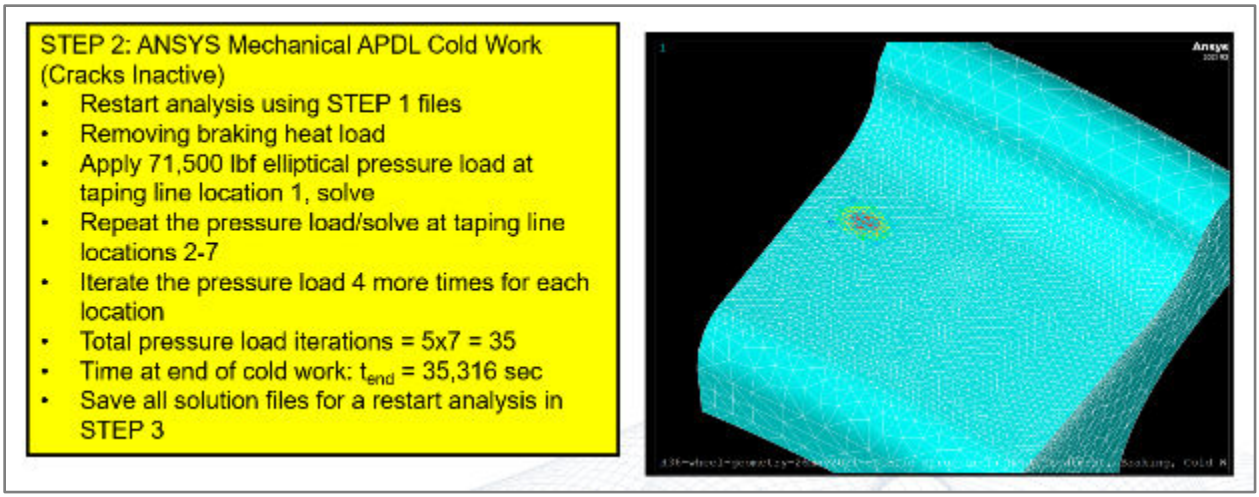

Figure 15. Solution Process Details: Step 2

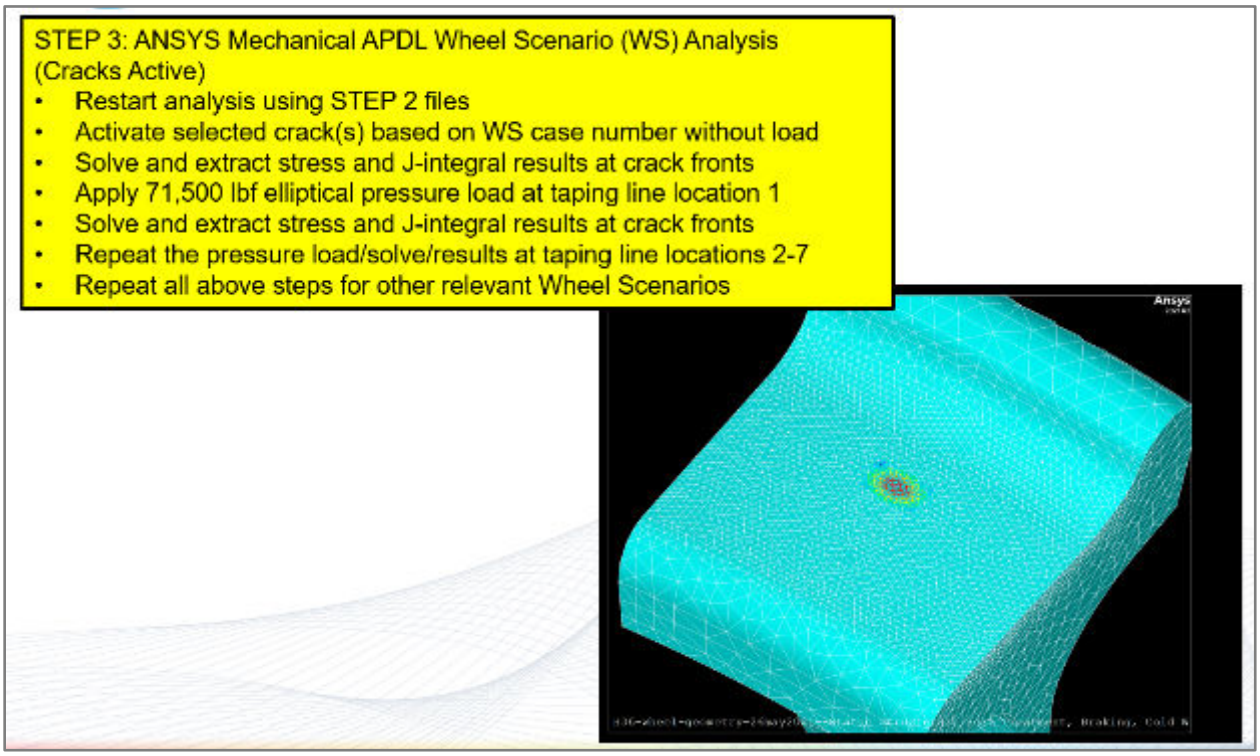

Figure 16. Solution Process Details: Step 3

3.4 Geometry Development

The team created the 1.5-inch rim thickness geometry profile using ANSYS SpaceClaim (Figure 17). This profile is typical of wheel geometry but does not conform to any particular manufacturer's proprietary design. This geometry profile was used to create a 2D model.

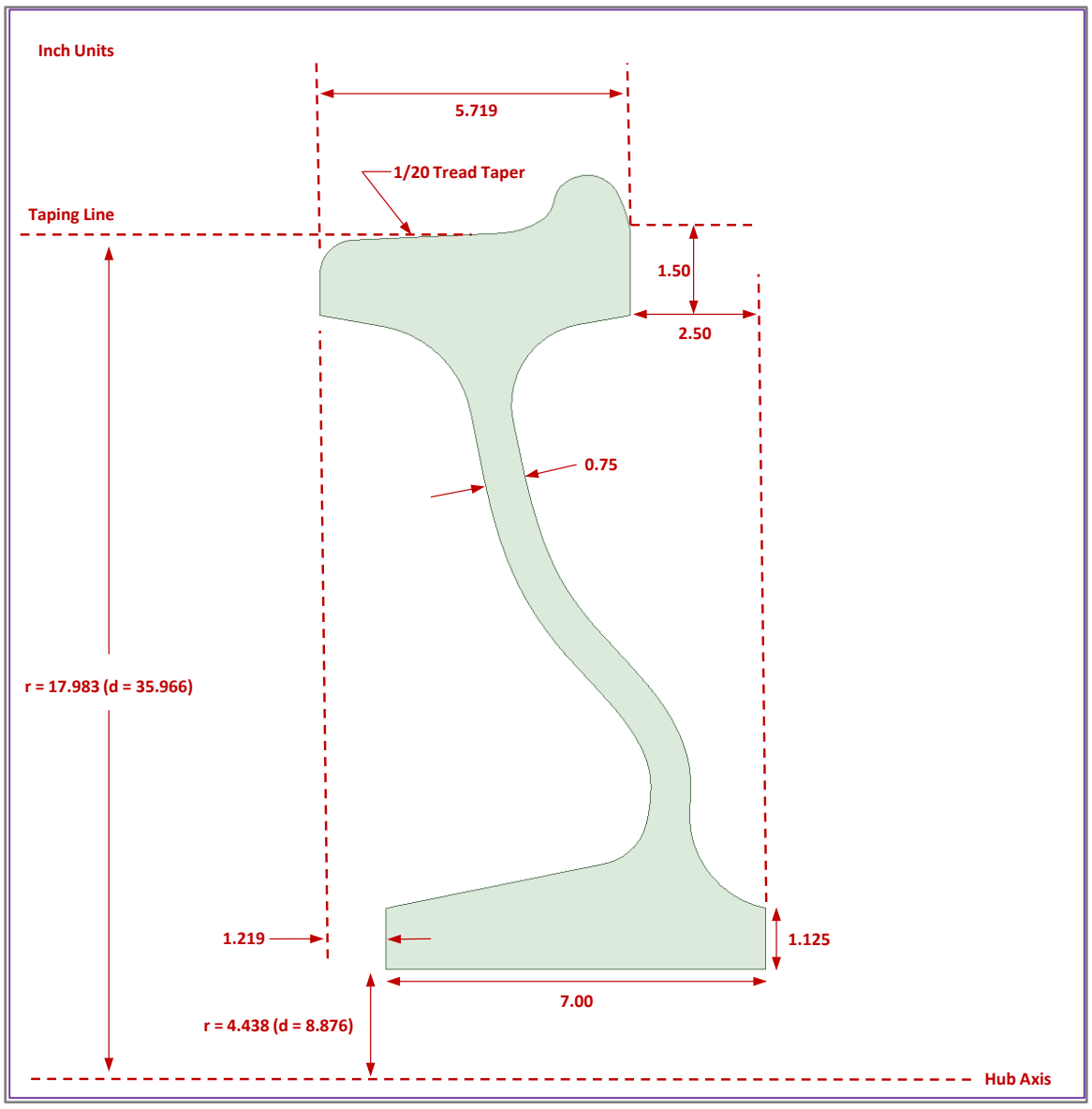

Figure 17. Stage II Wheel Geometry Profile

Following development of the 2D geometry profile, the geometry was extruded into the 15° sector model shown in Figure 18. ANSYS DesignModeler was used to divide the sector model and create the geometry of the seven subsurface cracks, as well as other details for application of the normal load on the tread taping line. Figures 19–21 illustrate the groups of horizontal cracks located at 0.1, 0.2, and 0.5 inches below the tread surface, as well as the local cylindrical coordinate systems assigned to each. Figure 22 provides similar detail for the single vertical crack. Figure 23 shows a section view of the new 1.5-inch rim thickness geometry with annotated crack information.

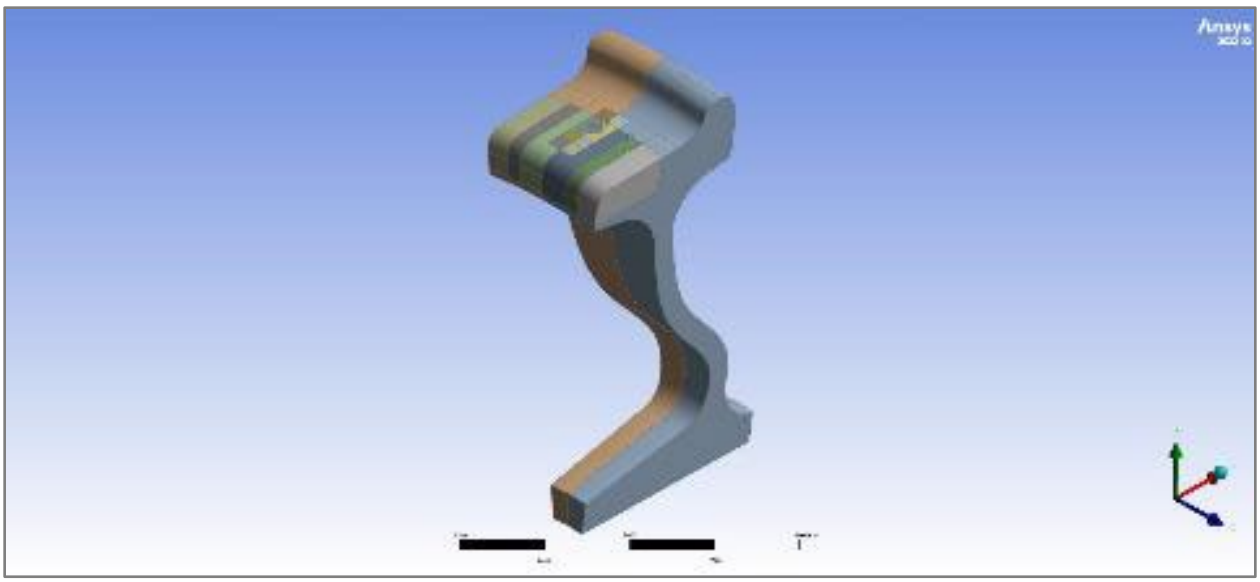

Figure 18. 15° 3D Rail Wheel Sector Model

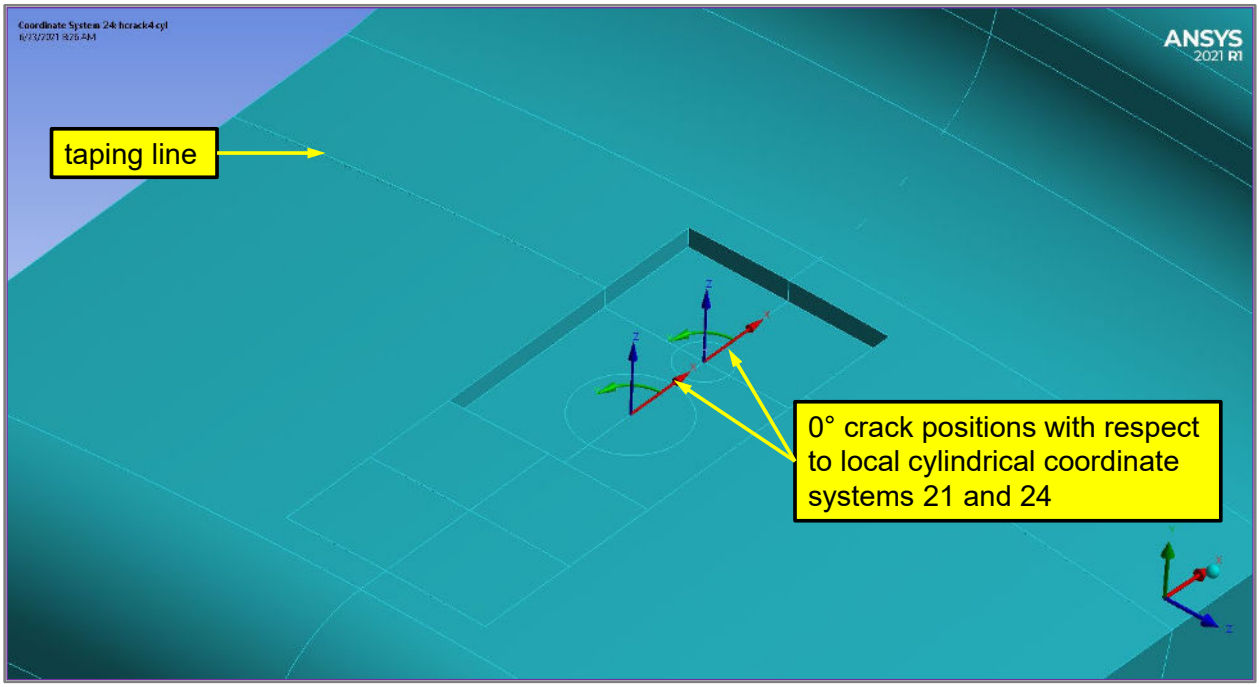

Figure 19. 0.1-Inch Deep, 0.25-Inch and 0.5-Inch Diameter Horizontal Cracks (HCRACK1, HCRACK3)

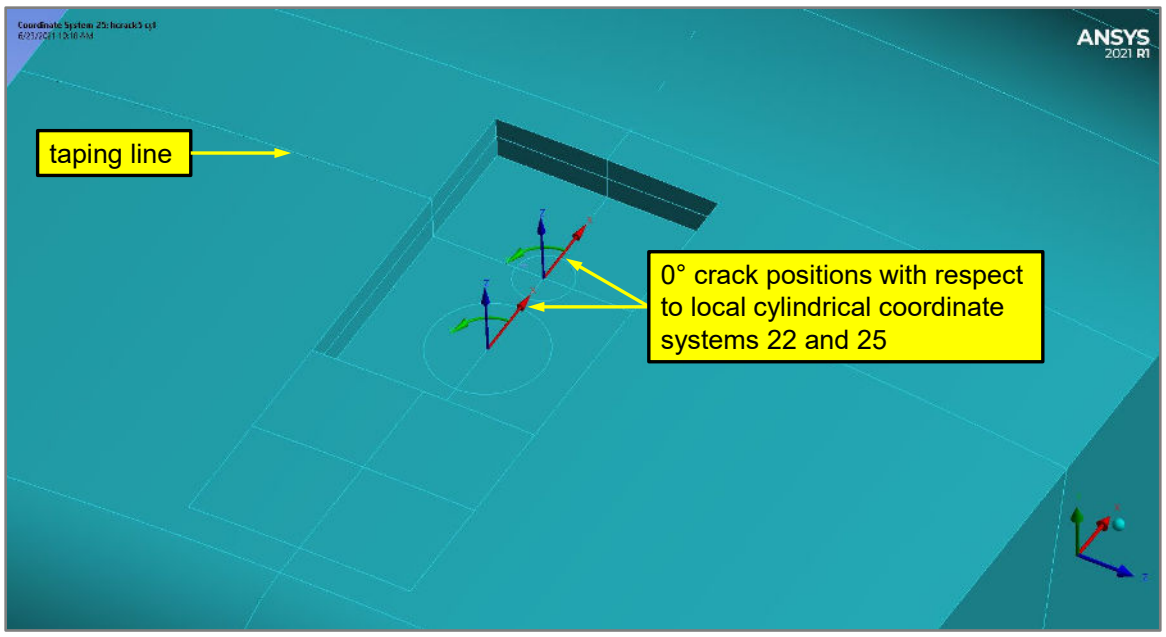

Figure 20. 0.2-Inch Deep, 0.25-Inch and 0.5-Inch Diameter Horizontal Cracks (HCRACK2, HCRACK5)

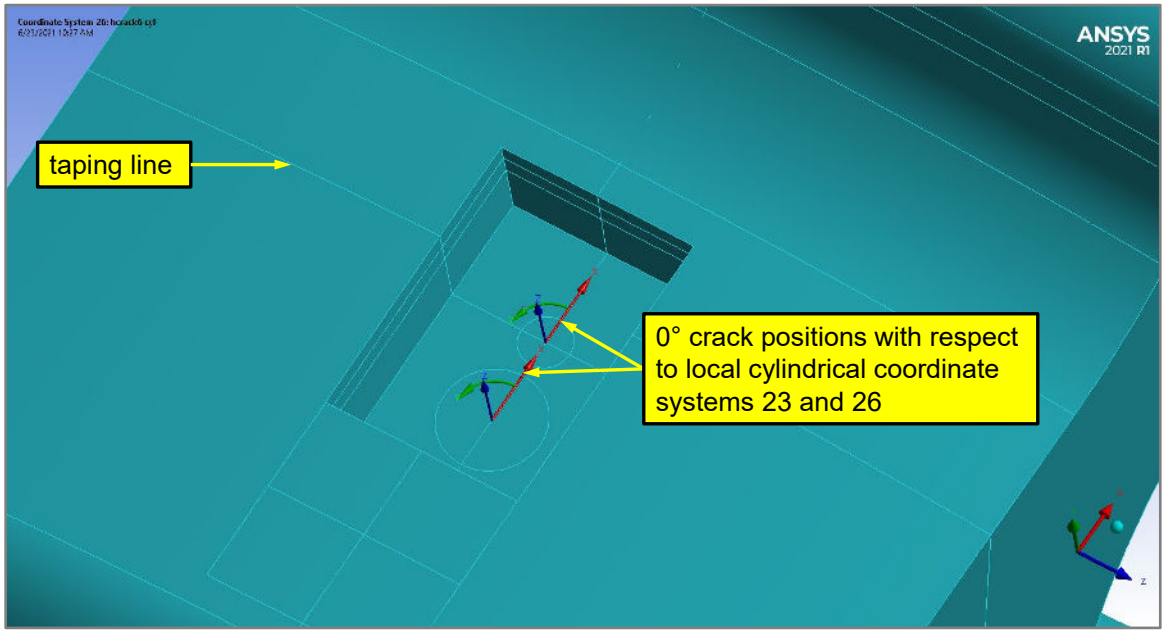

Figure 21. 0.5-Inch Deep, 0.25-Inch and 0.5-Inch Diameter Horizontal Cracks (HCRACK3, HCRACK6)

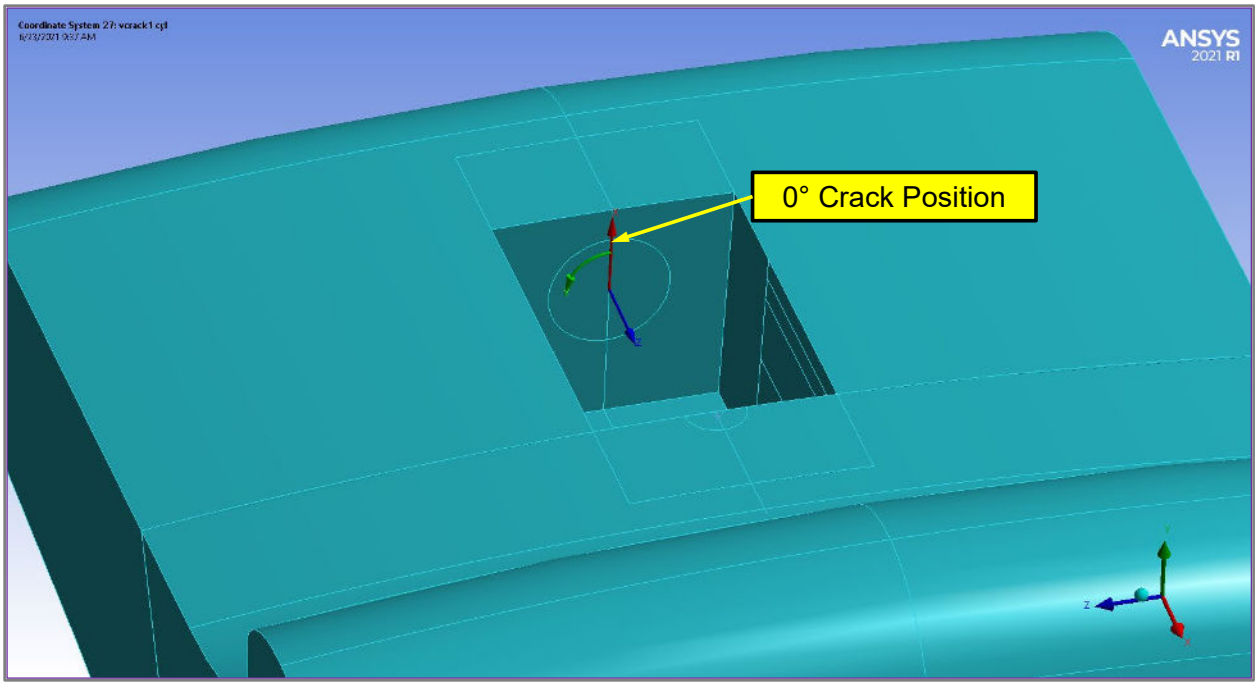

Figure 22. 0.5-Inch Diameter Vertical Crack (VCRACK1)

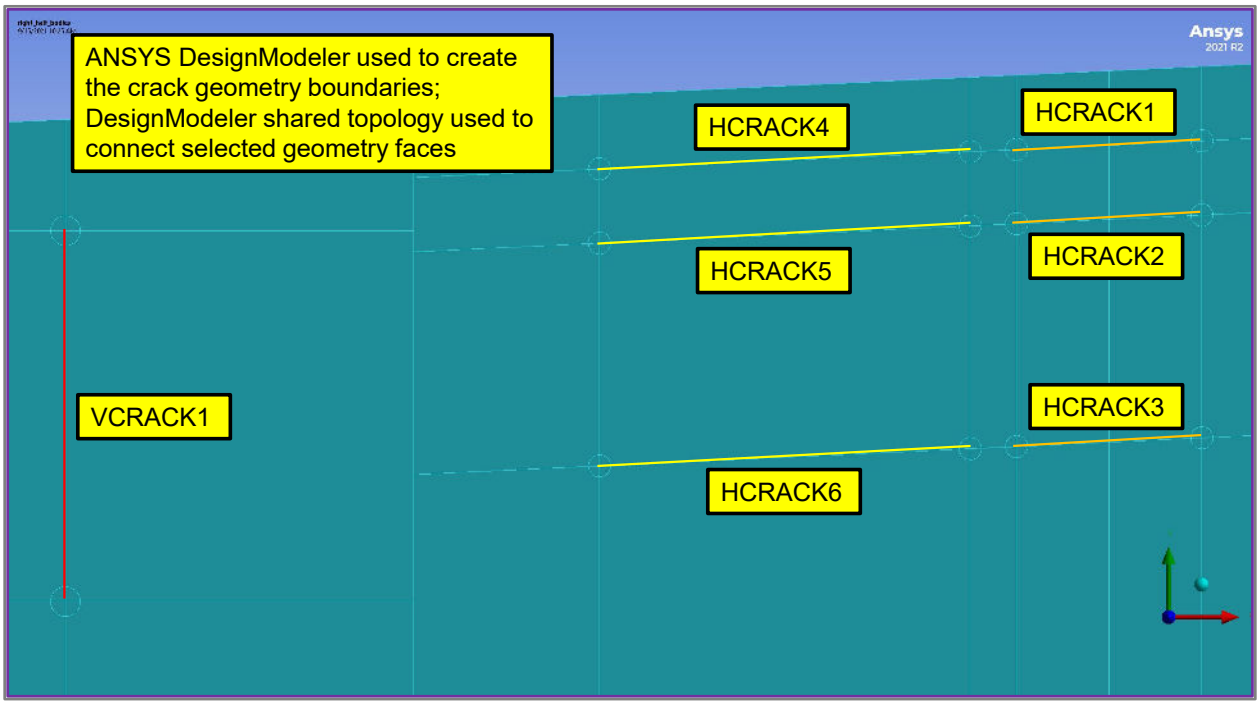

Figure 23. Section View of Embedded Cracks: 1.5 Inch Rim Thickness

Figure 24 compares the geometry profile of a new 1.5-inch rim thickness wheel to that of a worn 1-inch rim thickness wheel. For the worn wheel profile, geometry in red is removed from the new wheel profile but the positions of the subsurface cracks are the same with respect to the tread surface. Note also that the heat treatment process applies only to the new wheel profile. Once the worn 0.5-inch of material is removed from the new wheel, the heat treatment is not repeated on the worn wheel.

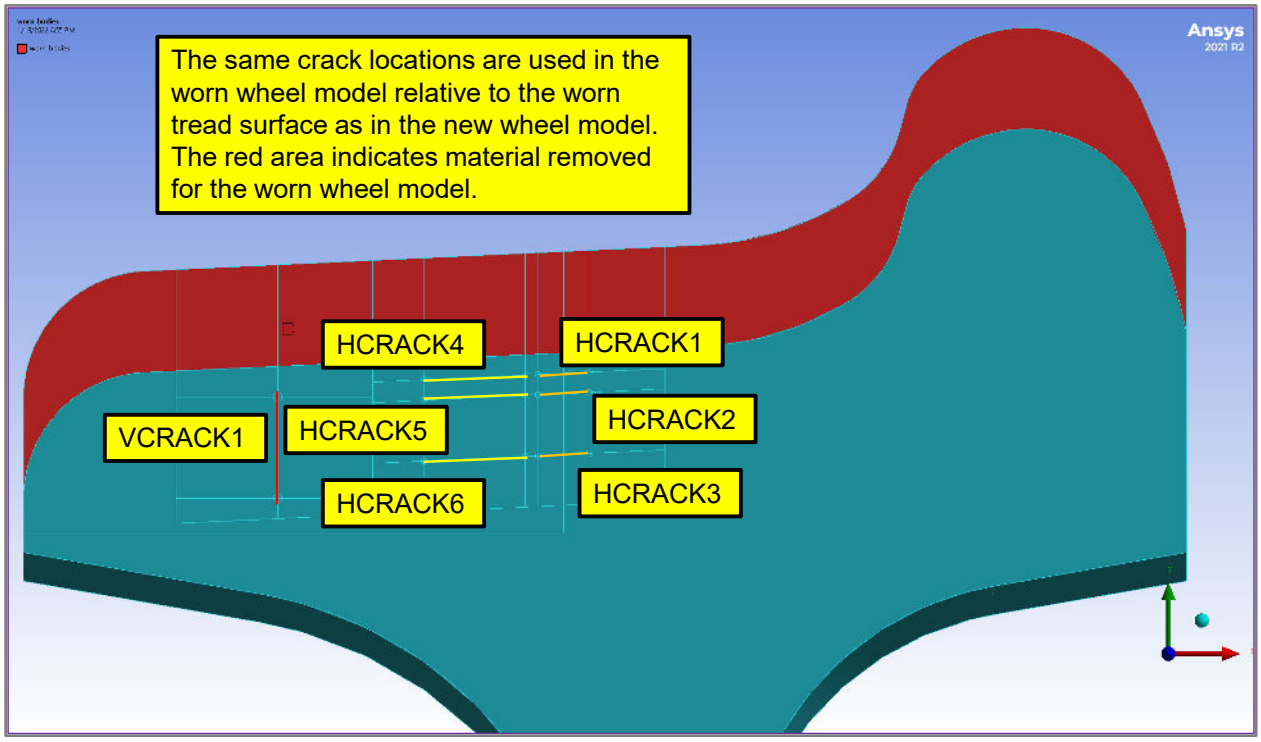

Figure 24. Section View of Embedded Cracks: 1 Inch Rim Thickness

3.5 Computational Mesh

The computational mesh developed for the 3D sector model is shown in Figure 25. It consists of a mix of ANSYS 10-noded tetrahedral (SOLID187) and 20-noded hexahedral (SOLID186) elements. Due to the significant number of load steps used in solving the thermal and structural models, and the use of multiple solution restarts, a compromise in mesh density was required to keep both solution time and disk space requirements within reason while still providing reliable results. Even so, disk space of up to 4 TB is recommended when solving the model. The model was solved on a 32-core workstation with 256 GB of RAM. Solution time is processor- and memory-dependent.

The 20-noded hexahedral elements were primarily employed in the region around the crack fronts, while 10-noded tetrahedral elements were used elsewhere. Figure 26 shows a cut-away view of the sector model interior, with mesh refinement at the embedded crack locations. Figure 27 illustrates the crack volume elements, which are hexahedral. Figure 28 is a cut-away view of one of the crack volumes (HCRACK3).

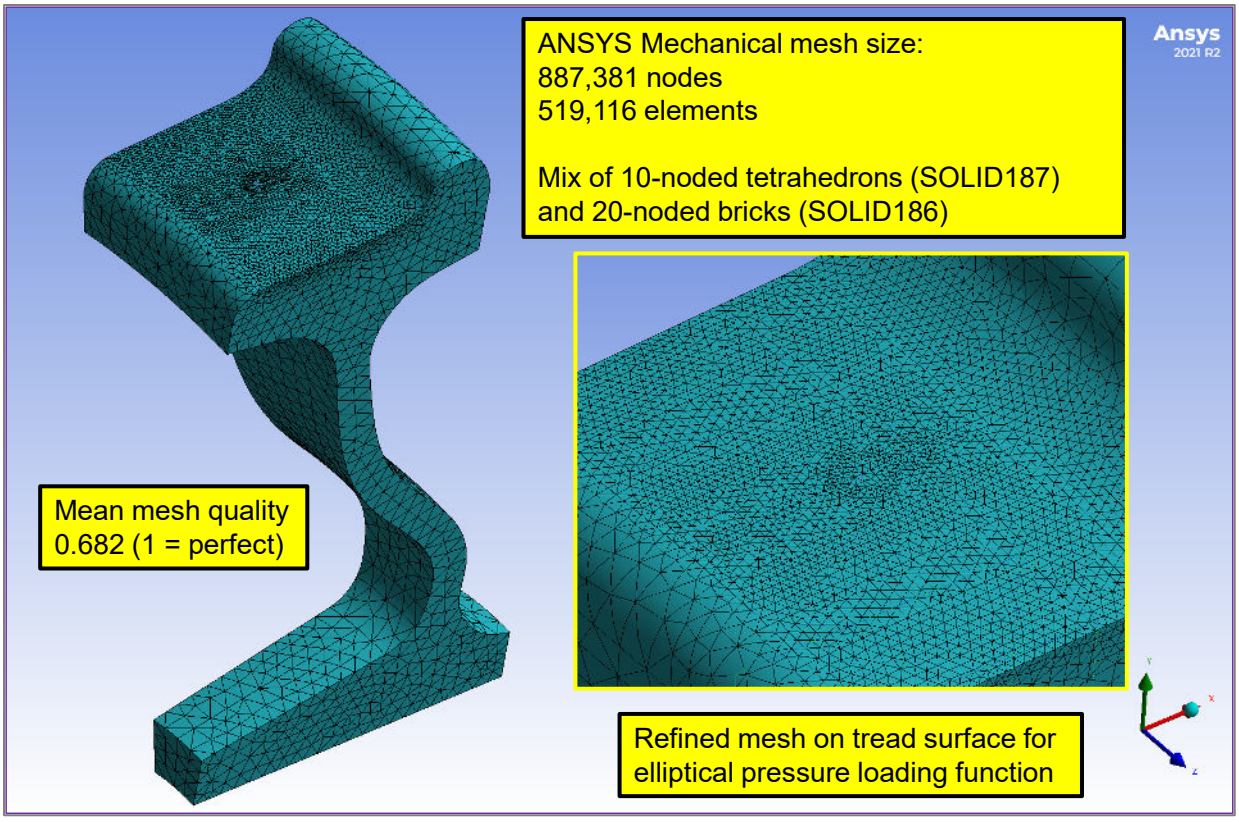

Figure 25. 3D Sector Model Baseline Computational Mesh

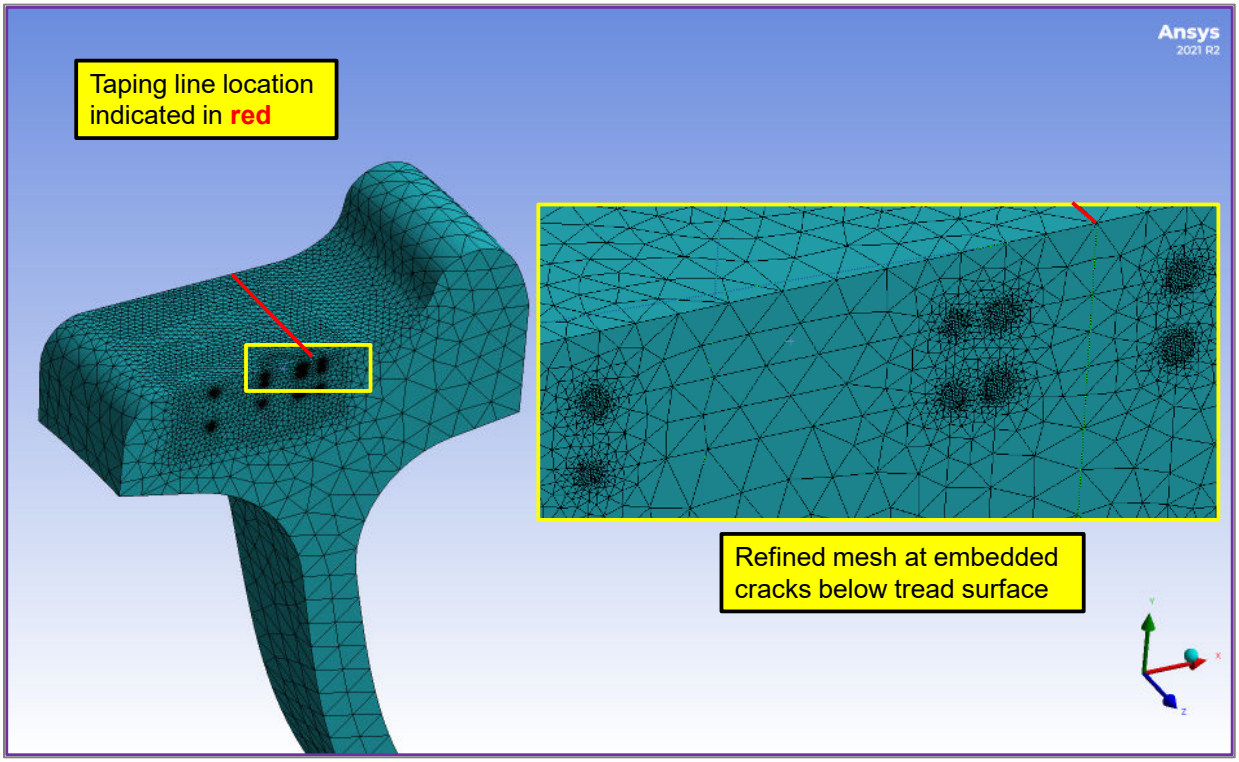

Figure 26. Refined Subsurface Computational Mesh

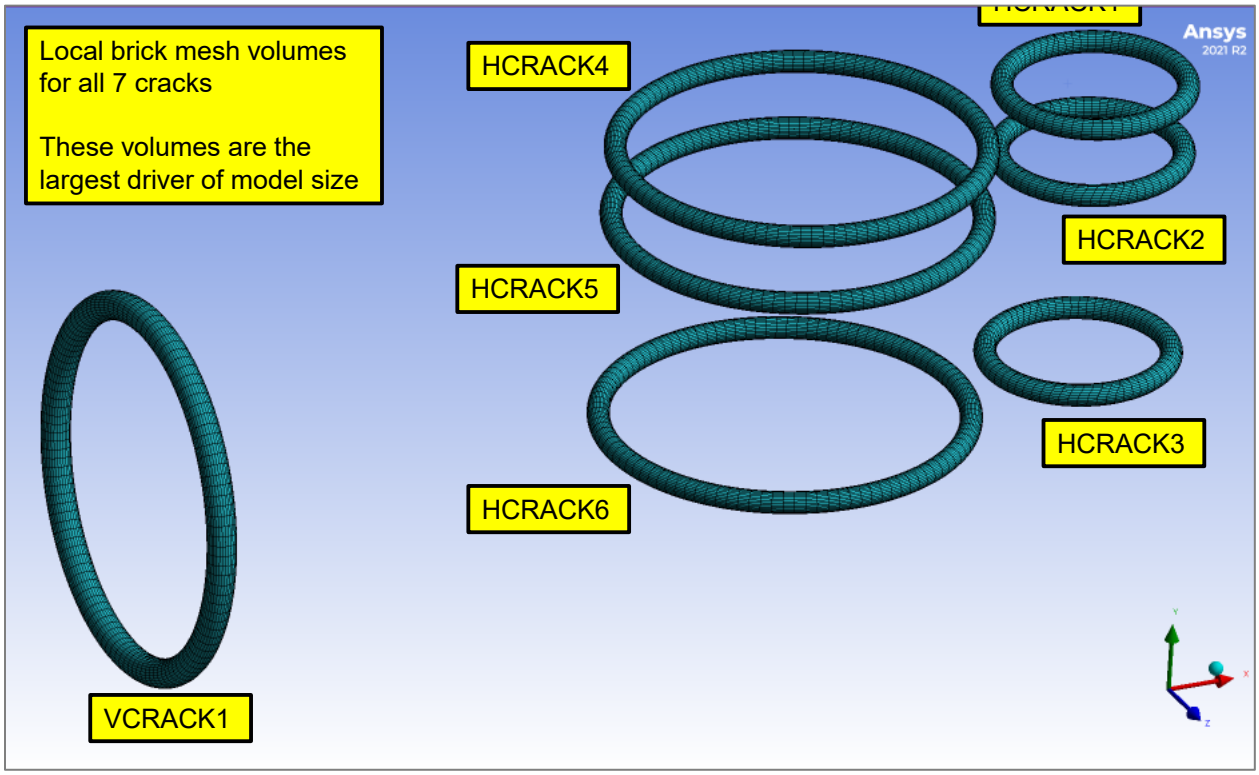

Figure 27. Refined Computational Mesh: Crack Volumes

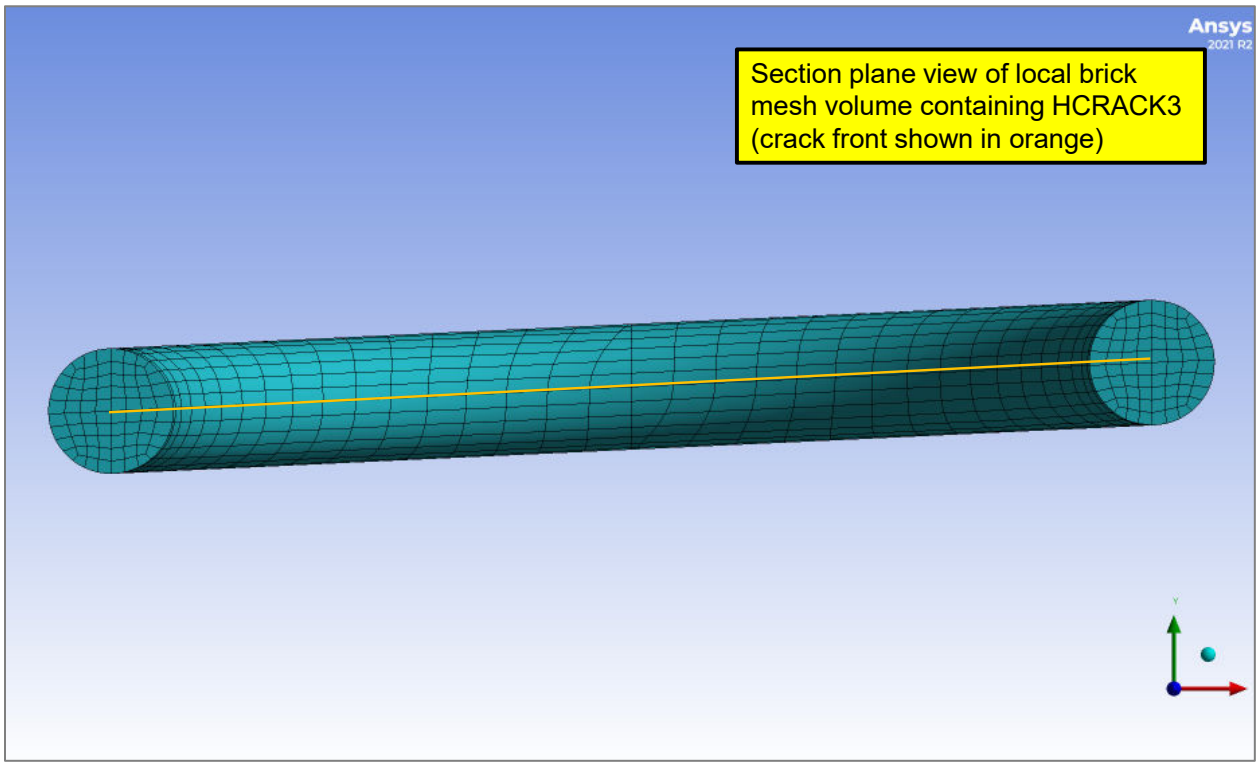

Figure 28. Refined Computational Mesh: Crack Volumes

3.5.1.1 Crack Contact Elements

In DesignModeler, shared topology connections were not defined between the top and bottom faces of the cracks (i.e., the crack faces were not connected). ANSYS contact elements are used to control whether the crack is inactive (faces connected) or active (faces unconnected). Bonded and frictionless contact pairs (ANSYS CONTA174 and TARGE170 elements) were defined between each crack top and bottom surface. Initially, the frictionless contacts were "killed" using the EKILL command, while the bonded contacts were retained, ensuring the cracks remained inactive.

In later analyses, the reverse occurred: bonded contact elements were killed while frictionless contact elements were made "live", rendering the crack active. Frictionless contact elements were used to prevent the top and bottom crack surfaces from interpenetrating when the crack closed. Figure 29 shows VCRACK1.

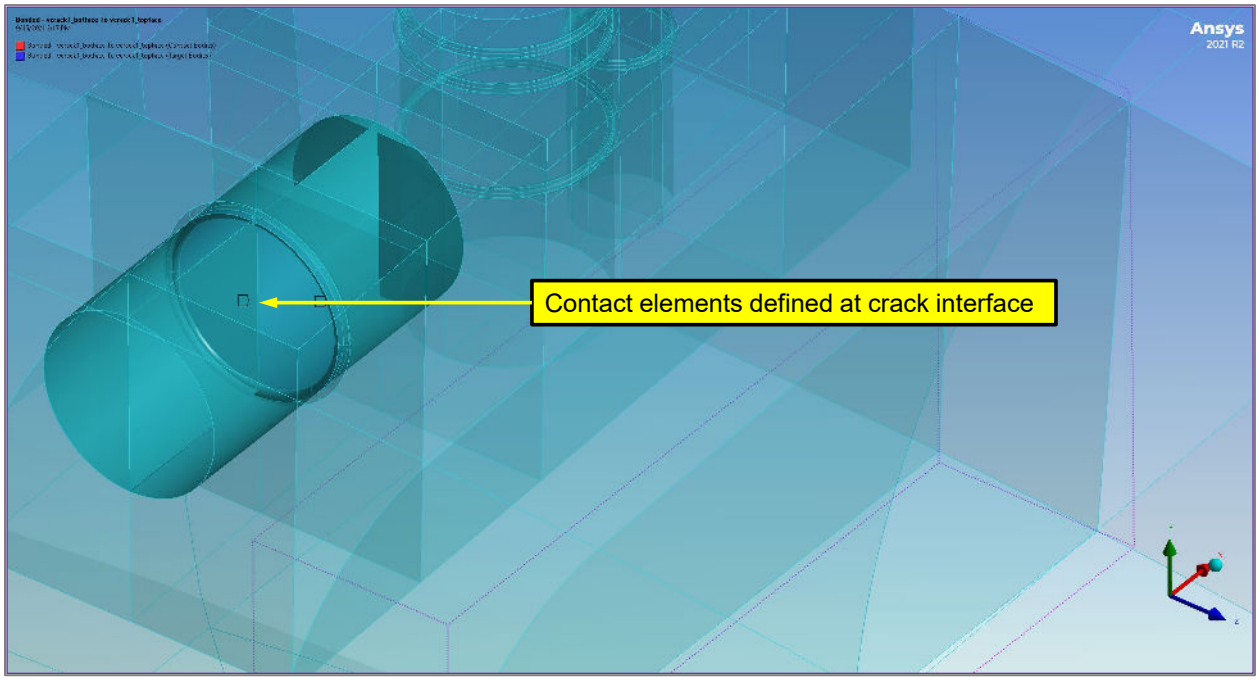

Figure 29. Crack Contact Elements

3.6 Material Properties

Material properties used in the analysis conform to those in S-669 of AAR MSRP Section G, Wheels and Axles [9], as shown in Figure 30 and Figure 31. The material properties are temperature-dependent and therefore non-linear. The creep strain definition conforms to a Norton creep model. It is necessary to convert effective stress σ_{eff} used in the creep equation from units of ksi to psi, which is part of the unit system used in ANSYS.

10.2 Material Properties (Temperature-Dependent) for Heat-Treatment Simulation

Table 10.1 Specific heat [8]

Temp (°F)	(BTU/lbm-°F)
0	0.1059
75	0.1106
1292	0.1866
1337	0.4079
1382	0.1487
1652	0.1309
1800	0.1309

Table 10.2 Thermal conductivity [7]

Temp (°F)	(BTU/sec-in-°F)
0	0.000672
75	0.000664
392	0.000629
1292	0.000403
1472	0.000329
1800	0.000361

10.3 Material Properties (Temperature-Dependent) for Stress Calculations

Table 10.3 Modulus of elasticity (E) and hardening modulus (Etan)

Temp (°F)	E (kips/in.^{2})	Etan [9, 10, 11, 12][a/] (kips/in.^{2})
0	29368	2016
75	29000	2192
100	28955	2250
200	28543	2484
300	28130	2719
400	27718	2953
500	27306	3187
600	26859	3028
700	26407	2804
800	25741	2514
900	24784	2151
1000	23553	1790
1100	20542	1431
1200	17531	1071
1300	14424	726
1400	11698	557
1500	9952	424
1600	9114	384
1700	8577	343
1800	7390	303

[a/] Temperature-dependent values for hardening modulus have been interpolated such that they are presented for the same temperatures as the modulus of elasticity.

Table 10.4 Poisson's ratio [9, 11, 13]

Temp (°F)	ν
0	0.2820
75	0.2838
514	0.2927
752	0.2980
932	0.3020
1292	0.3200
1472	0.3400
1800	0.3461

Table 10.5 Coefficient of thermal expansion [8]

Temp (°F)	Thermal Expansion Coefficient per °F
0	6.22E-06
75	6.22E-06
212	6.22E-06
400	8.58E-06
1292	8.58E-06
1472	9.61E-06
1800	9.61E-06

Figure 30. Material Properties [9]

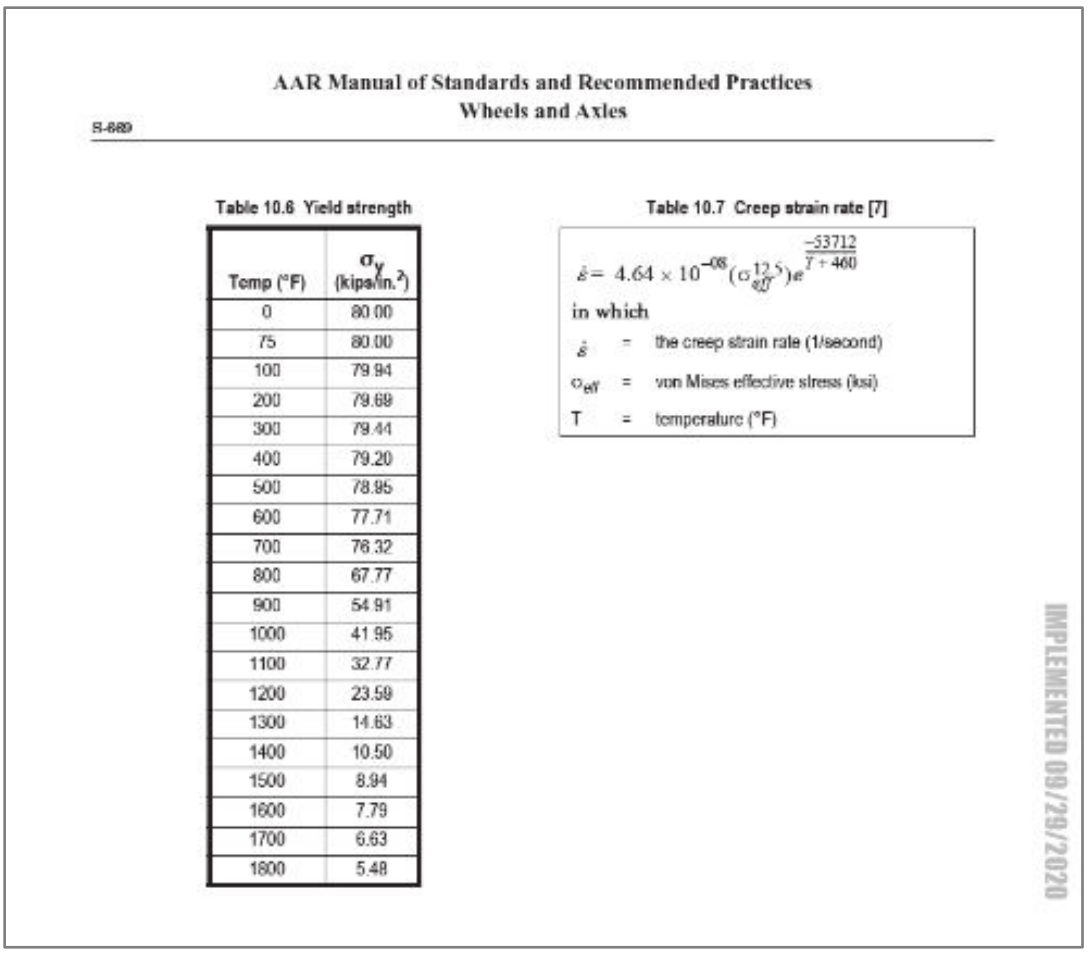

AAR Manual of Standards and Recommended Practices
Wheels and Axles
S-669

Table 10.6 Yield strength

Temp (°F)	σ_y (kips/in.^{2})
0	80.00
75	80.00
100	79.94
200	79.69
300	79.44
400	79.20
500	78.95
600	77.71
700	76.32
800	67.77
900	54.91
1000	41.95
1100	32.77
1200	23.59
1300	14.63
1400	10.50
1500	8.94
1600	7.79
1700	6.63
1800	5.48

Table 10.7 Creep strain rate [7]

$$\dot{\varepsilon} = 4.64 \times 10^{-08} (\sigma_{eff}^{12.5}) e^{\frac{-53712}{T+460}}$$

in which

$\dot{\varepsilon}$ = the creep strain rate (1/second)

σ_{eff} = von Mises effective stress (ksi)

T = temperature (°F)

IMPLEMENTED 09/29/2020

Figure 31. Material Properties — Continued [9]

3.7 Heat Treatment Process

The wheel heat treatment process was developed per general industry practices and does not conform to the proprietary process of any particular manufacturer. The total duration of the preliminary multi-step heat treatment process was 34,065 seconds and was implemented in ANSYS as a non-linear transient thermal analysis. Natural convection conditions assume a room temperature of 75°F. The preliminary heat treatment steps are shown in Table 2.

Table 2. Preliminary 1.5-Inch Rim Thickness Wheel Heat Treatment Process

ANSYS Load Step	Heat Treatment Load Step Description	Load Step Duration (sec)	Total Duration (sec)
1	Initial uniform wheel temperature, 1600°F	15	15
2	Uniform water spray quench, tread running surface	150	165
3	Air cool, 25 min	1500	1,665
4	Annealing furnace 932°F, 3 hr	10,800	12,465
5	Air cool, 6 hr	21,600	34,065

The forged, AAR Grade C, 36-inch carbon steel wheel has an approximate melting temperature T_m of 1450°C (2642°F), or 3102°R in absolute terms. Creep effects were considered when the temperature exceeded about 50 percent of the absolute melting temperature, or 1551°R (1091°F). Based on the heat treatment thermal simulation, $T \geq 0.5T_m$ predominantly occurred during heat treatment steps 1 and 2. Therefore, for the structural segment of the thermal-stress analysis, creep effects only needed to be activated for those steps. The heat treatment simulation was initially evaluated as a 2D problem. The 2D meshed wheel cross-section is shown in Figure 32.

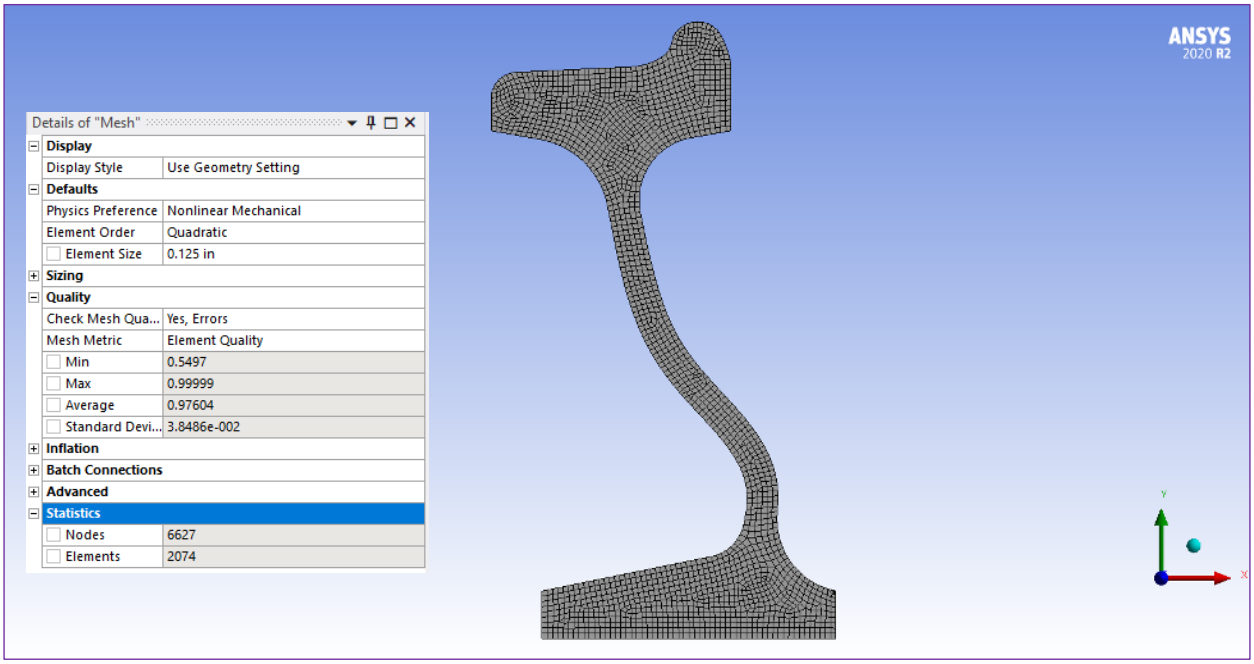

Figure 32. 2D Wheel Transient Thermal Model Computational Mesh

Figures 33–35 indicate the temperature results at the end of each transient thermal analysis load step. After reviewing the temperature results, the project team determined that the internal temperatures were not as low as desired after water quench step 2. They therefore decided to lengthen the duration of water quench from 165 to 180 seconds. The final wheel heat treatment process is shown in Table 3.

Table 3. Final 1.5-Inch Rim Thickness Wheel Heat Treatment Process

ANSYS Load Step	Heat Treatment Load Step Description	Load Step Duration (sec)	Total Duration (sec)
1	Initial uniform wheel temperature, 1600°F	15	15
2	Uniform water spray quench, tread running surface	165	180
3	Air cool, 25 minutes	1500	1,680
4	Annealing furnace 932°F, 3 hr	10,800	12,480
5	Air cool, 6 hr	21,600	34,080

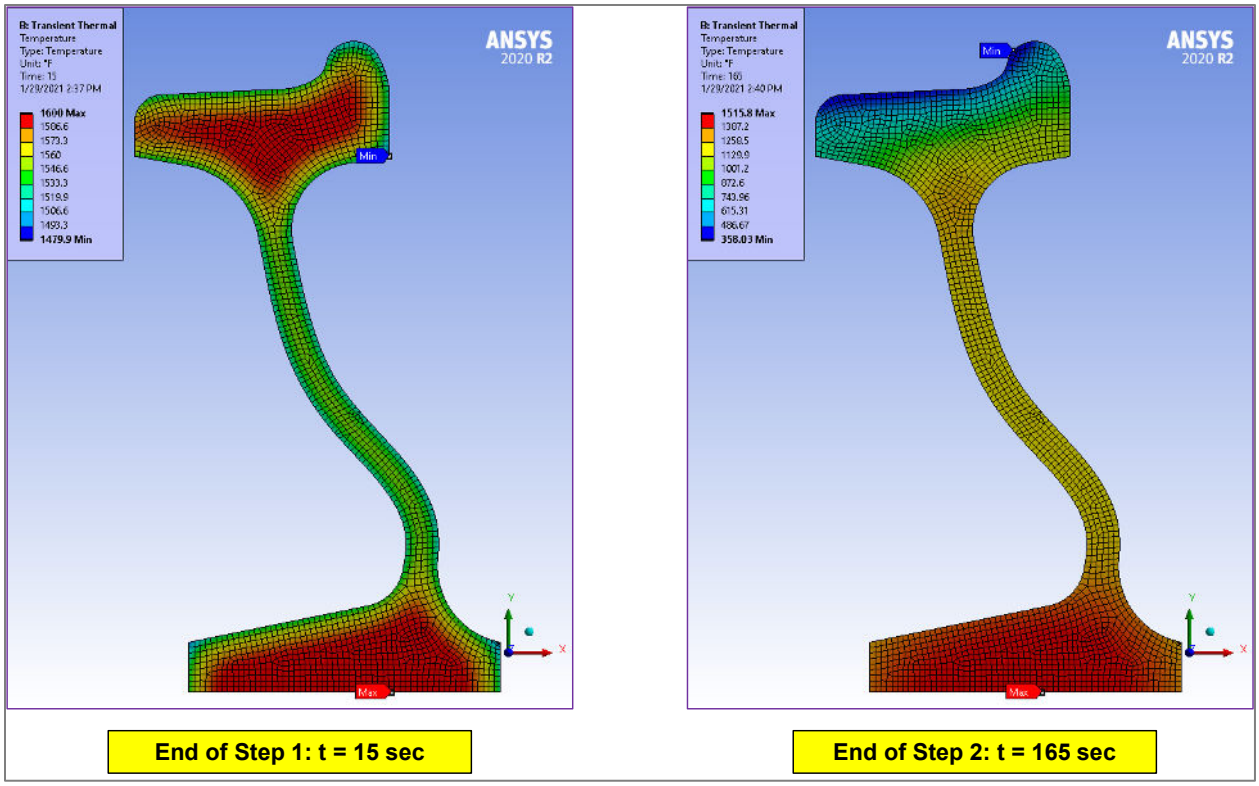

Figure 33. 2D Wheel Temperature Results: End of Steps 1 and 2

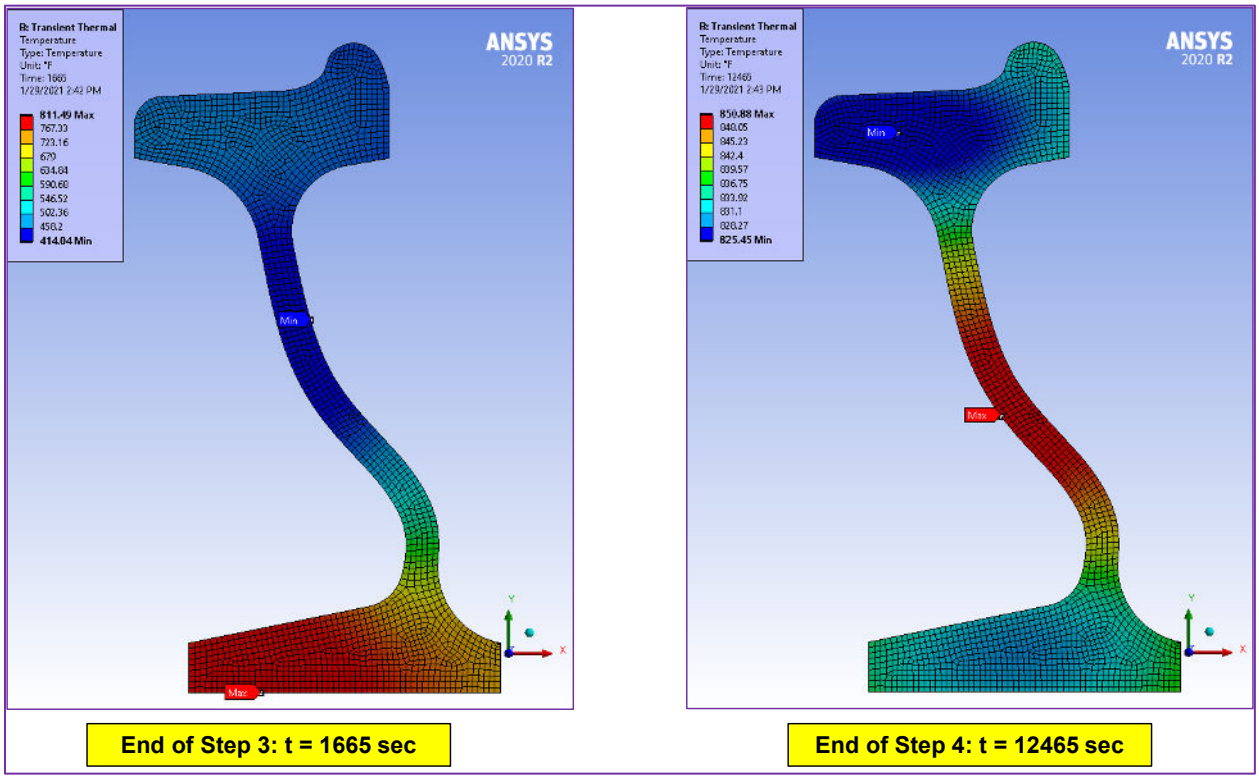

Figure 34. 2D Wheel Temperature Results: End of Steps 3 and 4

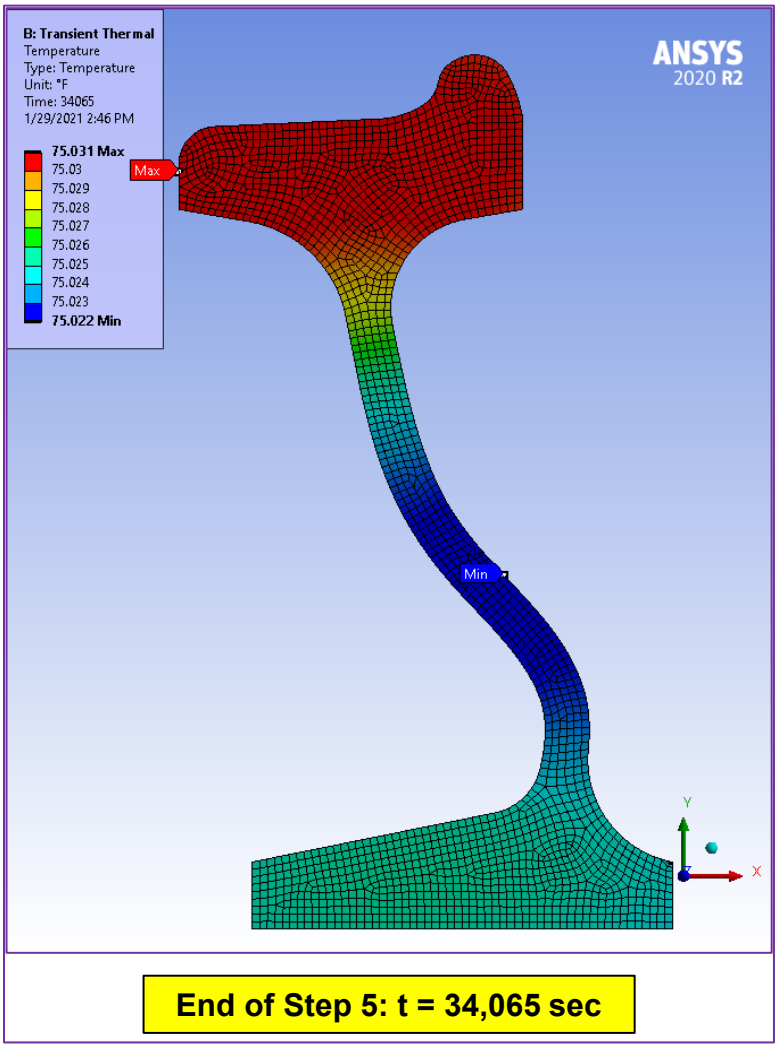

Figure 35. 2D Wheel Temperature Results: End of Step 5

The 2D wheel section was expanded to a 3D 15° sector model, and the final wheel heat treatment process in Table 3 was applied. Results at the end of steps 1 and 2 are shown in Figure 36 and Figure 37. The temperature results were transferred to a multi-step static structural analysis, and the model was solved to obtain thermal-stress results.

Figures 38–40 show the resulting hoop, radial, and axial residual stress components from the heat treatment process. There is significant compressive residual hoop stress at the tread surface as expected. The compressive residual stress also carries over to the front rim and flange. There is a sizeable pool of axial tensile residual stress below the tread surface.

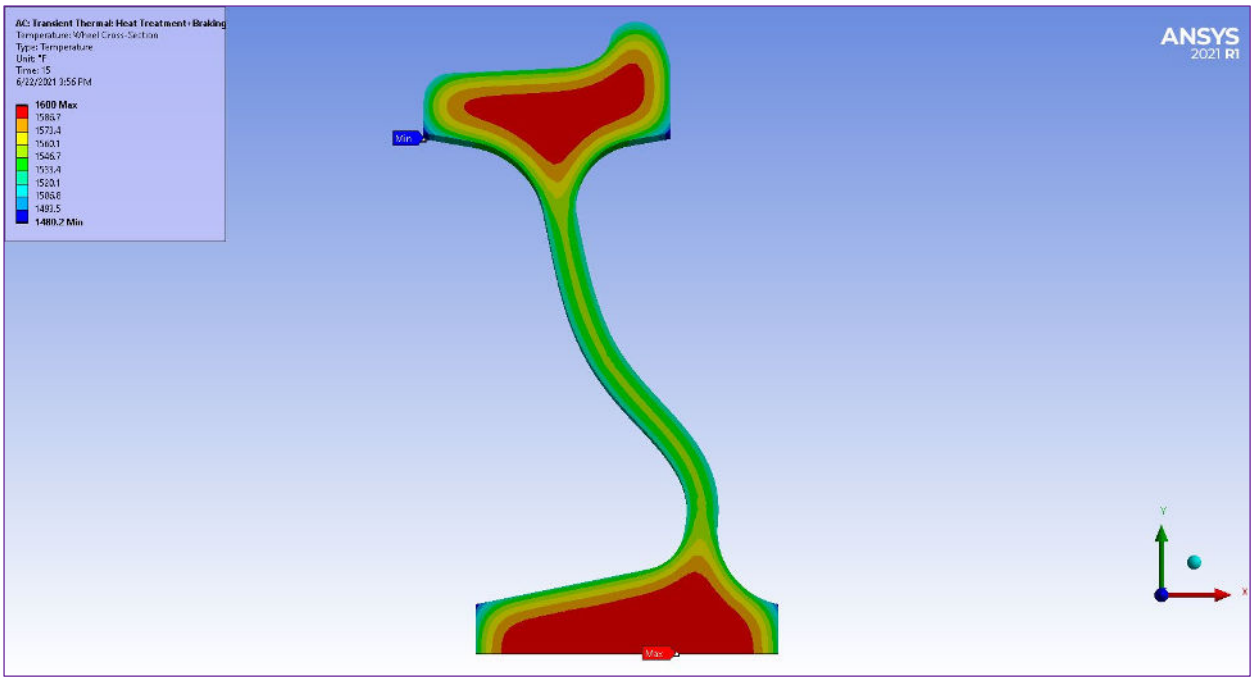

Figure 36. 3D Sector Temperature Results: End of Step 1 (t = 15 sec)

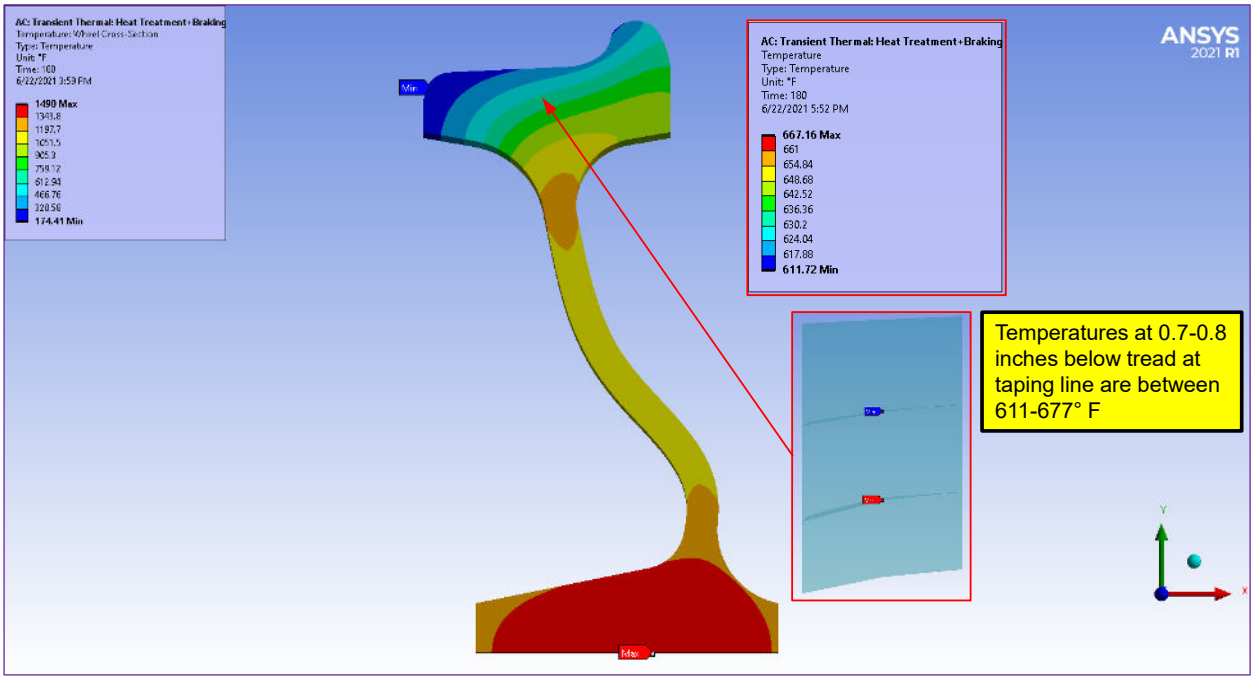

Figure 37. 3D Sector Temperature Results: End of Quench Step 2 (t = 180 sec)

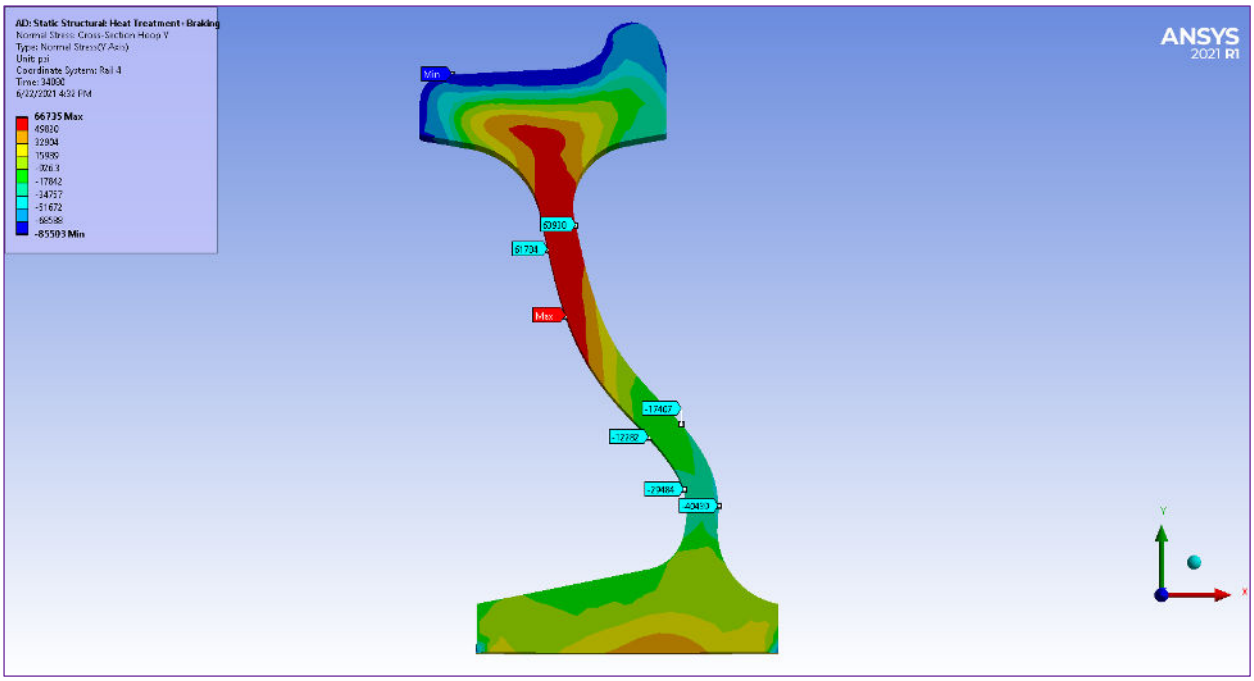

Figure 38. 3D Sector Model Hoop Stress Results

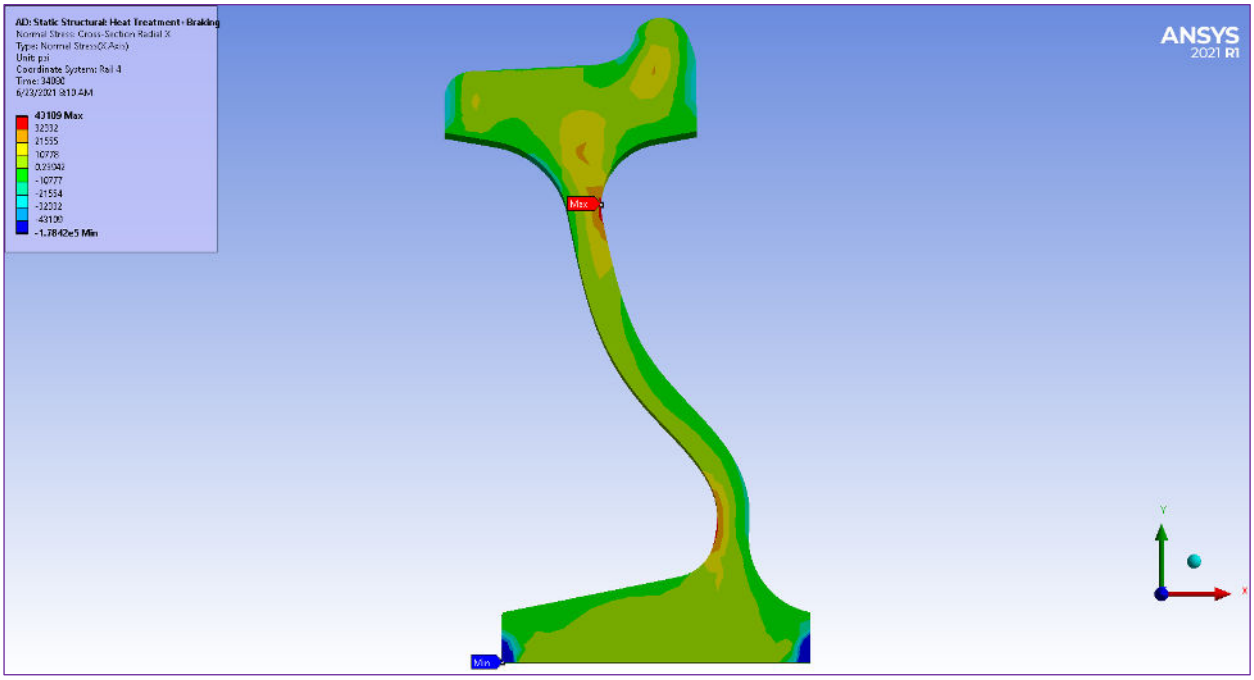

Figure 39. 3D Sector Model Radial Stress Results

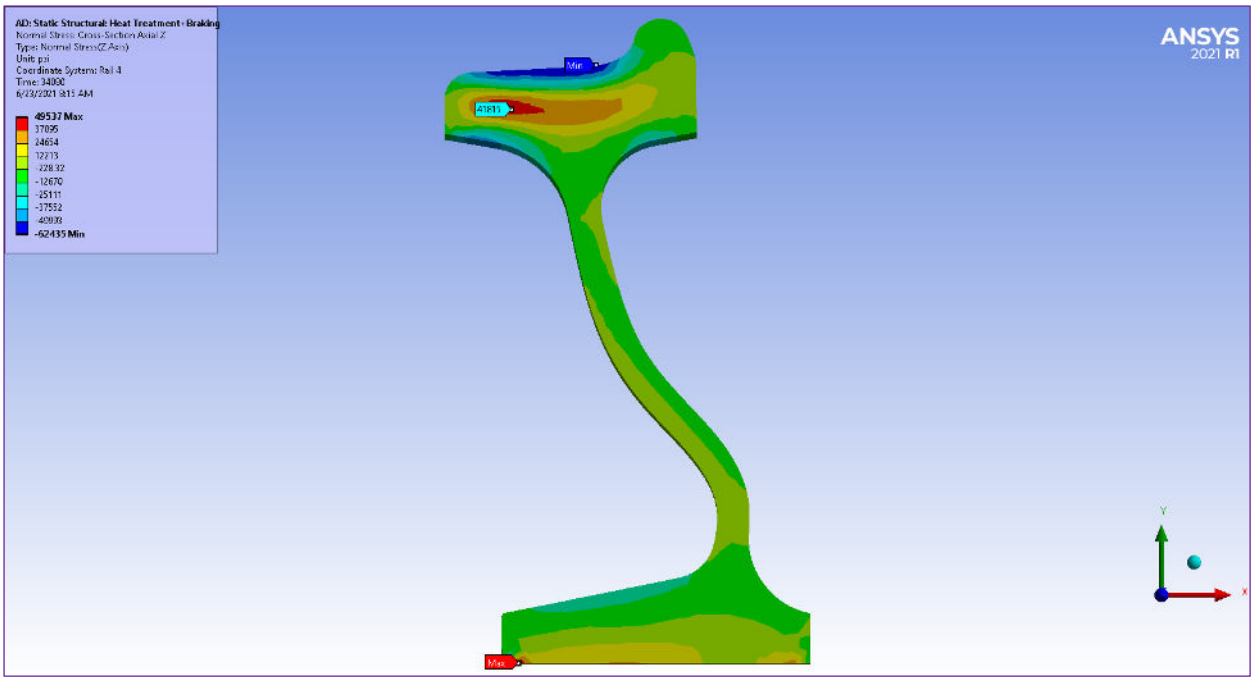

Figure 40. 3D Sector Model Axial Stress Results

3.8 Mechanical Loading

There are two types of mechanical loading. For the new 1.5-inch rim thickness wheel entering service, an initial series of normal loads was applied to the tread to generate cold work conditioning effects. After the cold work process, normal and tangential service loads were applied to the tread surface for wheel scenario analyses.

The magnitude of the normal load for both cold work and wheel scenario evaluations was 71,500 lbf, equivalent to two times the load from a 286,000 lbf rail car. Tangential load magnitude was half the normal load, or 35,750 lbf. The loads were applied at seven different sequential locations using an elliptical pressure distribution on the taping line. Figure 41 shows the progression of the elliptical pressure distribution from taping line positions 1 to 7.

The dimensions of the elliptical pressure area were derived using a Hertzian contact stress calculator, which required the material properties and radii of curvature of the wheel and rail, as well as the applied load. The major and minor radii of the ellipse were then calculated (Figure 42 and Figure 43). The elliptical pressure loading sequence is provided in Figure 44 in a top-down view of the tread surface.

Taping line diameter d = 35.966 in
radius r = d/2

Arc Length (in)	Angle (deg)
S	θ = (S/r)*(180°/π rad)
±1.5	4.779
±1.0	3.186
±0.5	1.593

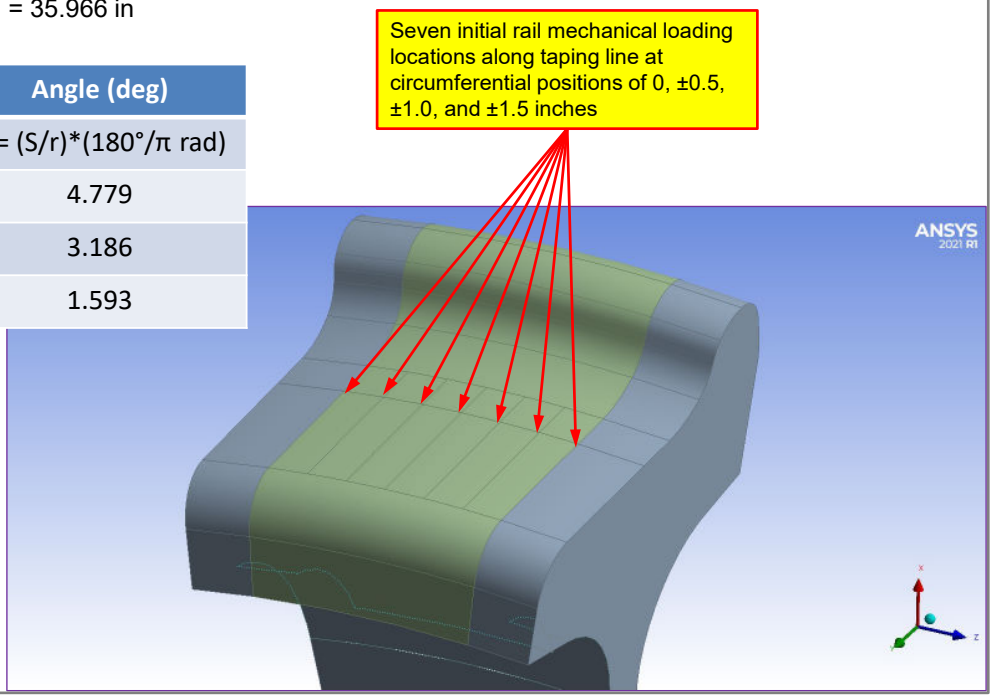

Figure 41. Taping Line Mechanical Loading Positions

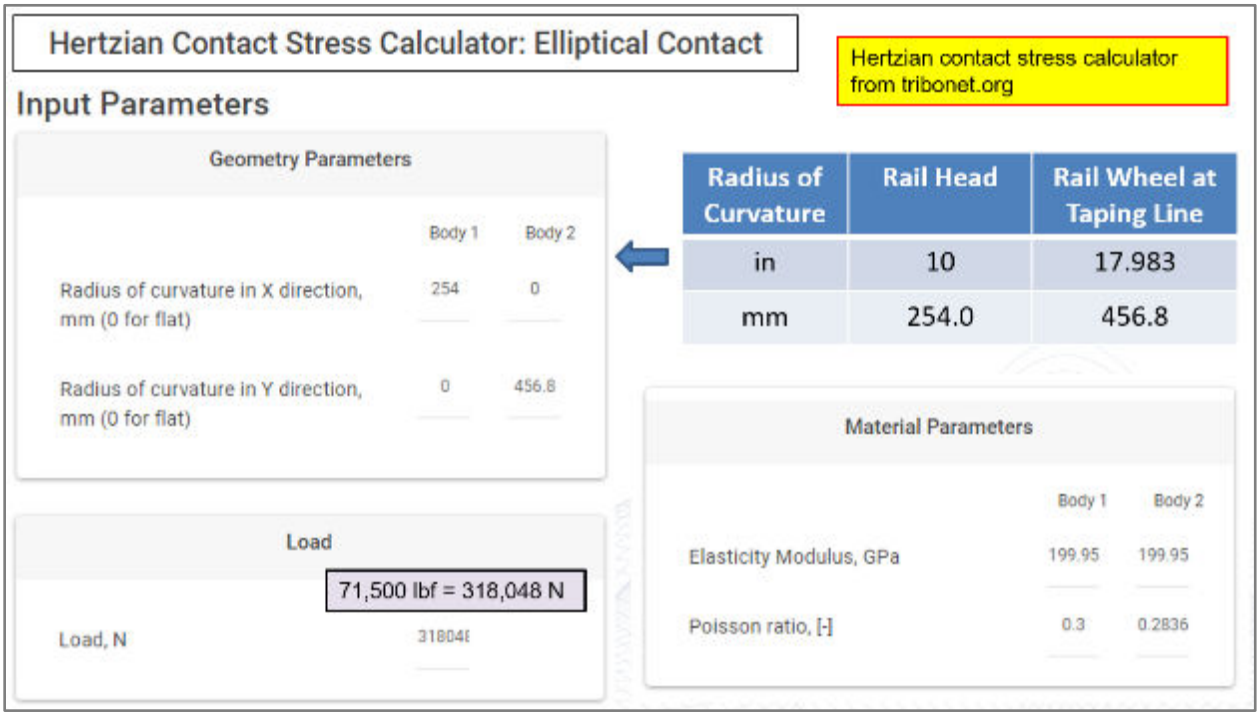

Radius of Curvature	Rail Head	Rail Wheel at Taping Line
in	10	17.983
mm	254.0	456.8

Figure 42. Hertzian Contact Stress Calculations

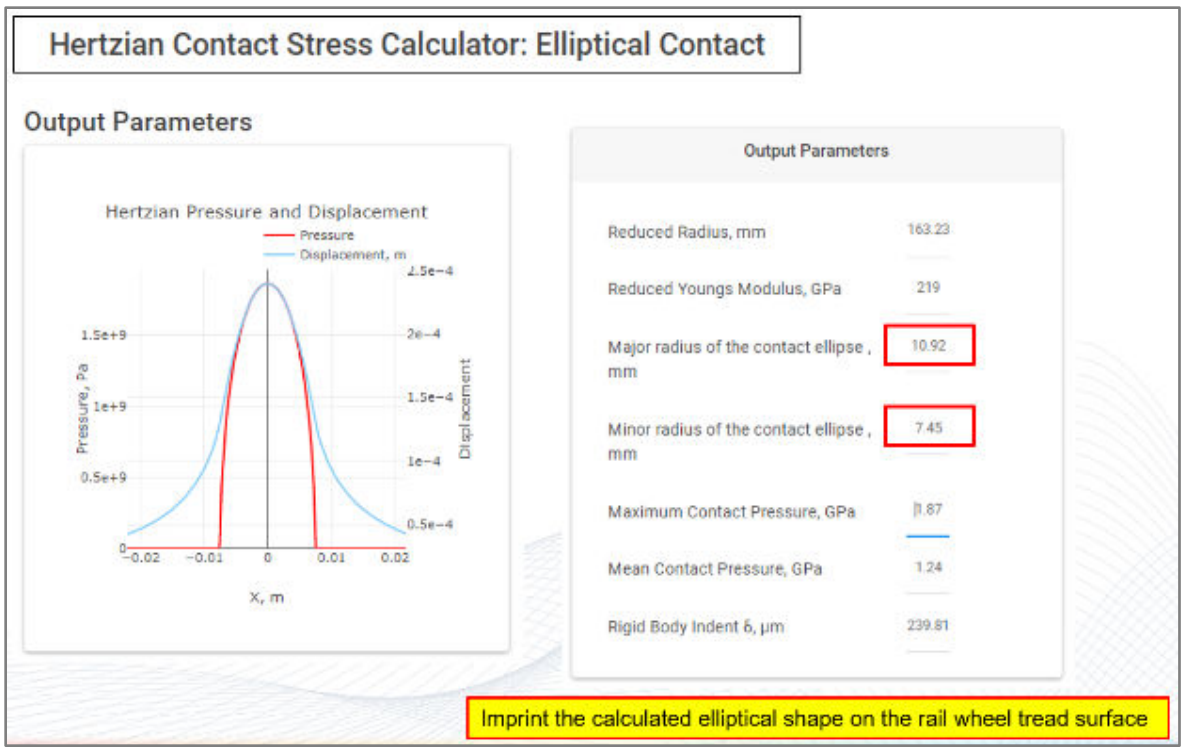

Figure 43. Hertzian Contact Stress Calculations (Continued)

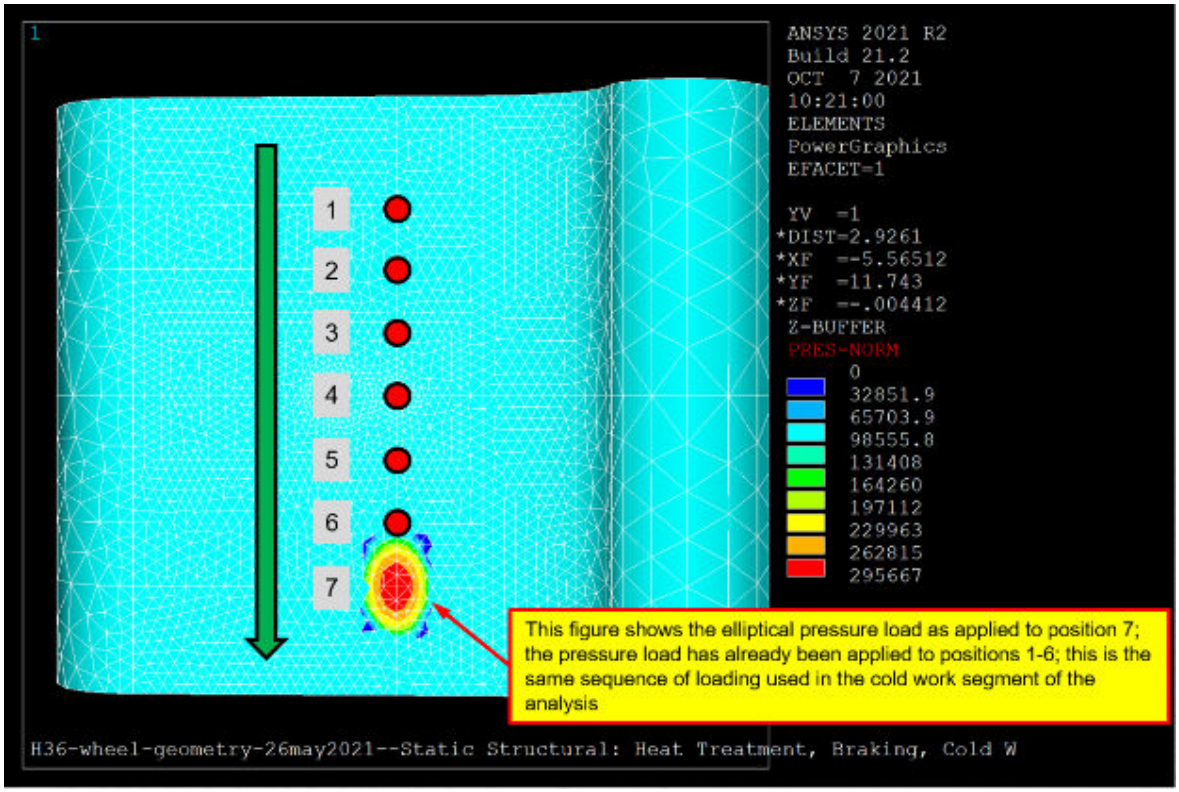

Figure 44. Elliptical Pressure Loading Sequence (1: first load application, 7: last, as depicted by the green arrow)

3.9 Effects of Braking

Three different levels of heat input due to braking were applied to the Stage II FEA model, depending on the wheel scenario. Figure 45, Figure 46, and Figure 47 illustrate the values used, from lowest heat input to highest. Braking heat loads were applied for a duration of 1200 seconds (20 minutes) in the transient thermal analysis. The developed temperature profile was applied to the structural model using data stored in the ANSYS thermal results file.

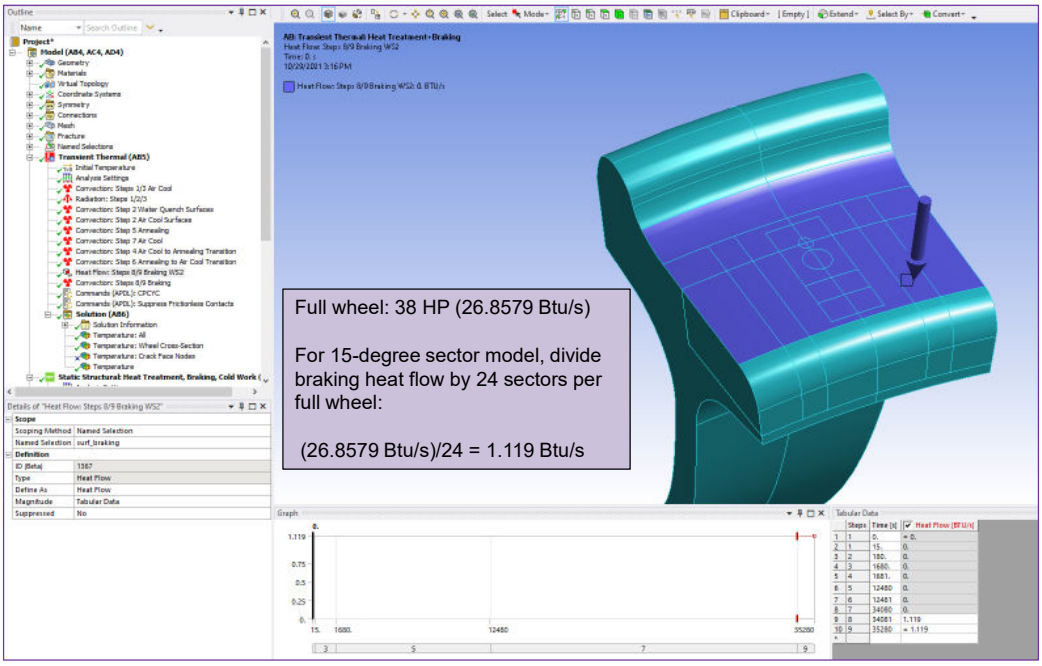

Figure 45. Stage II Model: Braking Heat Load Application (38 HP)

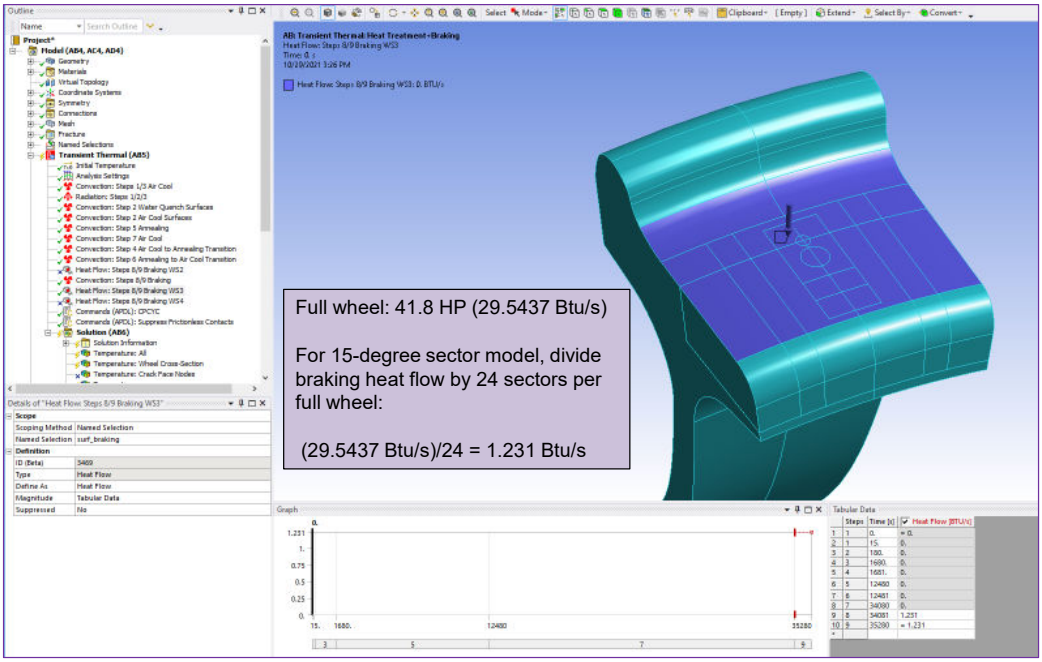

Figure 46. Stage II Model: Braking Heat Load Application (41.8 HP)

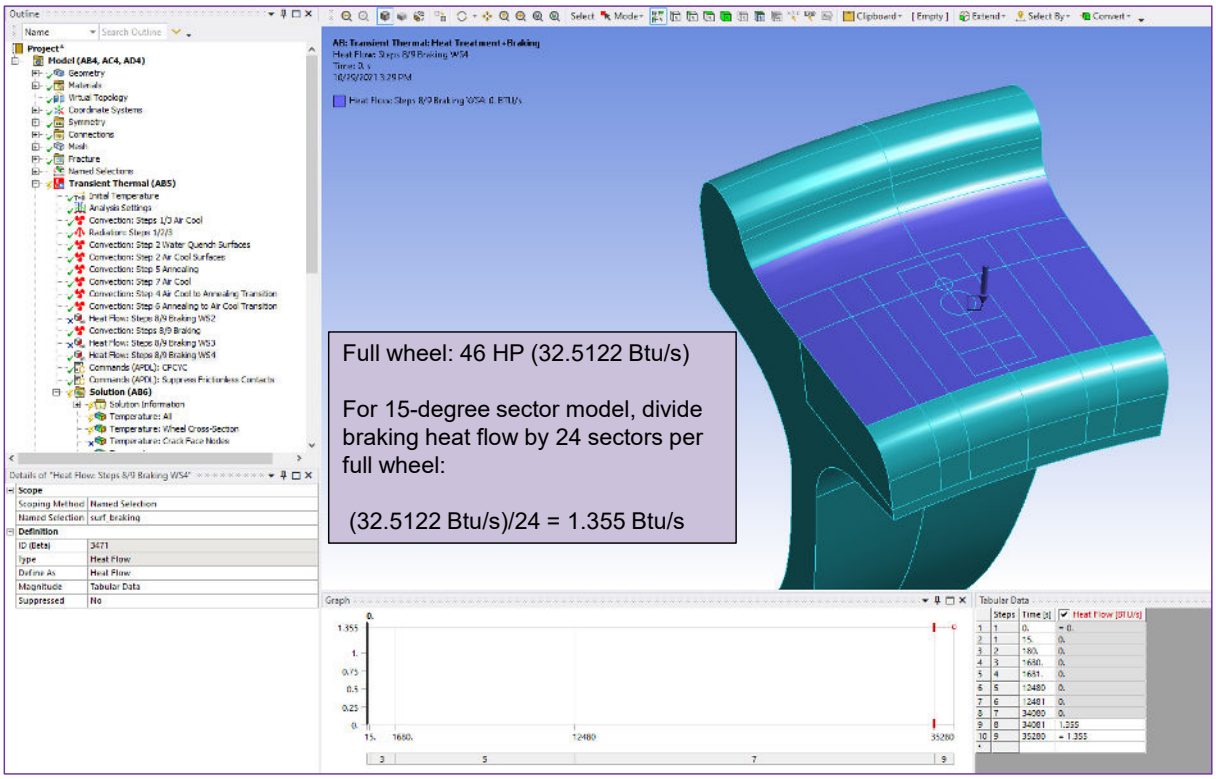

Figure 47. Stage II Model: Braking Heat Load Application (46 HP)

3.10 Analyzed Scenarios and Results

The research team analyzed thirteen wheel scenarios (WS; detailed description in Appendix A). A condensed summary is shown below in Table 4. During the project, the principal focus was on scenarios with only normal forces applied. This means that in addition to WS1, which investigates the effects of heat treatment and cold work without braking or mechanical forces, WS2–WS4 and WS8–WS10 were the primary analyses completed.

Table 4. Analysis Scenario Summary

Wheel Scenario	Rim Thickness (in)	Cracks Activated?	Braking Heat (HP)	Normal Force (kips)	Tangential Force (kips)	Analysis Completed?
WS1	New (1.5)	No	0	0	0	Yes
WS2	New (1.5)	Yes	38	71.5	0	Yes
WS3	New (1.5)	Yes	41.8	71.5	0	Yes
WS4	New (1.5)	Yes	46	71.5	0	Yes
WS5	New (1.5)	Yes	38	71.5	37.75	No
WS6	New (1.5)	Yes	41.8	71.5	37.75	No
WS7	New (1.5)	Yes	46	71.5	37.75	No
WS8	Worn (1.0)	Yes	38	71.5	0	Yes
WS9	Worn (1.0)	Yes	41.8	71.5	0	Yes
WS10	Worn (1.0)	Yes	46	71.5	0	Yes
WS11	Worn (1.0)	Yes	38	71.5	37.75	No
WS12	Worn (1.0)	Yes	41.8	71.5	37.75	No
WS13	Worn (1.0)	Yes	46	71.5	37.75	No

Additionally, the team attempted to complete WS11, which contained both normal and tangential forces; the tangential forces acted in the axial direction. Sampled J-integral values produced in this scenario were abnormally high and the project team had little confidence in the results. The effect of tangential forces was eventually excluded because a purely tangential force in rolling contact is unlikely unless a false flange condition exists. Phase 2 destructive testing of VSR failed wheels did not show a correlation to false flange conditions. Therefore, wheel scenarios WS5-WS7 and WS11-W13 were not analyzed.

3.10.1 WS1 Analysis Results Summary

For WS1, result items 2–4 show temperature gradients at specific times during the heat treatment process of the full rim thickness model and items 5–7 provide hoop, radial, and axial residual stress results. These items are documented in Section 3.7. Note that no mechanical forces have been applied in the results shown in Figure 48.

Result items 8–21 document the residual normal stress (hoop/radial/axial) and shear stress components at all seven cracks. Result item 22 shows the residual hoop/radial/axial stresses at the taping line center, from the tread surface to a depth of 0.5 inches. All results examined met the team's expectations. It should be reinforced that all cracks are inactive for WS1. For reference, result item 8 is shown below.

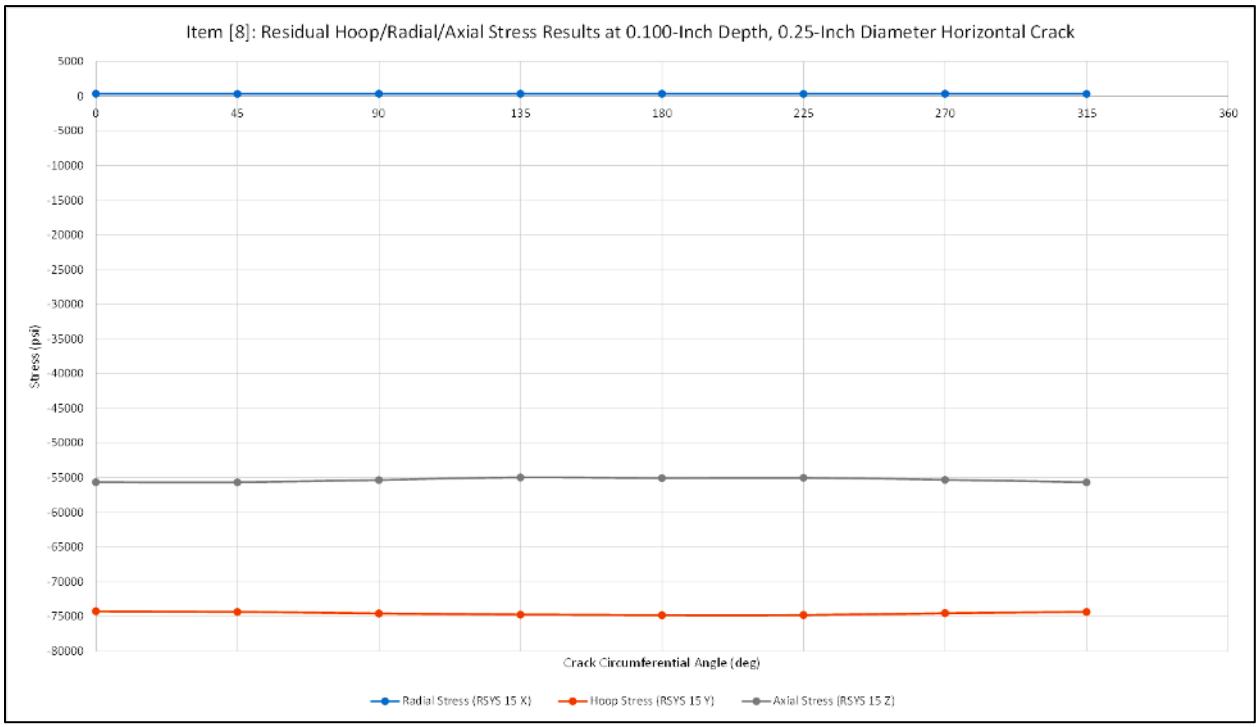

Figure 48. WS1 Result Item 8: Residual Hoop/Radial/Axial Stresses (HCRACK1)

3.10.2 WS2 Analysis Results Summary

Table 5 lists the result output items for WS2.

Table 5. WS2 Result Outputs

Result Items	Condition: Heat Treatment, No Cold Work, Cracks Inactive, 38 HP Braking (t_{end} = 35280 sec)
1	Temperature Gradient: T_{max} = 693.73° F
2-4	Normal Stress Components (Values?)
Result Items	**Condition: Heat Treatment, Cold Work, Cracks Inactive, 38 HP Braking (t_{end} = 35316 sec)**
5-6	Plastic Strain vs. Time, 0.050- and 0.100-Inch Depths Below Tread at Taping Line
7-8	Stress vs. Plastic Strain, 0.050- and 0.100-Inch Depths Below Tread at Taping Line
Result Items	**Condition: Heat Treatment, Cold Work, HCRACK1 Active, 38 HP Braking (t_{end} = 35324 sec)**
9-15	Normal Stress Components vs. Crack Circumferential Angle φ, Normal Contact Force Positions 1–7
16-22	Shear Stress Components vs. Crack Circumferential Angle φ, Normal Contact Force Positions 1–7
23-29	J-Integral vs. Crack Circumferential Angle φ, Normal Contact Force Positions 1–7
Result Items	**Condition: Heat Treatment, Cold Work, HCRACK4 Active, 38 HP Braking (t_{end} = 35324 sec)**
30-36	Same as Items 9–15
37-43	Same as Items 16–22
44-50	Same as Items 23–29
Result Items	**Condition: Heat Treatment, Cold Work, HCRACK2 Active, 38 HP Braking (t_{end} = 35324 sec)**
51-57	Same as Items 9–15
58-64	Same as Items 16–22
65-71	Same as Items 23–29
Result Items	**Condition: Heat Treatment, Cold Work, HCRACK5 Active, 38 HP Braking (t_{end} = 35324 sec)**
72-78	Same as Items 9–15
79-85	Same as Items 16–22
86-92	Same as Items 23–29
Result Items	**Condition: Heat Treatment, Cold Work, HCRACK3 Active, 38 HP Braking (t_{end} = 35324 sec)**
93-99	Same as Items 9–15
100-106	Same as Items 16–22
107-113	Same as Items 23–29
Result Items	**Condition: Heat Treatment, Cold Work, HCRACK6 Active, 38 HP Braking (t_{end} = 35324 sec)**
114-120	Same as Items 9–15
121-127	Same as Items 16–22
128-134	Same as Items 23–29
Result Items	**Condition: Heat Treatment, Cold Work, VCRACK1 Active, 38 HP Braking (t_{end} = 35324 sec)**
135-141	Same as Items 9–15
142-148	Same as Items 16–22
149-155	Same as Items 23–29

3.10.3 WS3, WS4, WS8 & WS10 Analysis Results

Section 4 consists of the most relevant results from the simulation.

3.11 Validation Exercises

Before the four-step model validation process was performed towards the end of the project, the model underwent several refinements of the elements mesh. All validation exercises showed the expected results, and the details are outlined in the appendices.

3.11.1 AAR MSRP S-660 Stress Check

Stress checks were performed on a full 3D model of the rail wheel per AAR MSRP S-660 [9]. See Appendix B for details.

3.11.2 Result Symmetry Check

A model check was conducted to determine the effect of heat treatment, cold work, crack activation, and normal load application positions on the symmetry behavior of stress results at 45° intervals around the crack circumference. See Appendix C for details.

3.11.3 Stress-Free Wheel

A model check was performed to verify that a stress-free wheel produced J-integral values equal to zero around the crack circumference. See Appendix D for details.

3.11.4 Mesh Sensitivity

A mesh sensitivity study was conducted to determine the effect on crack results. See Appendix E for details.

3.12 Additional Outputs

Analysis of fracture mechanics results was undertaken to predict the direction of crack propagation. This report section details the assumptions and calculations performed.

3.12.1 Crack Turn-In Prediction

The focus of the crack turn-in prediction was on HCRACK2 and HCRACK5, which are the cracks located at a depth of 0.2 inches from the tread surface. HCRACK2 lies on the taping line. See Figure 49.

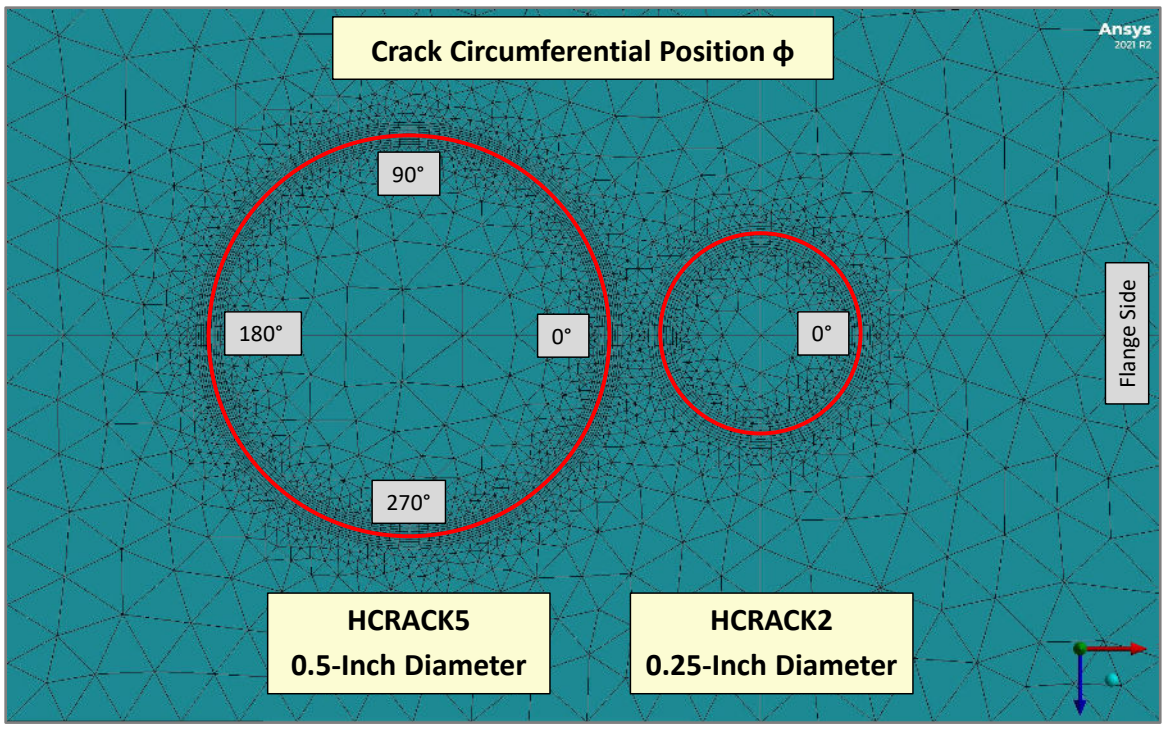

Figure 49. Cracks Located 0.2 Inches Below Tread Surface

The relationship between J-Integral, Energy Release Rate (G), and Stress Intensity Factor (SIF, or Fracture Toughness) K for fracture Modes I, II, and III is as follows, with the indicated assumptions:

- Material is isotropic, linear elastic, and plane strain applies.
- The crack extends straight ahead with respect to its original orientation.
- E = elastic modulus, ν = Poisson's ratio

$$J_{IC} = G_{IC} = K_{IC}^2\left(\frac{1-\vartheta^2}{E}\right)$$
$$J_{IIC} = G_{IIC} = K_{IIC}^2\left(\frac{1-\vartheta^2}{E}\right)$$
$$J_{IIIC} = G_{IIIC} = K_{IIIC}^2\left(\frac{1\mp\vartheta}{E}\right)$$

The critical Mode I J-Integral value (J_{IC}) for this railroad wheel steel alloy is 45 psi-inch. The critical mode I Fracture Toughness (K_{IC}) is therefore:

$$K_{IC} = \left[\frac{J_{IC}E}{1-\vartheta^2}\right]^{1/2} = \left[\frac{(45\ psi-in)(30E6\ psi)}{1-(0.3)^2}\right]^{1/2} = 38{,}516\ psi-in^{1/2}$$

There are several methods that can be used to predict crack propagation direction:

- T-Stress Results (Scalar)
  - T-stress is related to crack path stability.

- T < 0: Straight crack path stable
- T > 0: Straight crack path unstable (deviation from straight path)
- Use T-Stress results to identify preferential crack locations which may turn and deviate from a straight path.
- While T-stress is a readily available result from an ANSYS fracture mechanics solution, some references have called into question the accuracy of T-Stress predictions.

- Mode I and Mode II Stress-Intensity Factor Results
  - The ratio of Mode I (K_I) and Mode II (K_{II}) SIF results can predict the crack propagation angle θ.
  - Meggiolaro, et al. [10] have proposed the relationship, as shown in the equation below and Figure 50.

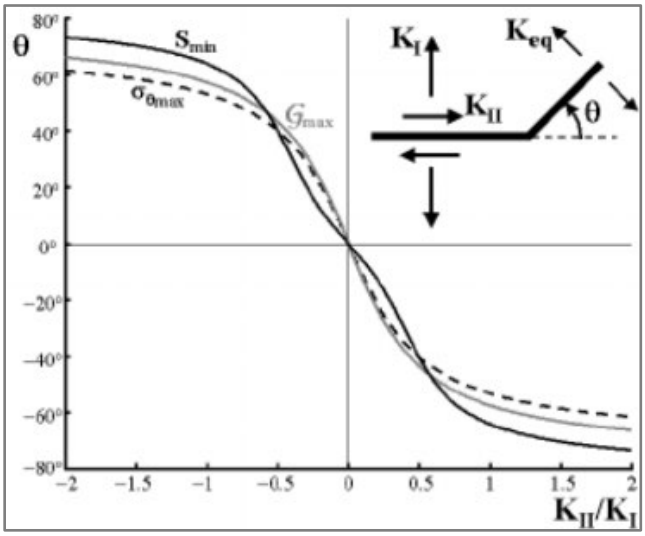

Figure 50. Crack Propagation Angle θ Prediction

  - From the equation, the crack propagation angle θ will have a positive or negative sense.
  - Figure 51 illustrates a representative volume element in the wheel with a crack; both normal and shear stress components are indicated, as well as four major crack circumferential positions (φ = 0°, 90°, 180°, and 270°).
  - At crack positions 0° and 180°, the primary shear stress component of interest is τ_{rz}.
  - At crack positions 90° and 270°, the primary shear stress component of interest is $\tau_{r\theta}$.
  - By the right-hand rule, $+\tau_{rz}$ or $+\tau_{r\theta}$ would cause the crack to turn downward toward the hub; negative values would cause the crack to turn upward toward the tread.

$$\theta_0'' = 2\arctan\left(\frac{1}{4}\frac{K_I}{K_{II}} \pm \frac{1}{4}\sqrt{\left(\frac{K_I}{K_{II}}\right)^2 + 8}\right)$$

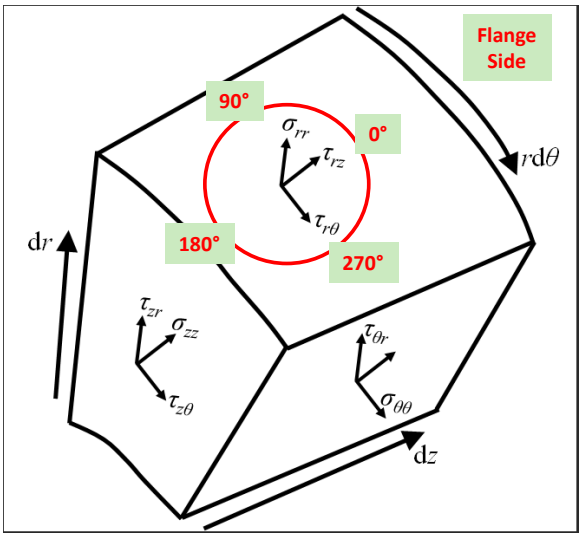

Figure 51. Volume Element Normal and Shear Stress Components, Cylindrical Coordinate System

- Principal Stresses and Direction Cosines
  - This method is more difficult to visualize and will therefore not be used.

Crack propagation direction results for HCRACK2 are shown in Table 6, with five different combinations of conditions considered. The research team is particularly interested to understand under what conditions the crack at φ = 180° (which points toward the rim) turns down toward the hub. Results show that conditions 4 and 5 induced downward turning of HCRACK2 (with the normal load at position 3) and had the highest braking heat input from WS10, causing the most pronounced effect. Note also that HCRACK2 lies directly under the taping line.

Table 6. HCRACK2 Propagation Results

Condition	**Crack Circum. Position φ (deg)**	**K_{II}/K_I Ratio**	**Crack Propagation Angle θ** [10]	**Crack Propagation Direction**
1. After Crack Activation	0	3.51	-65.19	UP
	90	0.60	-44.13	UP
	180	3.34	-64.93	UP
	270	-0.83	+50.13	DOWN
2. After WS8 Braking Heat Load	0	4.31	-66.17	UP
	90	0.73	-47.89	UP
	180	4.00	-65.83	UP
	270	-0.97	+52.73	DOWN
3. After WS10 Braking Heat Load	0	4.87	-66.66	UP
	90	0.88	-51.11	UP
	180	4.04	-65.88	UP
	270	-0.96	+52.44	DOWN

Condition	Crack Circum. Position φ (deg)	K_{II}/K_I Ratio	Crack Propagation Angle θ [10]	Crack Propagation Direction
4. After WS8 Braking Heat Load + Normal Load Position 3	0	0.29	-28.72	UP
	90	1.22	-56.01	UP
	180	-0.08	+8.89	DOWN
	270	-19.93	+69.57	DOWN
5. After WS10 Braking Heat Load + Normal Load Position 3	0	0.02	-2.21	UP
	90	1.43	-57.94	UP
	180	-0.53	+41.38	DOWN
	270	-13.64	+69.13	DOWN

Crack propagation direction results for HCRACK5 are shown in Table 7, with the same five combinations of conditions considered. The results are considerably different than the results for HCRACK2 because HCRACK5 is further from the taping line and is only marginally exposed to the normal load at position 3.

Table 7. HCRACK5 Propagation Direction Results

Condition	Crack Circum. Position φ (deg)	K_{II}/K_I Ratio	Crack Propagation Angle θ (deg) [10] [4]	Crack Propagation Direction
1. After Crack Activation	0	1.91	-60.95	UP
	90	0.09	-10.12	UP
	180	0.46	-38.44	UP
	270	-0.10	+11.01	DOWN
2. After WS8 Braking Heat Load	0	1.36	-57.36	UP
	90	0.03	-3.60	UP
	180	0.34	-31.81	UP
	270	-0.13	+14.84	DOWN
3. After WS10 Braking Heat Load	0	1.21	-55.85	UP
	90	-0.002	+0.23	DOWN
	180	0.41	-35.98	UP
	270	-0.15	+16.60	DOWN
4. After WS8 Braking Heat Load + Normal Load Position 3	0	1.08	-54.30	UP
	90	14.48	-69.21	UP
	180	1.29	-56.67	UP
	270	0.43	-36.84	UP
5. After WS10 Braking Heat Load + Normal Load Position 3	0	1.50	-58.49	UP
	90	2.13	-61.88	UP
	180	1.12	-54.84	UP
	270	0.43	-37.14	UP

4. Analyses of the Results

The analysis methodology focused on establishing correlations for all physical characteristics to identify the dominant contributors. The first step was to identify the wealth of data produced by the simulations, maximum values for stresses (radial, hoop, axial, and shear), and J-integral. These data were evaluated after each step of the simulation (heat treatment, cold work, crack activation, and heat load) for each crack. The next step was to calculate the Pearson Correlation Coefficient [11] for each stress component in terms of depth, size, and position of the cracks. Each step of the simulation was isolated in a way that the correlation illustrates the level of influence of each factor.

The research team compared wheel scenarios 8 and 10: both had worn wheels, but the brake load was 38 HP for WS8 and was 46 HP for WS 10. For WS8, in crack 2, position 3, only 21 of the J-integral results were larger than 45 psi-in$^{1/2}$. For WS10, the number of results exceeding 45 psi-in$^{1/2}$ increased to 28, which is a strong indicator of the influence of heat. These results are shown in Table 8. This value is the equivalent to the critical mode I SIF (fracture toughness) value of 38.5 ksi-in$^{1/2}$.

Table 8. Exceedences above 45 psi-in$^{1/2}$ for WS8 and WS10

	Position / Exceedences above 45 psi-in$^{1/2}$							Distance	J-Int Max	
Scenario 8	1	2	3	4	5	6	7			
Crack1	0	0	10	24	1	0	0	0.164	295.25	
Crack2	0	0	21	26	1	0	0	0.241	191.57	
Crack3	1	1	1	0	0	0	0	0.521	71.83	
Crack4	3	3	3	14	8	6	6	0.7	148.23	
Crack5	2	2	2	6	1	2	2	0.725	76.9	
Crack6	0	0	0	1	1	0	0	0.87	49.2	
Crack7	0	0	0	0	0	0	0	1.577	2.98	
Crack5	2	2	2	7	1	2	2	0.725	76.17	
Scenario 10									S10 J-Int Max	S8 J-Int Max
Crack2	0	0	28	25	1	0	0	0.241	241.84	191.57
Crack5	2	2	2	8	0	1	1	0.725	220.06	76.89

Table 9: Correlations found in the analyses

Correlations	Radial	Hoop	Axial	Shear	J-Int
By Depth	0.33	**0.98**	-0.03	0.43	**0.80**
By Size	-0.68	-0.19	-0.02	-0.73	**-0.81**
By Distance	**0.96**	**0.96**	**0.90**	-0.30	**-0.86**

[1] *The correlations are computed after applying brake heat and mechanical loading.*
[2] *Mechanical load position at centerline of cracks (position 4 – see Figure 5.)*
[3] *Perfect correlations would be 1 or -1.*
[4] *Positive correlations have direct relationship to the measured result.*
[5] *Negatives indicate an inverse relationship.*

Table 9 depicts further progress in the analyses, which included the isolation of correlations excluding the only vertical crack in the model, which behaves in its own peculiar form. Correlations that only include horizontal cracks are even stronger.

Analysis of SIF results was undertaken to predict the direction of crack propagation. The approach from Meggiolaro, et al. [10] was used to determine whether the crack turned up toward the tread, or more importantly, down toward the hub, indicative of VSR behavior. A significant relationship was detected between both braking heat input and position of the normal load relative to the crack. The crack circumferential position closest to the front rim was found to turn downward and was more pronounced with higher heat input.

5. Conclusions and Recommendations

This section summarizes conclusions from phase 3 of the wheel failure study and provides potential mitigation strategies to reduce the incidence of VSRs and recommendations for further investigations.

The research team aimed to answer the following questions in Phase 3 of the project:

1. What are the major factors that cause subsurface cracks to turn towards the surface of the rim?
2. What are the relative roles of contact mechanics and operating conditions in the development of VSR, including the development of thermal stresses in the wheel?
3. Given what the team learned from this FEA and historical research, what information can industry collect to identify conditions that could be indicators of at-risk wheels, either presently or in the future?

The team drew the following conclusions from the efforts conducted under phase 3 and prior research activities:

1. The likelihood of a VSR increases with increased brake heating. Without brake heating, the probability of a VSR is diminished.
2. In order of importance, the contributing factors to the development of a VSR are brake heating, subsurface crack size, and distance from the tread contact point with the rail to the crack tip.
3. A very large percentage of subsurface cracks will break out to the tread, creating an out-of-round condition and high impact readings from wayside detectors. Those which turn away from the tread (and generate a VSR) need high thermal gradients to generate the thermal stresses necessary to drive crack growth thermal stresses.
4. Manufacturing residual compressive stresses prevents the subsurface crack from breaking out to the front rim face, instead forcing a crack path to the rim inner diameter.
5. Wheel-rail contact loads cause crack initiation (likely in the presence of some material anomaly) and propagation. The larger the crack gets, the less important wheel-rail contact becomes, since the distance to the crack tip gets larger, and stresses decrease.
6. Unstable crack growth occurs when the crack tip progresses away from the tread surface and into a tensile residual stress pool resulting from manufacturing residual stresses due to heat treatment.

The following recommendations to prevent and/or mitigate the formation of VSRs are under discussion with the industry:

1. Improve microcleanliness. Based on the information from the investigation, cleaner steel will minimize the formation of subsurface cracks. Almost all VSRs initiate from a subsurface crack which typically begins at a material anomaly.
2. Improve fracture toughness by altering steelmaking practice (lower sulfur, alter deoxidation, etc.) Consider microalloying to improve yield strength and fracture toughness.

3. Alter heat treatment processes to reduce compressive hoop stresses at front rim faces. The compressive stress prevents the crack from breaking out to the front face, thereby promoting the turn-in of the crack. Although this will not eliminate shelling of the tread, it will likely reduce the possibility of a VSR.
4. Test to a tighter ultrasonic standard, aiming to find more defects that could potentially evolve into a VSR.
5. Tighten the upper limit range of carbon content without sacrificing wear resistance.
6. Improve braking systems to prevent failures and avoid extremely high temperature events in wheels.

6. References

[1] Dick, M., Sundaram, N., and Sherrock, E., "Wheel Failure Investigation Program: Phase 1," U.S. Department of Transportation, Federal Railroad Administration, Washington, D.C., Technical Report No. DOT/FRA/ORD-21/04, 2020.

[2] S. Chrismer, E. Sherrock, D. Stone, and A. Alvarez-Reyes, "Wheel Failure Investigation Program: Phase 2," U.S. Department of Transportation, Federal Railroad Administration, Washington, DC, DOT/FRA/ORD-21/36, 2021.

[3] C. Lonsdale, T. Rusin, and T. Hay, "Research to Understand the Effects of Wheel Impact Loads on Wheel Stress Levels," in *Proceedings of the 2009 ASME Joint Rail Conference*, Pueblo, CO, 2009.

[4] Lonsdale, C. and Oliver, J., "Wheel Rim Axial Residual Stresses and a Proposed Mechanism for Vertical Split Rims," in *Proceedings of ASME 2011 Rail Transportation Division Fall Technical Conference*, New York City, NY, 2011.

[5] H. Tournay and K. Jones, "Investigation: Root Causes of Vertical Split Rim Wheel Failures," in *Association of American Railroads 21st Annual Research Review*, Pueblo, CO, 2016.

[6] D. H. Stone and S. L. Dedmon, "Crack Growth Rates of Vertical Split Rim Wheel Fractures," in *Joint Rail Conference*, New York City, NY, 2017.

[7] S. L. Demdon, D. H. Stone, and H. Guzel, "Development of tread cracks in class c wheels," in *International Heavy Haul Association*, Calgary, Alberta, Canada, 2011.

[8] T. Hiroshi, Paris, P. C., and Irwin, G. R., "The stress analysis of cracks handbook", The American Society of Mechanical Engineers, New York City, NY, 2000.

[9] The Association of American Railroads, "Manual of Standards and Recommended Practices", Washington, D.C., 2022.

[10] M. A. Meggiolaro, A. O. Miranda, J. P. Castro, and L. F. Martha, "Bifurcated fatigue crack path and life predicitions," *Mechanics of Solids in Brazil*, Brazilian Society of Mechanical Sciences and Engineering, pp. 329-340.

[11] M.T. Puth, M. Neuhäuser, and G. D. Ruxton, "Effective use of Pearson's product-moment correlation coefficient," *Animal Behaviour,* vol. 93, pp. 183-189, ISSN 0003-3472, 2014.

Appendix A: Stage II Railroad Wheel – Scenarios to be Analyzed

This appendix contains details of the 13 Stage II scenarios to be analyzed.

Scenario 1	New Rim Thickness, No Cracks, No Braking, No External Forces	
Rim Thickness	1-1/2"	
Heat Treatment	Yes	
Braking	None	
Rolling Contact Condition	None	
Total No. of Simulations:	4	
Case Number	Time After Leaving Furnace	No. of Illustrations
1-1	10 seconds after leaving furnace	1
1-2	just before quenching	1
1-3	just after quenching	1
1-4	at end of cool down	19
Thermal Data Product(s) Cases 1-1 through 1-4	(1) 2D temperature gradient of the wheel radial cross section at time intervals described above (Total of 4 Illustrations for Cases 1-1 through 1-4).	
Structural Data Products Case 1-4	(1)Resulting hoop, radial and axial residual stress contour plots of the new 1-1/2" rim thickness radial cross section at the end of heat treatment cool down (Total of 3 Illustrations for Case 1-4). (2) The final residual hoop, radial, axial stresses (on one graph) and final residual shear stress (on one graph) at nodes 45-degrees apart around the circumference of where the 0.100-inch deep 0.25-inch and 0.50-inch diameter embedded cracks will be; note that the cracks will not actually be present in this model. (Total of 4 Illustrations for Case 1-4). (3) The final residual hoop, radial, axial stresses (on one graph) and final residual shear stress (on one graph) at nodes 45-degrees apart around the circumference of where the 0.200-inch deep 0.25-inch and 0.50-inch diameter embedded cracks will be; note that the cracks will not actually be present in this model. (Total of 4 Illustrations for Case 1-4). (4) The final residual hoop, radial, axial stresses (on one graph) and final residual shear stress (on one graph) at nodes 45-degrees apart around the circumference of where the 0.500-inch deep 0.25-inch and 0.50-inch diameter embedded cracks will be; note that the cracks will not actually be present in this model. (Total of 4 Illustrations for Case 1-4). ((4) The final residual hoop, radial, axial stresses (on one graph) and final residual shear stress (on one graph) at nodes 45-degrees apart around the circumference of where the vertical embedded crack will be; note that the crack will not actually be present in this model. (Total of 2 Illustration for Case 1-4). (3) Resulting hoop, axial and radial stress vs. depth of a line of nodes located at the taping line to a depth of 0.50" to quantify the results of heat treatment (1 Illustration for Case 1-4).	
	Total Anticipated Number of Illustrations/Graphs	22

Scenario 2	New Rim Thickness with Cracks, 38 HP Braking, Normal Force			
Rim Thickness	1-1/2"			
Heat Treatment	Yes			
Braking	38 HP			
Rolling Contact Condition	Normal Force = 71.5K			
Total No. of Simulations:	7			
Case Number	Lateral Crack Diameter(s)	Crack Depth	Vertical Crack	No. of Graphs
2-1	0.25"	0.100"	-	21
2-2	0.25" + 0.50"	0.100"	-	21
2-3	0.25"	0.200"	-	21
2-4	0.25" + 0.50"	0.200"	-	21
2-5	0.25"	0.500"	-	21
2-6	0.25" + 0.50"	0.500"	-	21
2-7	-	-	0.50"	21
Thermal Data Products - Once per Scenario	(1) 2D temperature gradient of the wheel radial cross section 20 minutes after 38 HP braking heat flux has been applied to the tread.			1
Structural Data Products Once Per Scenario	(1) Resulting hoop, radial and axial residual stress contour plots of the new 1-1/2" rim thickness radial cross section due to the combined effects of heat treatment and tread braking energy input before applying the distributed load (to simulate cold work) and before bringing the cracks into existence (Total of 3 Illustrations for This Scenario). (2) Graph of plastic strain vs. time after contact loads have been applied but before cracks have been introduced to determine when the material is cold worked at nodes located 0.050 [in] and 0.100 [in] below the tread at the taping line; it is assumed that ~5 time steps will be required (Total of 2 Illustrations for This Scenario). (3) Graph stress vs. plastic strain after contact loads have been applied but before cracks have been introduced to determine when the material is cold worked at nodes located 0.050 [in] and 0.100 [in] below the tread at the taping line (Total of 2 Illustrations for This Scenario)			7
Structural Data Products Required for Each Case	(1) For each crack configuration and seven contact force positions, graph the resultant 3 normal stresses vs. theta (on one graph with different colors) and 3 shear stresses vs. theta (all three shears on one graph with different colors) around the largest embedded crack, resulting in two separate illustrations for each of the seven contact force positions. (2) For each crack configuration and seven contact force positions, graph J-integral vs. theta around the largest embedded crack.			See Above
	Total Anticipated Number of Illustrations/Graphs			155

Scenario 3	New Rim Thickness with Cracks, 41.8 HP Braking, Normal Force			
Rim Thickness	1-1/2"			
Heat Treatment	Yes			
Braking	41.8			
Rolling Contact Condition	Normal Force = 71.5K			
Total No. of Simulations:	7			
Case Number	Lateral Crack Diameter(s)	Crack Depth	Vertical Crack	No. of Graphs
3-1	0.25"	0.100"	-	21
3-2	0.25" + 0.50"	0.100"	-	21
3-3	0.25"	0.200"	-	21
3-4	0.25" + 0.50"	0.200"	-	21
3-5	0.25"	0.500"	-	21
3-6	0.25" + 0.50"	0.500"	-	21
3-7	-	-	0.50"	21
Thermal Data Products - Once per Scenario	(1) 2D temperature gradient of the wheel radial cross section 20 minutes after 38 HP braking heat flux has been applied to the tread.			1
Structural Data Products Once Per Scenario	(1) Resulting hoop, radial and axial residual stress contour plots of the new 1-1/2" rim thickness radial cross section due to the combined effects of heat treatment and tread braking energy input before applying the distributed load (to simulate cold work) and before bringing the cracks into existence (Total of 3 Illustrations for This Scenario). (2) Graph of plastic strain vs. time after contact loads have been applied but before cracks have been introduced to determine when the material is cold worked at nodes located 0.050 [in] and 0.100 [in] below the tread at the taping line; it is assumed that ~5 time steps will be required (Total of 2 Illustrations for This Scenario). (3) Graph stress vs. plastic strain after contact loads have been applied but before cracks have been introduced to determine when the material is cold worked at nodes located 0.050 [in] and 0.100 [in] below the tread at the taping line (Total of 2 Illustrations for This Scenario)			7
Structural Data Products Required for Each Case	(1) For each crack configuration and seven contact force positions, graph the resultant 3 normal stresses vs. theta (on one graph with different colors) and 3 shear stresses vs. theta (all three shears on one graph with different colors) around the largest embedded crack, resulting in two separate illustrations for each of the seven contact force positions. (2) For each crack configuration and seven contact force positions, graph J-integral vs. theta around the largest embedded crack.			See Above
	Total Anticipated Number of Illustrations/Graphs			155

Scenario 4	New Rim Thickness with Cracks, 46 HP Braking, Normal Force			
Rim Thickness	1-1/2"			
Heat Treatment	Yes			
Braking	46 HP			
Rolling Contact Condition	Normal Force = 71.5K			
Total No. of Simulations:	7			
Case Number	Lateral Crack Diameter(s)	Crack Depth	Vertical Crack	No. of Graphs
4-1	0.25"	0.100"	-	21
4-2	0.25" + 0.50"	0.100"	-	21
4-3	0.25"	0.200"	-	21
4-4	0.25" + 0.50"	0.200"	-	21
4-5	0.25"	0.500"	-	21
4-6	0.25" + 0.50"	0.500"	-	21
4-7	-	-	0.50"	21
Thermal Data Products - Once per Scenario	(1) 2D temperature gradient of the wheel radial cross section 20 minutes after 38 HP braking heat flux has been applied to the tread.			1
Structural Data Products Once Per Scenario	(1) Resulting hoop, radial and axial residual stress contour plots of the new 1-1/2" rim thickness radial cross section due to the combined effects of heat treatment and tread braking energy input before applying the distributed load (to simulate cold work) and before bringing the cracks into existence (Total of 3 Illustrations for This Scenario). (2) Graph of plastic strain vs. time after contact loads have been applied but before cracks have been introduced to determine when the material is cold worked at nodes located 0.050 [in] and 0.100 [in] below the tread at the taping line; it is assumed that ~5 time steps will be required (Total of 2 Illustrations for This Scenario). (3) Graph stress vs. plastic strain after contact loads have been applied but before cracks have been introduced to determine when the material is cold worked at nodes located 0.050 [in] and 0.100 [in] below the tread at the taping line (Total of 2 Illustrations for This Scenario)			7
Structural Data Products Required for Each Case	(1) For each crack configuration and seven contact force positions, graph the resultant 3 normal stresses vs. theta (on one graph with different colors) and 3 shear stresses vs. theta (all three shears on one graph with different colors) around the largest embedded crack, resulting in two separate illustrations for each of the seven contact force positions. (2) For each crack configuration and seven contact force positions, graph J-integral vs. theta around the largest embedded crack.			See Above
	Total Anticipated Number of Illustrations/Graphs			155

Scenario 5	New Rim Thickness with Cracks, 38 HP Braking, Normal & Tangential Force			
Rim Thickness	1-1/2"			
Heat Treatment	Yes			
Braking	38 HP			
Rolling Contact Condition	Normal Force = 71.5K, Tangential Force = 37.75K			
Total No. of Simulations:	7			
Case Number	Lateral Crack Diameter(s)	Crack Depth	Vertical Crack	No. of Graphs
5-1	0.25"	0.100"	-	21
5-2	0.25" + 0.50"	0.100"	-	21
5-3	0.25"	0.200"	-	21
5-4	0.25" + 0.50"	0.200"	-	21
5-5	0.25"	0.500"	-	21
5-6	0.25" + 0.50"	0.500"	-	21
5-7	-	-	0.50"	21
Thermal Data Products - Once per Scenario	(1) 2D temperature gradient of the wheel radial cross section 20 minutes after 38 HP braking heat flux has been applied to the tread.			1
Structural Data Products Once Per Scenario	(1) Resulting hoop, radial and axial residual stress contour plots of the new 1-1/2" rim thickness radial cross section due to the combined effects of heat treatment and tread braking energy input before applying the distributed load (to simulate cold work) and before bringing the cracks into existence (Total of 3 Illustrations for This Scenario). (2) Graph of plastic strain vs. time after contact loads have been applied but before cracks have been introduced to determine when the material is cold worked at nodes located 0.050 [in] and 0.100 [in] below the tread at the taping line; it is assumed that ~5 time steps will be required (Total of 2 Illustrations for This Scenario). (3) Graph stress vs. plastic strain after contact loads have been applied but before cracks have been introduced to determine when the material is cold worked at nodes located 0.050 [in] and 0.100 [in] below the tread at the taping line (Total of 2 Illustrations for This Scenario)			7
Structural Data Products Required for Each Case	(1) For each crack configuration and seven contact force positions, graph the resultant 3 normal stresses vs. theta (on one graph with different colors) and 3 shear stresses vs. theta (all three shears on one graph with different colors) around the largest embedded crack, resulting in two separate illustrations for each of the seven contact force positions. (2) For each crack configuration and seven contact force positions, graph J-integral vs. theta around the largest embedded crack.			See Above
	Total Anticipated Number of Illustrations/Graphs			155

Scenario 6	New Rim Thickness with Cracks, 41.8 HP Braking, Normal & Tangential Force			
Rim Thickness	1-1/2"			
Heat Treatment	Yes			
Braking	41.8 HP			
Rolling Contact Condition	Normal Force = 71.5K, Tangential Force = 37.75K			
Total No. of Simulations:	7			
Case Number	Lateral Crack Diameter(s)	Crack Depth	Vertical Crack	No. of Graphs
6-1	0.25"	0.100"	-	21
6-2	0.25" + 0.50"	0.100"	-	21
6-3	0.25"	0.200"	-	21
6-4	0.25" + 0.50"	0.200"	-	21
6-5	0.25"	0.500"	-	21
6-6	0.25" + 0.50"	0.500"	-	21
6-7	-	-	0.50"	21
Thermal Data Products - Once per Scenario	(1) 2D temperature gradient of the wheel radial cross section 20 minutes after 38 HP braking heat flux has been applied to the tread.			1
Structural Data Products Once Per Scenario	(1) Resulting hoop, radial and axial residual stress contour plots of the new 1-1/2" rim thickness radial cross section due to the combined effects of heat treatment and tread braking energy input before applying the distributed load (to simulate cold work) and before bringing the cracks into existence (Total of 3 Illustrations for This Scenario). (2) Graph of plastic strain vs. time after contact loads have been applied but before cracks have been introduced to determine when the material is cold worked at nodes located 0.050 [in] and 0.100 [in] below the tread at the taping line; it is assumed that ~5 time steps will be required (Total of 2 Illustrations for This Scenario). (3) Graph stress vs. plastic strain after contact loads have been applied but before cracks have been introduced to determine when the material is cold worked at nodes located 0.050 [in] and 0.100 [in] below the tread at the taping line (Total of 2 Illustrations for This Scenario)			7
Structural Data Products Required for Each Case	(1) For each crack configuration and seven contact force positions, graph the resultant 3 normal stresses vs. theta (on one graph with different colors) and 3 shear stresses vs. theta (all three shears on one graph with different colors) around the largest embedded crack, resulting in two separate illustrations for each of the seven contact force positions. (2) For each crack configuration and seven contact force positions, graph J-integral vs. theta around the largest embedded crack.			See Above
	Total Anticipated Number of Illustrations/Graphs			155

Scenario 7	New Rim Thickness with Cracks, 46 HP Braking, Normal & Tangential Force			
Rim Thickness	1-1/2"			
Heat Treatment	Yes			
Braking	46 HP			
Rolling Contact Condition	Normal Force = 71.5K, Tangential Force = 37.75K			
Total No. of Simulations:	7			
Case Number	Lateral Crack Diameter(s)	Crack Depth	Vertical Crack	No. of Graphs
7-1	0.25"	0.100"	-	21
7-2	0.25" + 0.50"	0.100"	-	21
7-3	0.25"	0.200"	-	21
7-4	0.25" + 0.50"	0.200"	-	21
7-5	0.25"	0.500"	-	21
7-6	0.25" + 0.50"	0.500"	-	21
7-7	-	-	0.50"	21
Thermal Data Products - Once per Scenario	(1) 2D temperature gradient of the wheel radial cross section 20 minutes after 38 HP braking heat flux has been applied to the tread.			1
Structural Data Products Once Per Scenario	(1) Resulting hoop, radial and axial residual stress contour plots of the new 1-1/2" rim thickness radial cross section due to the combined effects of heat treatment and tread braking energy input before applying the distributed load (to simulate cold work) and before bringing the cracks into existence (Total of 3 Illustrations for This Scenario). (2) Graph of plastic strain vs. time after contact loads have been applied but before cracks have been introduced to determine when the material is cold worked at nodes located 0.050 [in] and 0.100 [in] below the tread at the taping line; it is assumed that ~5 time steps will be required (Total of 2 Illustrations for This Scenario). (3) Graph stress vs. plastic strain after contact loads have been applied but before cracks have been introduced to determine when the material is cold worked at nodes located 0.050 [in] and 0.100 [in] below the tread at the taping line (Total of 2 Illustrations for This Scenario)			7
Structural Data Products Required for Each Case	(1) For each crack configuration and seven contact force positions, graph the resultant 3 normal stresses vs. theta (on one graph with different colors) and 3 shear stresses vs. theta (all three shears on one graph with different colors) around the largest embedded crack, resulting in two separate illustrations for each of the seven contact force positions. (2) For each crack configuration and seven contact force positions, graph J-integral vs. theta around the largest embedded crack.			See Above
	Total Anticipated Number of Illustrations/Graphs			155

Scenario 8	Heavy Rim Wear with Cracks, 38 HP Braking, Normal Force			
Rim Thickness	1"			
Heat Treatment	Yes			
Braking	38 HP			
Rolling Contact Condition	Normal Force = 71.5K			
Total No. of Simulations:	2			
Case Number	Lateral Crack Diameter(s)	Crack Depth	Vertical Crack	No. of Graphs
8-1	0.25"	0.100"	-	21
8-2	0.25" + 0.50"	0.100"	-	21
Thermal Data Products - Once per Scenario	(1) 2D temperature gradient of the wheel radial cross section 20 minutes after 38 HP braking heat flux has been applied to the tread.			1
Structural Data Products Once Per Scenario	(1) Resulting hoop, radial and axial residual stress contour plots of the worn 1" rim thickness radial cross section due to the combined effects of heat treatment and tread braking energy input before applying the distributed load (to simulate cold work) and before bringing the cracks into existence (Total of 3 Illustrations for This Scenario). (2) Graph of plastic strain vs. time after contact loads have been applied but before cracks have been introduced to determine when the material is cold worked at nodes located 0.050 [in] and 0.100 [in] below the tread at the taping line; it is assumed that ~5 time steps will be required (Total of 2 Illustrations for This Scenario). (3) Graph stress vs. plastic strain after contact loads have been applied but before cracks have been introduced to determine when the material is cold worked at nodes located 0.050 [in] and 0.100 [in] below the tread at the taping line (Total of 2 Illustrations for This Scenario)			7
Structural Data Products Required for Each Case	(1) For each crack configuration and seven contact force positions, graph the resultant 3 normal stresses vs. theta (on one graph with different colors) and 3 shear stresses vs. theta (all three shears on one graph with different colors) around the largest embedded crack, resulting in two separate illustrations for each of the seven contact force positions. (2) For each crack configuration and seven contact force positions, graph J-integral vs. theta around the largest embedded crack.			See Above
	Total Anticipated Number of Illustrations/Graphs			50

Scenario 9	Heavy Rim Wear with Cracks, 41.8 HP Braking, Normal Force			
Rim Thickness	1"			
Heat Treatment	Yes			
Braking	41.8			
Rolling Contact Condition	Normal Force = 71.5K			
Total No. of Simulations:	2			
Case Number	Lateral Crack Diameter(s)	Crack Depth	Vertical Crack	No. of Graphs
9-1	0.25"	0.100"	-	21
9-2	0.25" + 0.50"	0.100"	-	21
Thermal Data Products - Once per Scenario	(1) 2D temperature gradient of the wheel radial cross section 20 minutes after 38 HP braking heat flux has been applied to the tread.			1
Structural Data Products Once Per Scenario	(1) Resulting hoop, radial and axial residual stress contour plots of the worn 1" rim thickness radial cross section due to the combined effects of heat treatment and tread braking energy input before applying the distributed load (to simulate cold work) and before bringing the cracks into existence (Total of 3 Illustrations for This Scenario). (2) Graph of plastic strain vs. time after contact loads have been applied but before cracks have been introduced to determine when the material is cold worked at nodes located 0.050 [in] and 0.100 [in] below the tread at the taping line; it is assumed that ~5 time steps will be required (Total of 2 Illustrations for This Scenario). (3) Graph stress vs. plastic strain after contact loads have been applied but before cracks have been introduced to determine when the material is cold worked at nodes located 0.050 [in] and 0.100 [in] below the tread at the taping line (Total of 2 Illustrations for This Scenario)			7
Structural Data Products Required for Each Case	(1) For each crack configuration and seven contact force positions, graph the resultant 3 normal stresses vs. theta (on one graph with different colors) and 3 shear stresses vs. theta (all three shears on one graph with different colors) around the largest embedded crack, resulting in two separate illustrations for each of the seven contact force positions. (2) For each crack configuration and seven contact force positions, graph J-integral vs. theta around the largest embedded crack.			See Above
	Total Anticipated Number of Illustrations/Graphs			50

Scenario 10	Heavy Rim Wear with Cracks, 46 HP Braking, Normal Force			
Rim Thickness	1"			
Heat Treatment	Yes			
Braking	46			
Rolling Contact Condition	Normal Force = 71.5K			
Total No. of Simulations:	2			
Case Number	Lateral Crack Diameter(s)	Crack Depth	Vertical Crack	No. of Graphs
10-1	0.25"	0.100"	-	21
10-2	0.25" + 0.50"	0.100"	-	21
Thermal Data Products - Once per Scenario	(1) 2D temperature gradient of the wheel radial cross section 20 minutes after 38 HP braking heat flux has been applied to the tread.			1
Structural Data Products Once Per Scenario	(1) Resulting hoop, radial and axial residual stress contour plots of the worn 1" rim thickness radial cross section due to the combined effects of heat treatment and tread braking energy input before applying the distributed load (to simulate cold work) and before bringing the cracks into existence (Total of 3 Illustrations for This Scenario). (2) Graph of plastic strain vs. time after contact loads have been applied but before cracks have been introduced to determine when the material is cold worked at nodes located 0.050 [in] and 0.100 [in] below the tread at the taping line; it is assumed that ~5 time steps will be required (Total of 2 Illustrations for This Scenario). (3) Graph stress vs. plastic strain after contact loads have been applied but before cracks have been introduced to determine when the material is cold worked at nodes located 0.050 [in] and 0.100 [in] below the tread at the taping line (Total of 2 Illustrations for This Scenario)			7
Structural Data Products Required for Each Case	(1) For each crack configuration and seven contact force positions, graph the resultant 3 normal stresses vs. theta (on one graph with different colors) and 3 shear stresses vs. theta (all three shears on one graph with different colors) around the largest embedded crack, resulting in two separate illustrations for each of the seven contact force positions. (2) For each crack configuration and seven contact force positions, graph J-integral vs. theta around the largest embedded crack.			See Above
	Total Anticipated Number of Illustrations/Graphs			50

Scenario 11	Heavy Rim Wear with Cracks, 38 HP Braking, Normal & Tangential Force			
Rim Thickness	1"			
Heat Treatment	Yes			
Braking	38 HP			
Rolling Contact Condition	Normal Force = 71.5K, Tangential Force = 37.75K			
Total No. of Simulations:	2			
Case Number	Lateral Crack Diameter(s)	Crack Depth	Vertical Crack	No. of Graphs
11-1	0.25"	0.100"	-	21
11-2	0.25" + 0.50"	0.100"	-	21
Thermal Data Products - Once per Scenario	(1) 2D temperature gradient of the wheel radial cross section 20 minutes after 38 HP braking heat flux has been applied to the tread.			1
Structural Data Products Once Per Scenario	(1) Resulting hoop, radial and axial residual stress contour plots of the worn 1" rim thickness radial cross section due to the combined effects of heat treatment and tread braking energy input before applying the distributed load (to simulate cold work) and before bringing the cracks into existence (Total of 3 Illustrations for This Scenario). (2) Graph of plastic strain vs. time after contact loads have been applied but before cracks have been introduced to determine when the material is cold worked at nodes located 0.050 [in] and 0.100 [in] below the tread at the taping line; it is assumed that ~5 time steps will be required (Total of 2 Illustrations for This Scenario). (3) Graph stress vs. plastic strain after contact loads have been applied but before cracks have been introduced to determine when the material is cold worked at nodes located 0.050 [in] and 0.100 [in] below the tread at the taping line (Total of 2 Illustrations for This Scenario)			7
Structural Data Products Required for Each Case	(1) For each crack configuration and seven contact force positions, graph the resultant 3 normal stresses vs. theta (on one graph with different colors) and 3 shear stresses vs. theta (all three shears on one graph with different colors) around the largest embedded crack, resulting in two separate illustrations for each of the seven contact force positions. (2) For each crack configuration and seven contact force positions, graph J-integral vs. theta around the largest embedded crack.			See Above
	Total Anticipated Number of Illustrations/Graphs			50

Scenario 12	Heavy Rim Wear with Cracks, 41.8 HP Braking, Normal & Tangential Force			
Rim Thickness	1"			
Heat Treatment	Yes			
Braking	41.8 HP			
Rolling Contact Condition	Normal Force = 71.5K, Tangential Force = 37.75K			
Total No. of Simulations:	2			
Case Number	Lateral Crack Diameter(s)	Crack Depth	Vertical Crack	No. of Graphs
12-1	0.25"	0.100"	-	21
12-2	0.25" + 0.50"	0.100"	-	21
Thermal Data Products - Once per Scenario	(1) 2D temperature gradient of the wheel radial cross section 20 minutes after 38 HP braking heat flux has been applied to the tread.			1
Structural Data Products Once Per Scenario	(1) Resulting hoop, radial and axial residual stress contour plots of the worn 1" rim thickness radial cross section due to the combined effects of heat treatment and tread braking energy input before applying the distributed load (to simulate cold work) and before bringing the cracks into existence (Total of 3 Illustrations for This Scenario). (2) Graph of plastic strain vs. time after contact loads have been applied but before cracks have been introduced to determine when the material is cold worked at nodes located 0.050 [in] and 0.100 [in] below the tread at the taping line; it is assumed that ~5 time steps will be required (Total of 2 Illustrations for This Scenario). (3) Graph stress vs. plastic strain after contact loads have been applied but before cracks have been introduced to determine when the material is cold worked at nodes located 0.050 [in] and 0.100 [in] below the tread at the taping line (Total of 2 Illustrations for This Scenario)			7
Structural Data Products Required for Each Case	(1) For each crack configuration and seven contact force positions, graph the resultant 3 normal stresses vs. theta (on one graph with different colors) and 3 shear stresses vs. theta (all three shears on one graph with different colors) around the largest embedded crack, resulting in two separate illustrations for each of the seven contact force positions. (2) For each crack configuration and seven contact force positions, graph J-integral vs. theta around the largest embedded crack.			See Above
	Total Anticipated Number of Illustrations/Graphs			50

Scenario 13	Heavy Rim Wear with Cracks, 46 HP Braking, Normal & Tangential Force			
Rim Thickness	1"			
Heat Treatment	Yes			
Braking	46 HP			
Rolling Contact Condition	Normal Force = 71.5K, Tangential Force = 37.75K			
Total No. of Simulations:	2			
Case Number	Lateral Crack Diameter(s)	Crack Depth	Vertical Crack	No. of Graphs
13-1	0.25"	0.100"	-	21
13-2	0.25" + 0.50"	0.100"	-	21
Thermal Data Products - Once per Scenario	(1) 2D temperature gradient of the wheel radial cross section 20 minutes after 38 HP braking heat flux has been applied to the tread.			1
Structural Data Products Once Per Scenario	(1) Resulting hoop, radial and axial residual stress contour plots of the worn 1" rim thickness radial cross section due to the combined effects of heat treatment and tread braking energy input before applying the distributed load (to simulate cold work) and before bringing the cracks into existence (Total of 3 Illustrations for This Scenario). (2) Graph of plastic strain vs. time after contact loads have been applied but before cracks have been introduced to determine when the material is cold worked at nodes located 0.050 [in] and 0.100 [in] below the tread at the taping line; it is assumed that ~5 time steps will be required (Total of 2 Illustrations for This Scenario). (3) Graph stress vs. plastic strain after contact loads have been applied but before cracks have been introduced to determine when the material is cold worked at nodes located 0.050 [in] and 0.100 [in] below the tread at the taping line (Total of 2 Illustrations for This Scenario)			7
Structural Data Products Required for Each Case	(1) For each crack configuration and seven contact force positions, graph the resultant 3 normal stresses vs. theta (on one graph with different colors) and 3 shear stresses vs. theta (all three shears on one graph with different colors) around the largest embedded crack, resulting in two separate illustrations for each of the seven contact force positions. (2) For each crack configuration and seven contact force positions, graph J-integral vs. theta around the largest embedded crack.			See Above
	Total Anticipated Number of Illustrations/Graphs			50

Appendix B: AAR MSRP S-660 Stress Check

A coupled thermal-structural physics simulation was conducted for the S-660 stress check on the stage II wheel design. Stresses on the front and rear plate sections of the wheel were of particular interest. The prescribed loads are shown in Figure 52. The 2D wheel profile was revolved to create a full 3D wheel. A computational mesh was generated on the 3D wheel (Figure 53). The mesh consists of a mix of ANSYS SOLID187 quadratic tetrahedral and SOLID186 hexahedral elements.

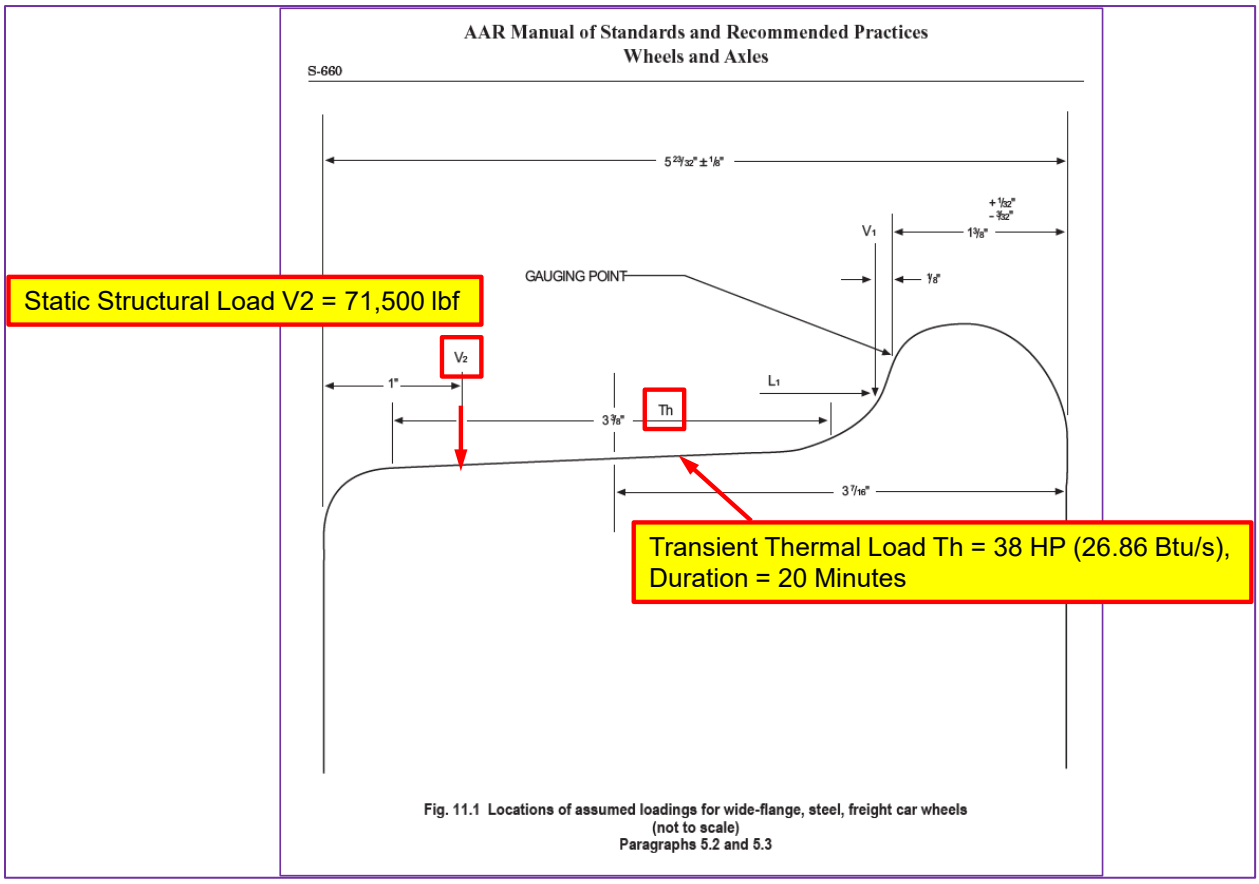

Figure 52. AAR MSRP S-660 Stress Check Thermal and Structural Loads

A transient thermal analysis was solved first to determine the wheel temperature distribution when a 38 HP braking load was applied for 20 minutes (see Figure 54). The resulting temperature distribution is shown in Figure 55, with a maximum value of 746°F on the tread surface. The temperature results were then applied to a static structural model to create thermal-stress effects. In conjunction with the applied temperature distribution, a structural load of 71,500 lbf was applied on the tread. Figure 56 indicates the location of load application and Figure 57 shows the fixed boundary condition at the hub.

Figures 58 and 59 show von Mises stress results on the front and rear plate regions. Stresses were in the 50,000–70,000 psi range and these values generally agree with expectations.

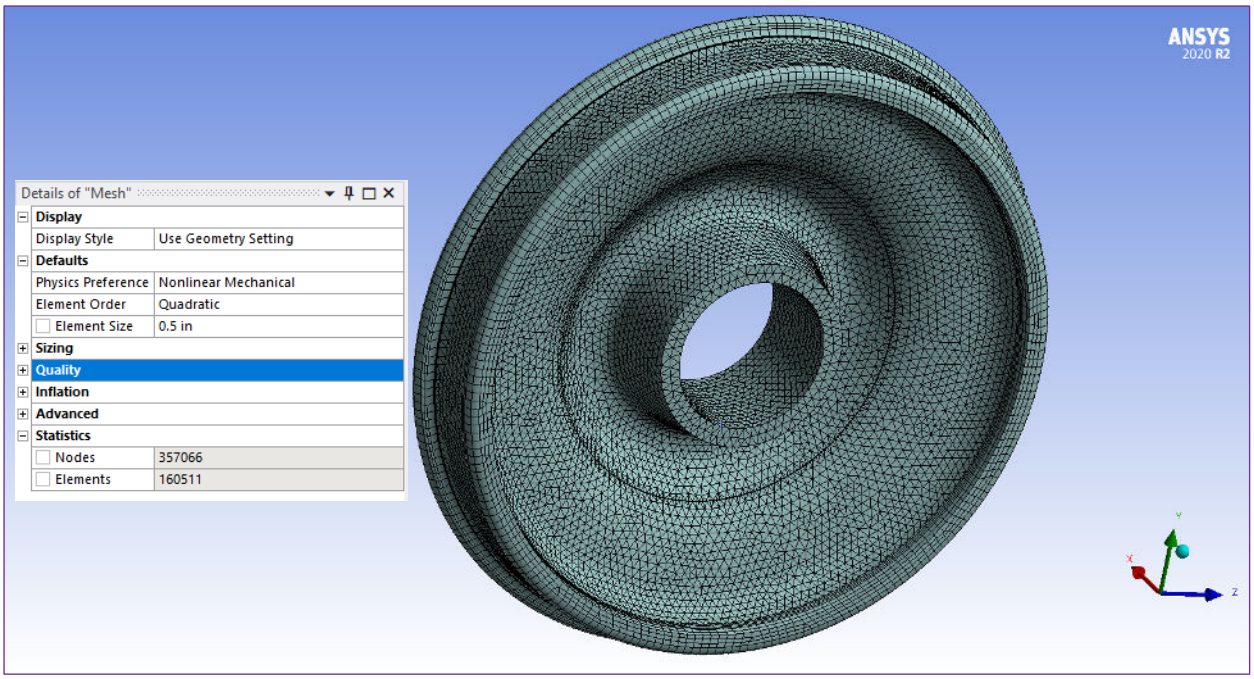

Figure 53. Full 3D Wheel Computational Mesh

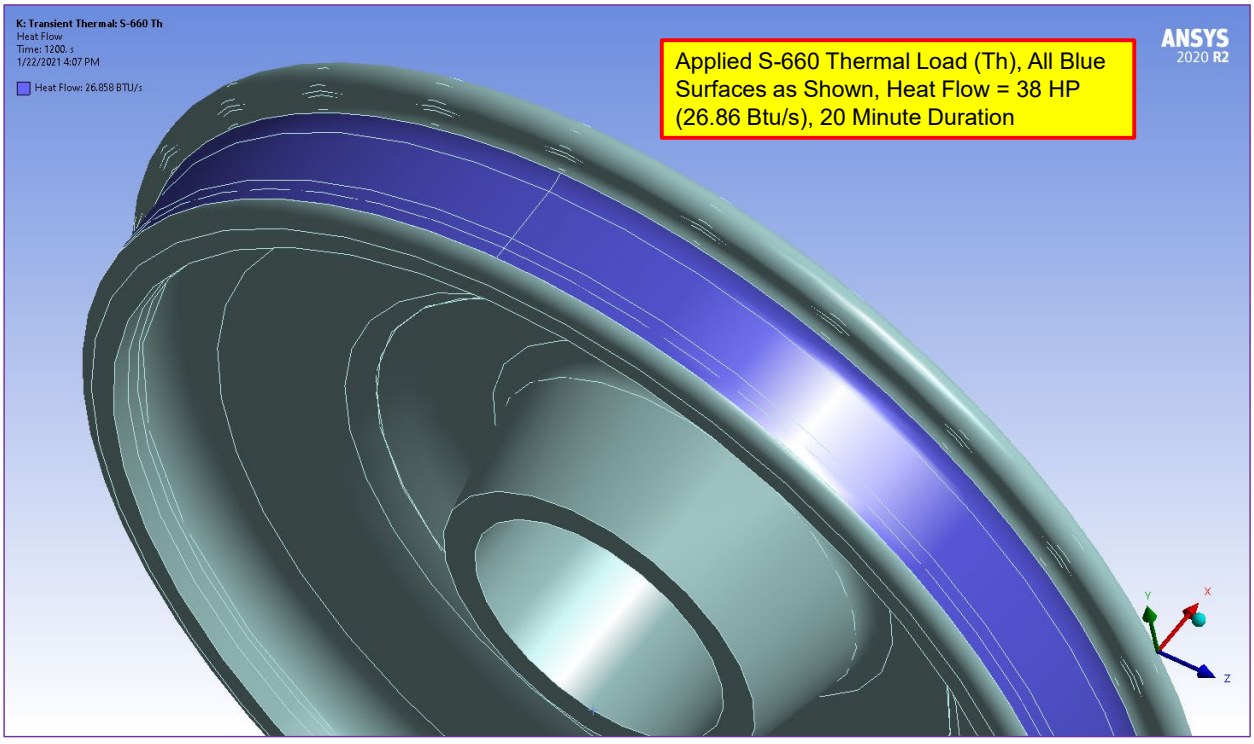

Figure 54. Applied Transient Thermal Load

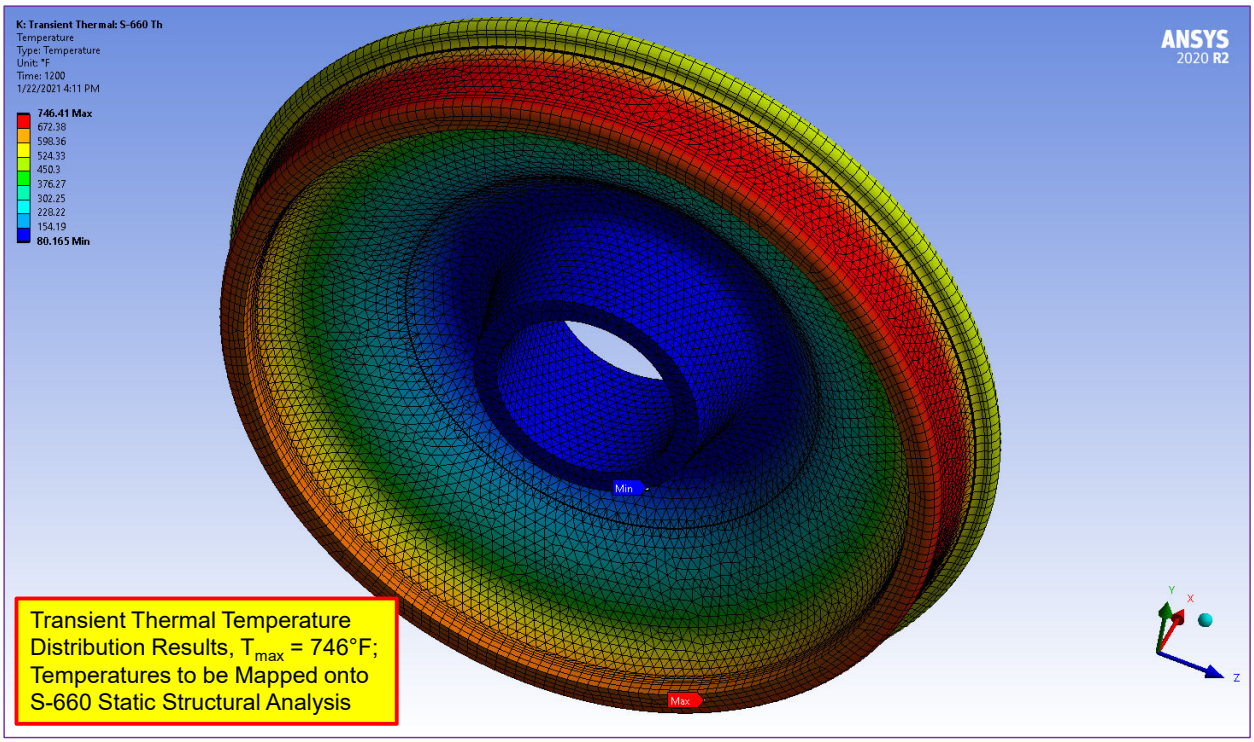

Figure 55. Applied Transient Thermal Analysis Temperature Results

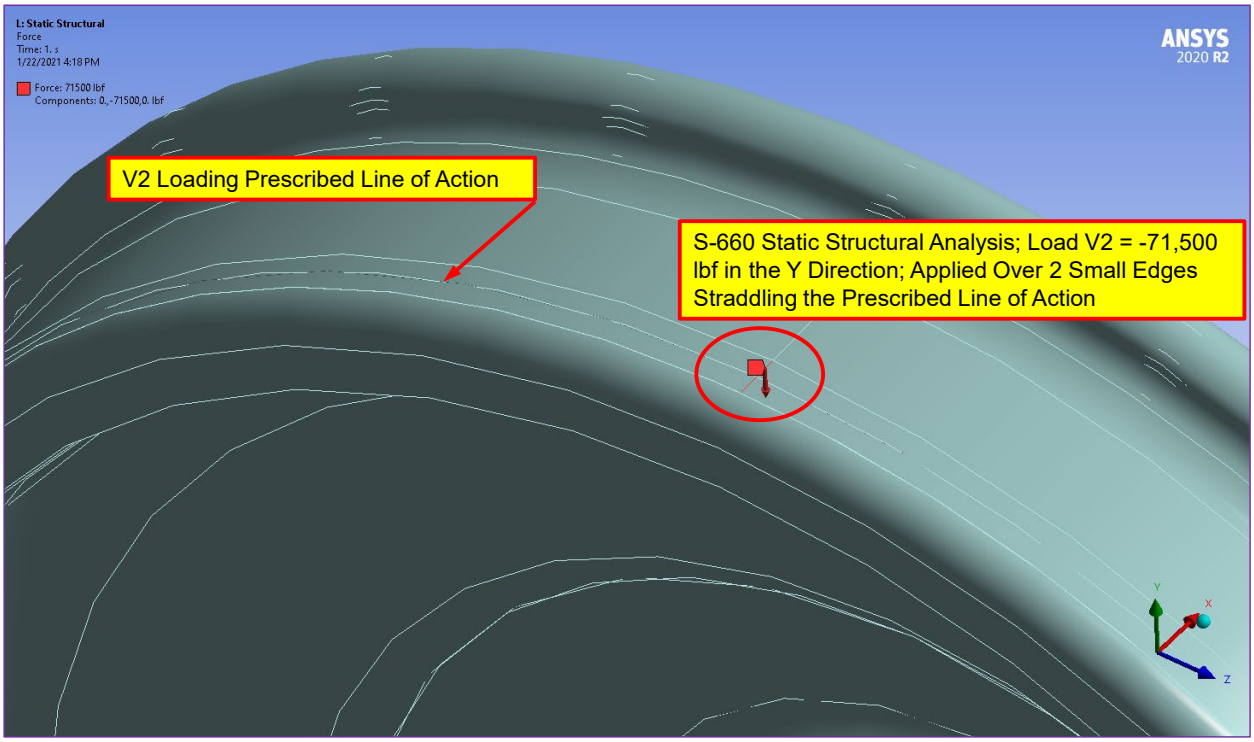

Figure 56. Applied Structural Load

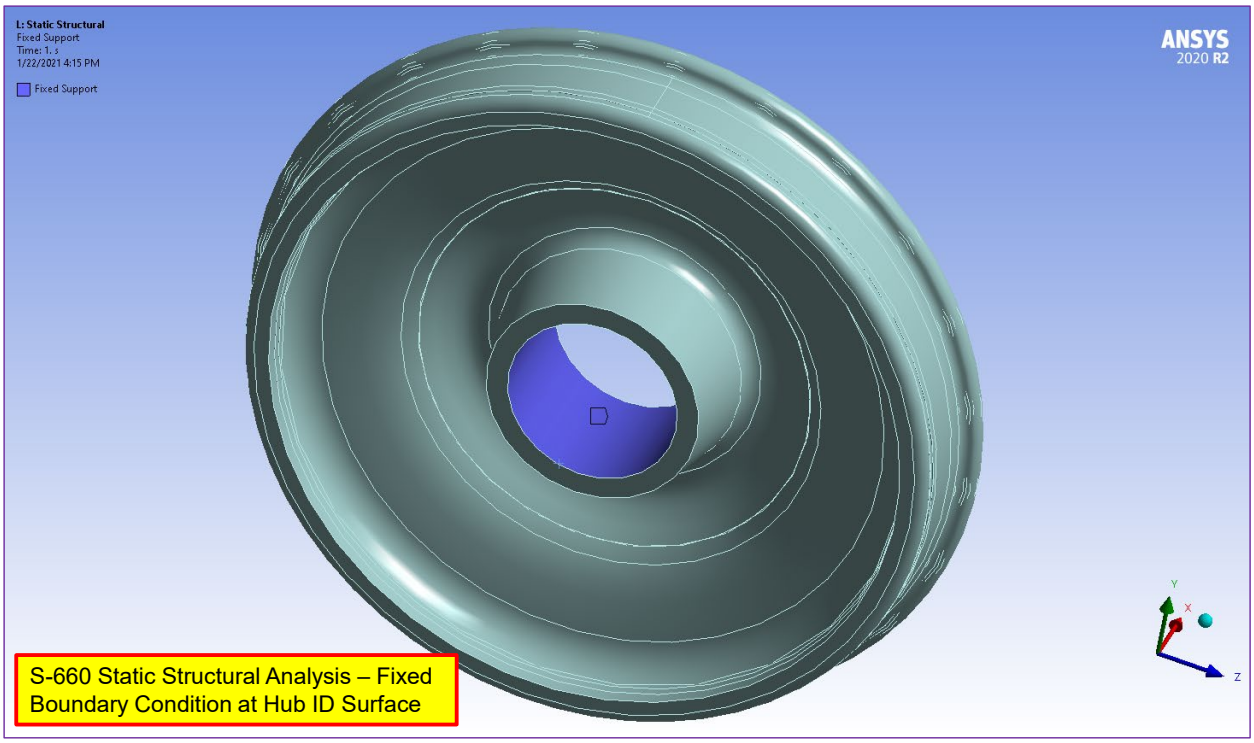

Figure 57. Hub Fixed Boundary Condition

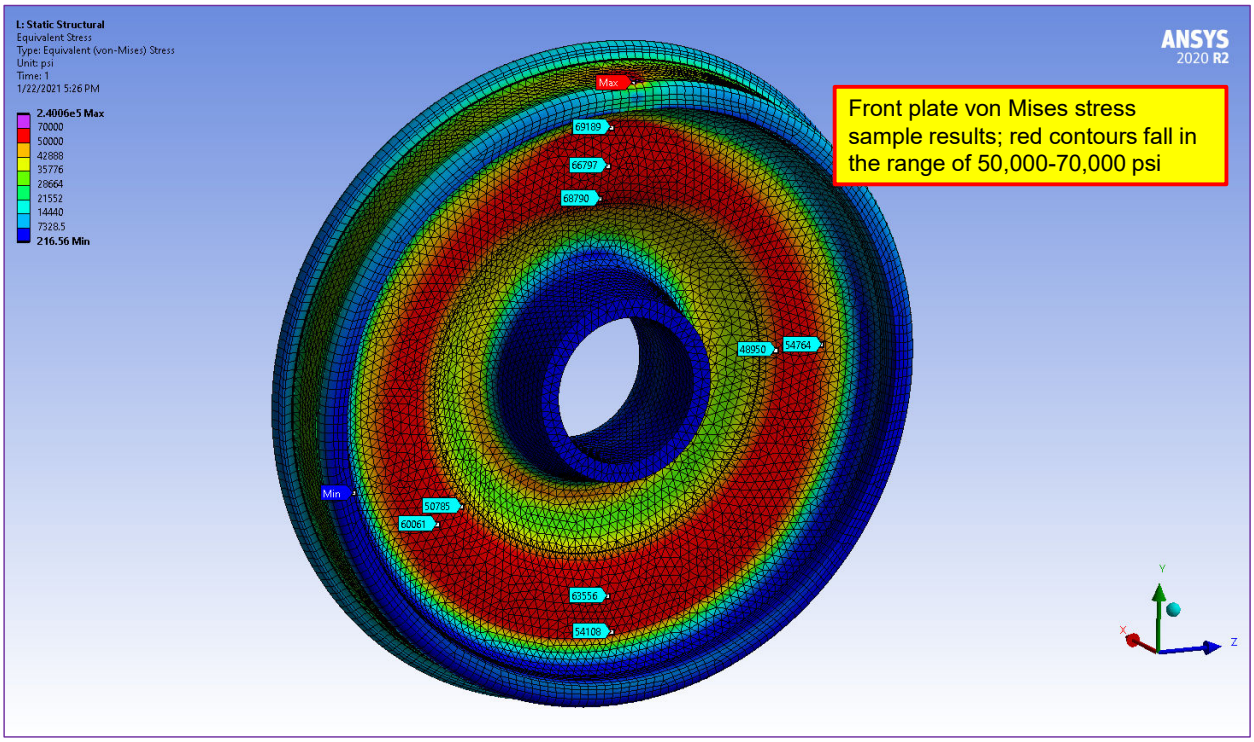

Figure 58. Front Plate von Mises Stress Results

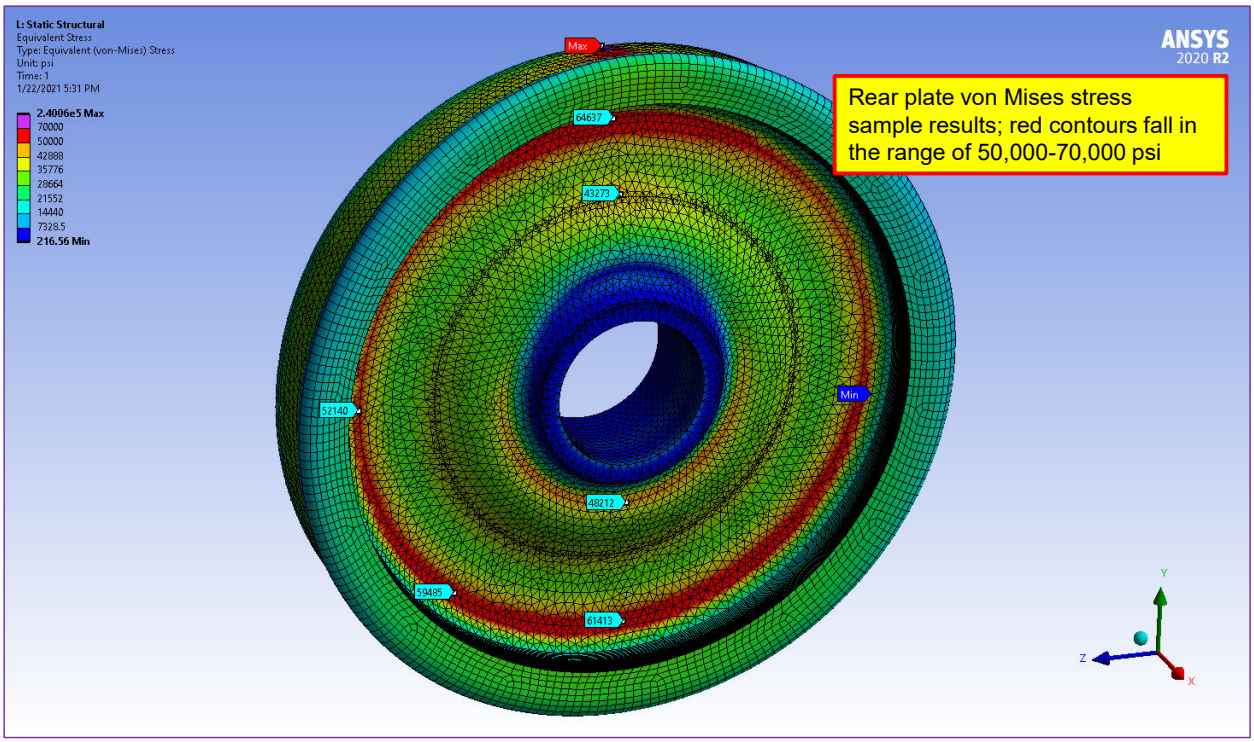

Figure 59. Rear Plate von Mises Stress Results

Appendix C: Result Symmetry Check

The result symmetry check examined radial, hoop, and axial stress results around the circumference of HCRACK1, which was centered on the taping line and closest to the tread surface. The symmetry of stress results was compared during different phases of the analysis process, including after heat treatment, after cold work, after crack activation, and during normal load application at different positions along the taping line.

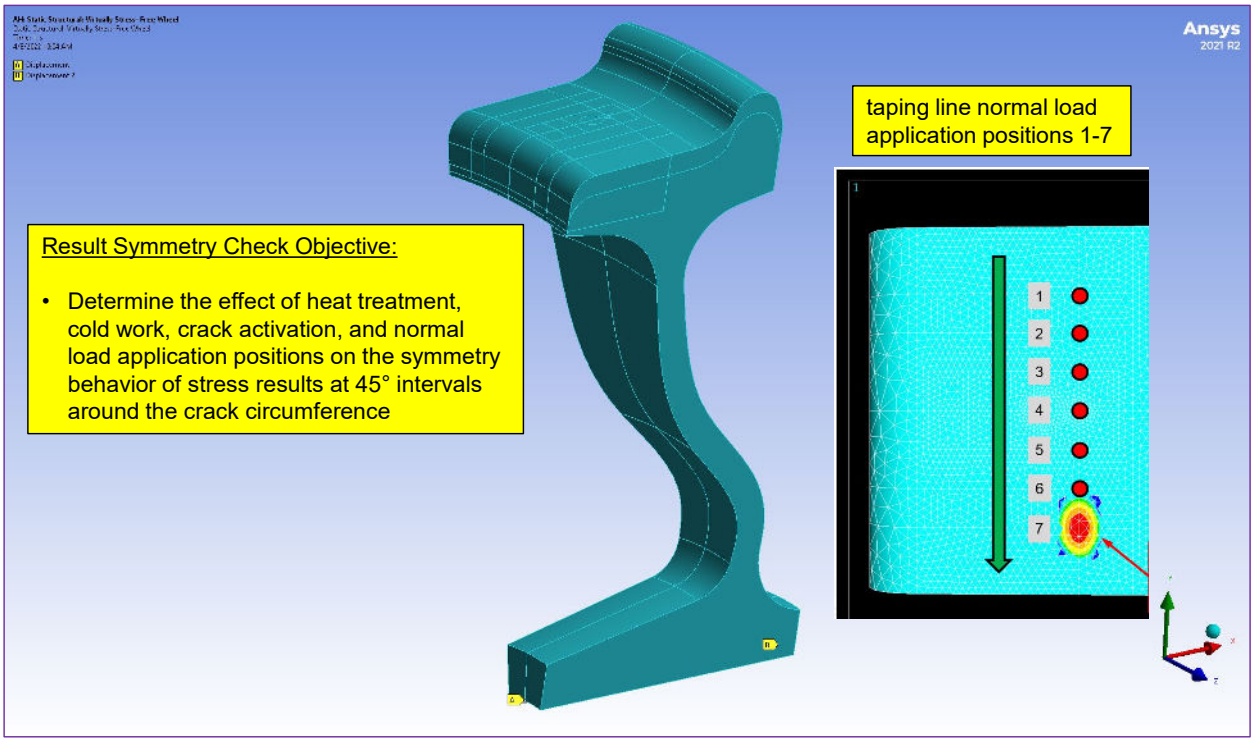

Figure 60. Result Symmetry Check Objective

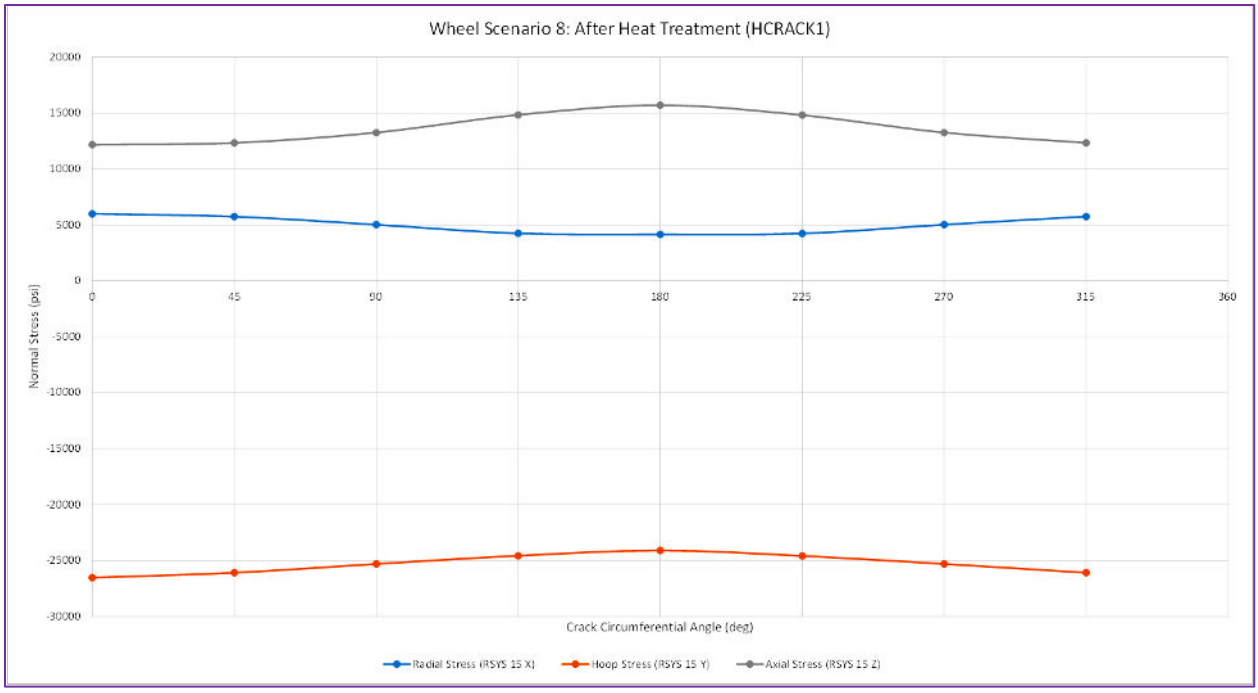

Figure 61. Result Symmetry Check after heat treatment. Stress components at all inactive crack circumferential locations show symmetric behavior. This chart plots HCRACK1 normal stress components with respect to circumferential angle.

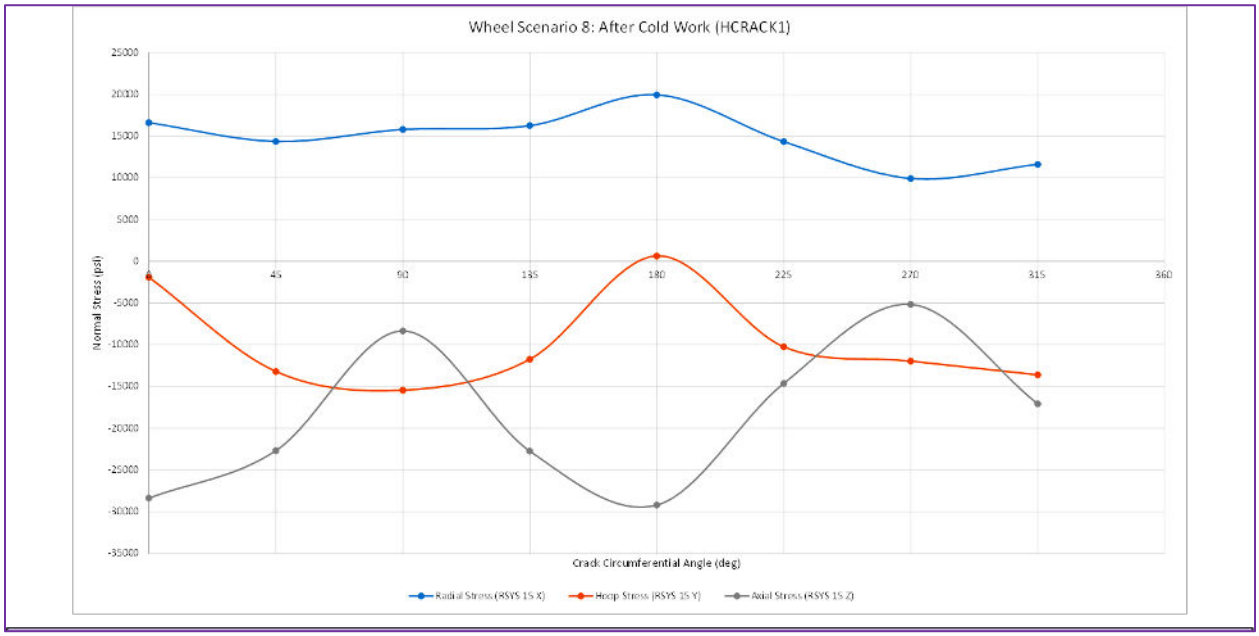

Figure 62. Result Symmetry Check after cold work. Stress components at most inactive crack circumferential locations show some asymmetric behavior; this is likely due to the amount of cold work performed. Asymmetry is most pronounced at taping line cracks HCRACK1–HCRACK3, less pronounced at HCRACK4–HCRACK6, and there is no effect at the vertical crack VCRACK1.

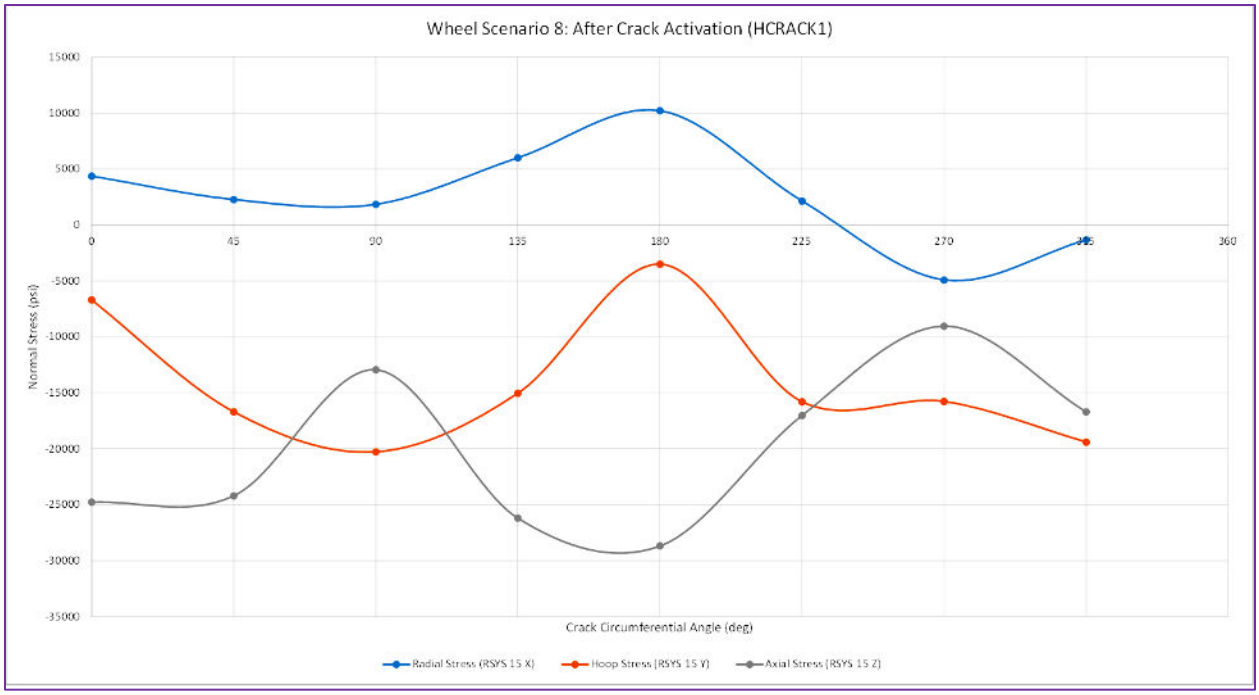

Figure 63. Result Symmetry Check after crack activation. Stress components show asymmetric behavior similar to post cold work results.

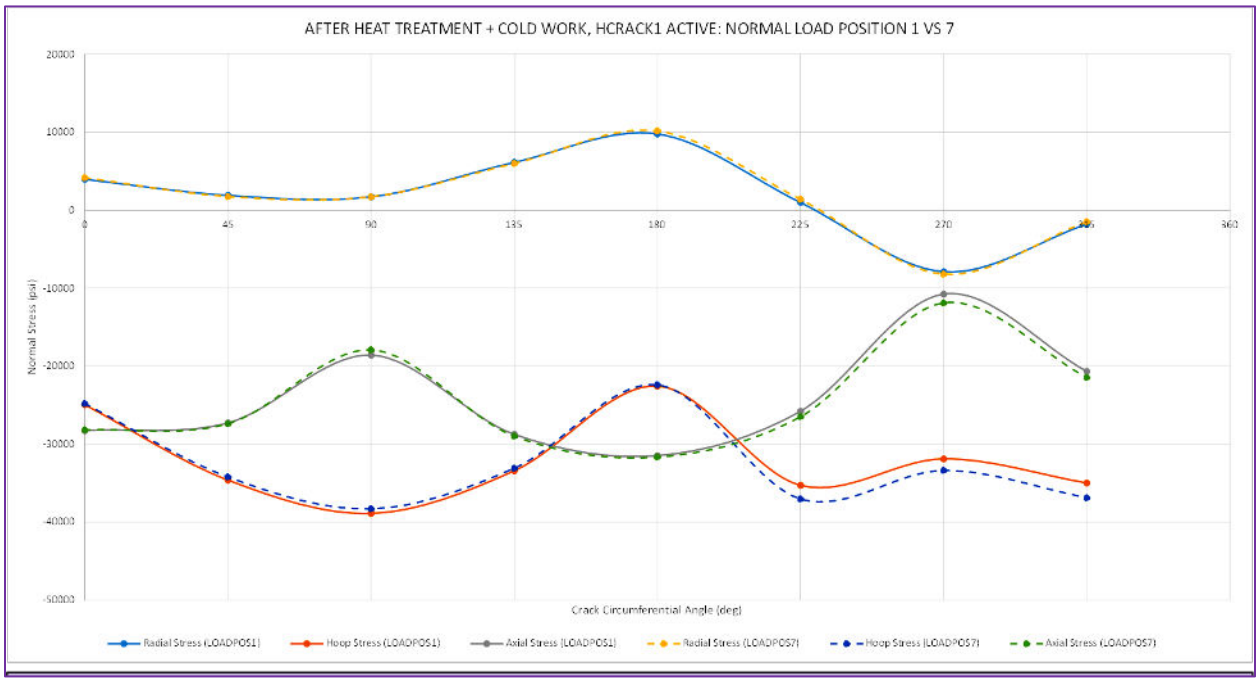

Figure 64. Result Symmetry Check for Normal Load Application Positions 1 and 7. The load is remote relative to the HCRACK1 location; therefore, there is little change in the stress results compared to post crack activation data.

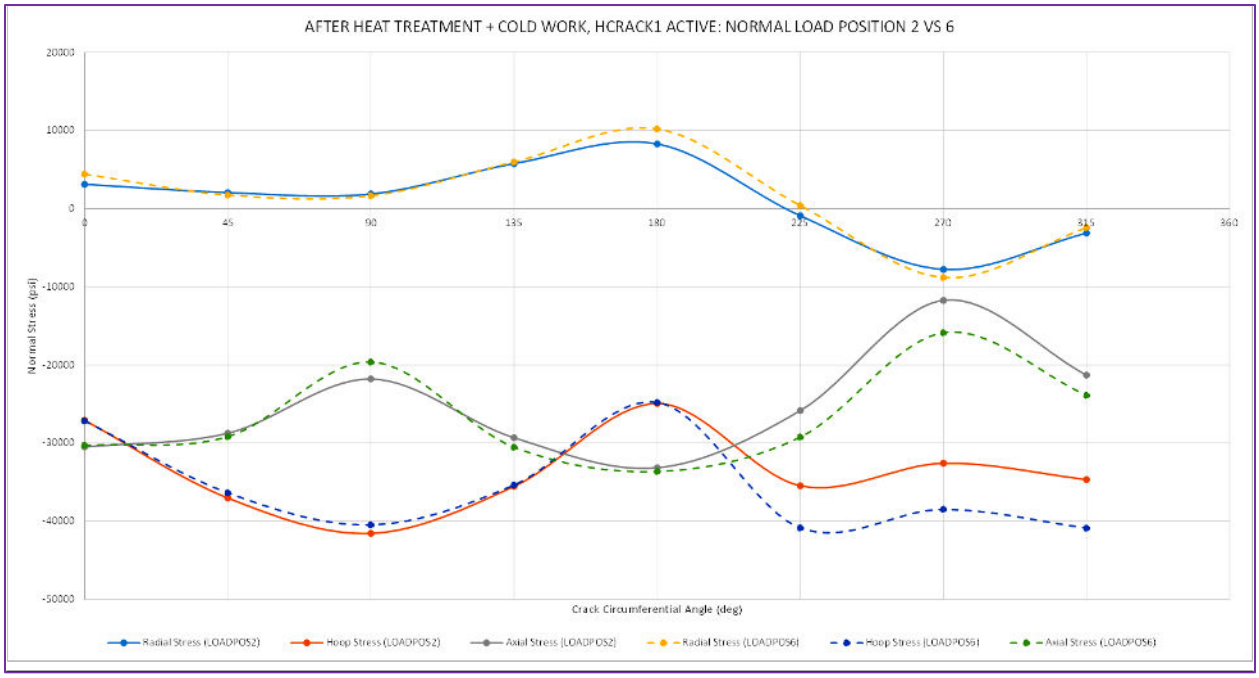

Figure 65. Result Symmetry Check for Normal Load Application Positions 2 and 6. The load is closer to the HCRACK1 location; there are minor changes is the stress results compared to post crack activation data, but the asymmetry is not significantly changed.

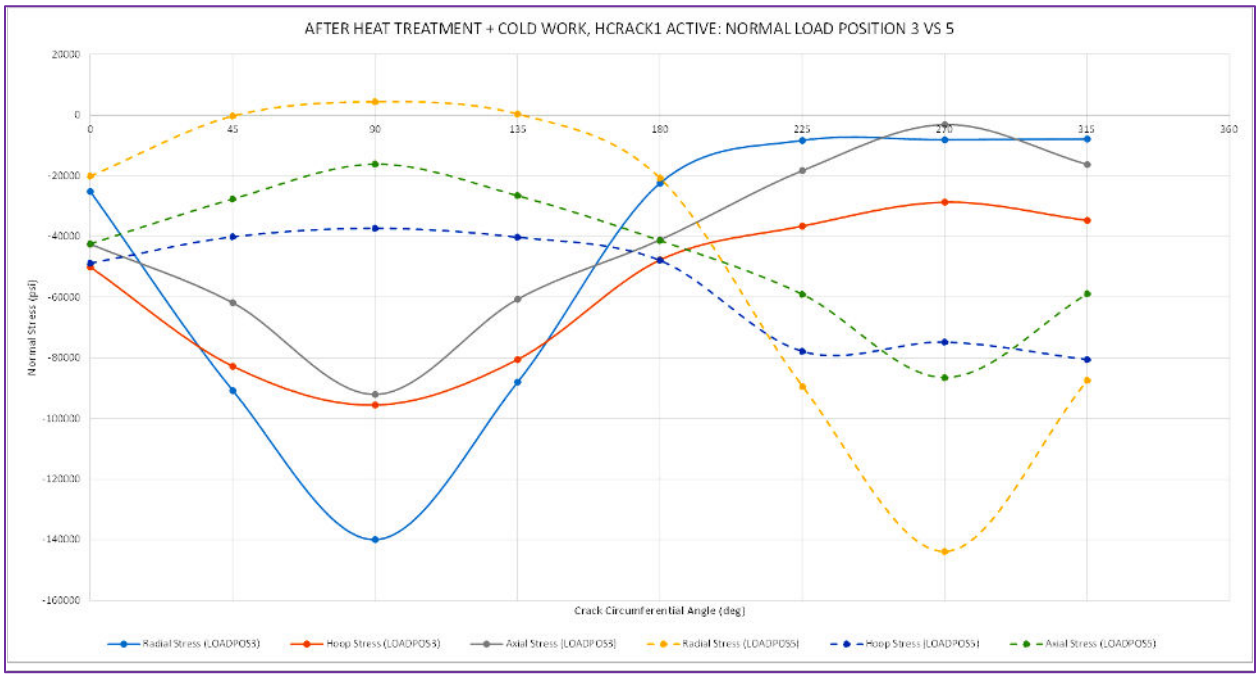

Figure 66. Result Symmetry Check for Normal Load Application Positions 3 and 5. They are directly adjacent to the HCRACK1 location and have the largest influence on the crack stress field; however, a degree of symmetry still exists.

Appendix D: Stress Free Wheel

The stress-free wheel check examines J-integral values on the wheel sector model. When various cracks are activated and no heat treatment, cold work, braking, or normal loads are applied, J-integral results should be zero. The results confirm this. See Figures 67–70.

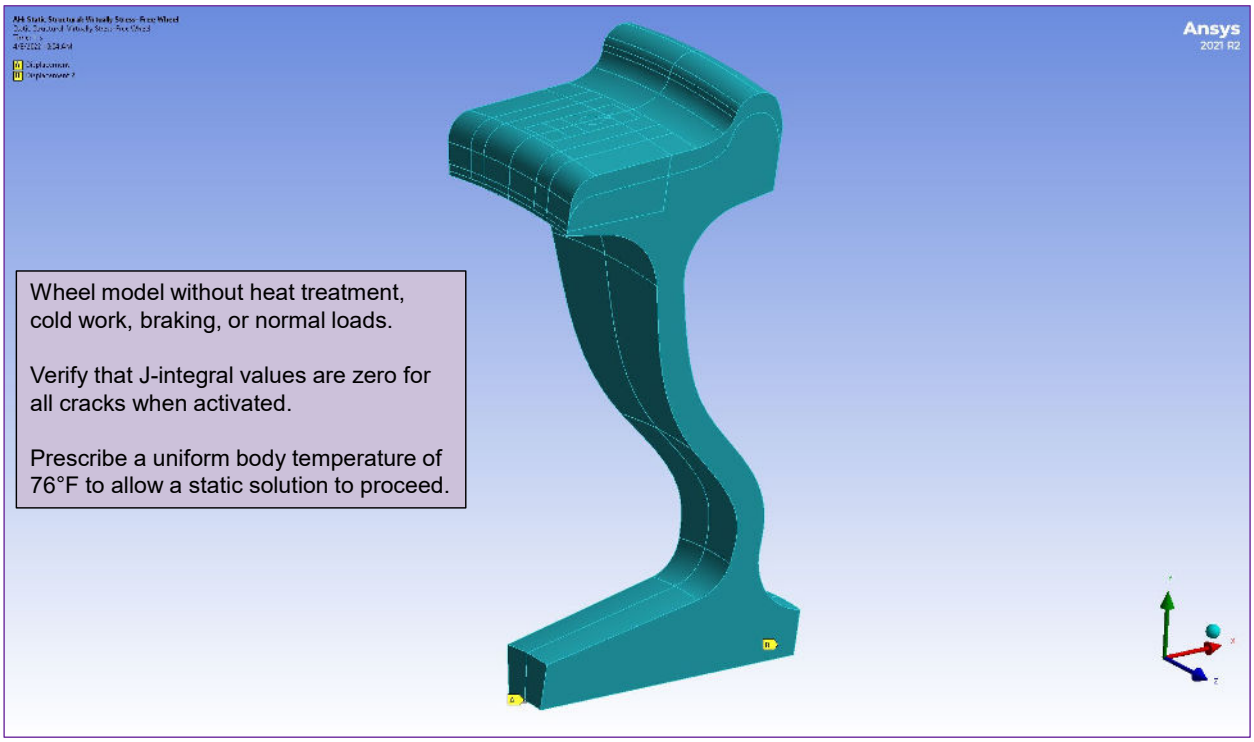

Figure 67. Stress-Free Wheel

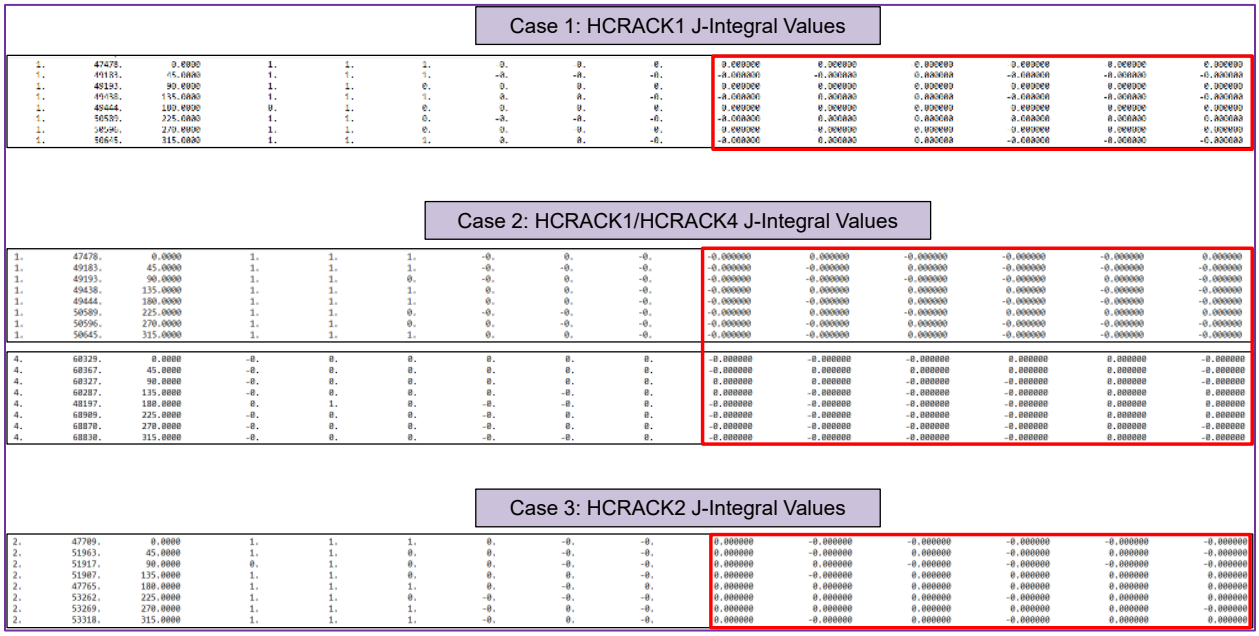

Figure 68. Stress-Free Wheel: Results for Crack Activation Cases 1–3

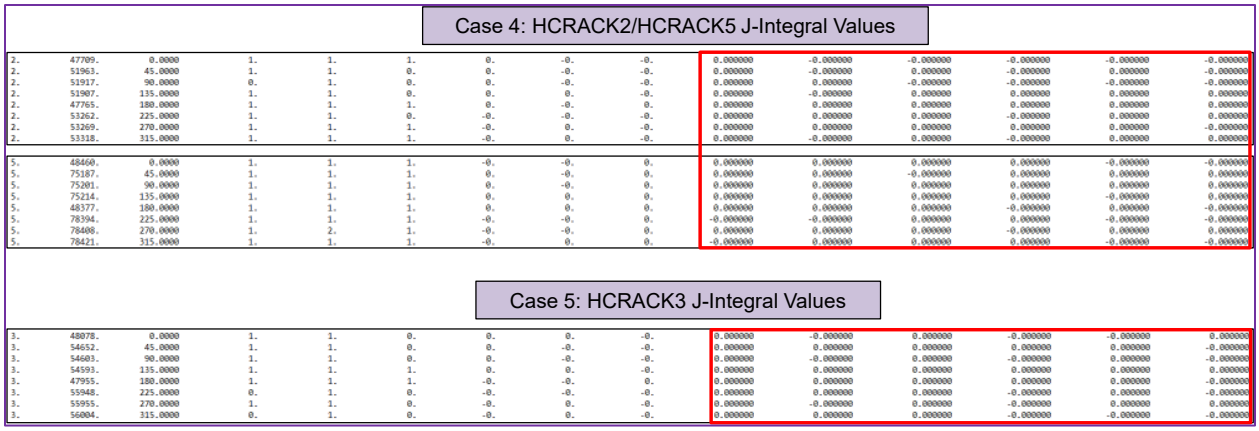

Figure 69. Stress-Free Wheel: Results for Crack Activation Cases 4–5

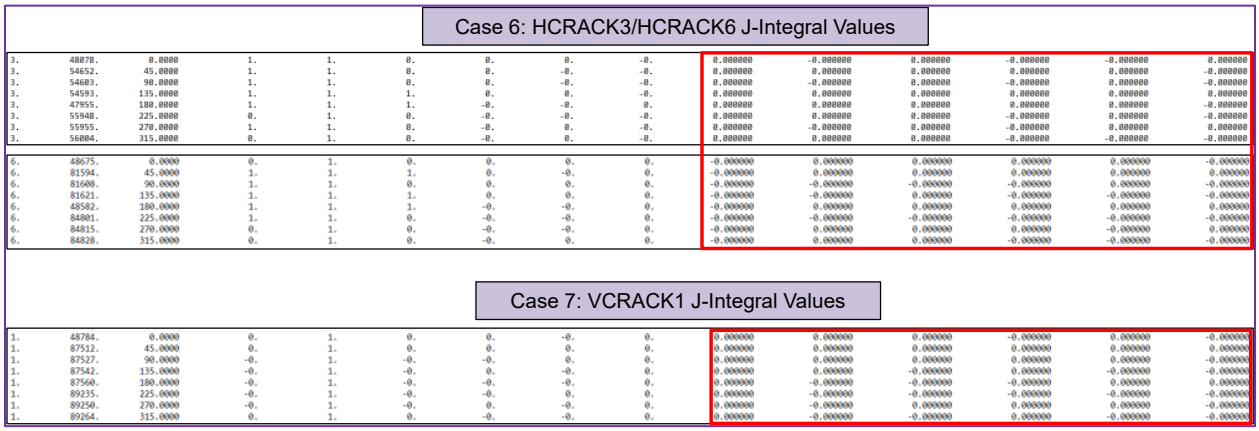

Figure 70. Stress-Free Wheel: Results for Crack Activation Cases 6–7

Appendix E: Mesh Sensitivity Study

A mesh sensitivity study was performed to determine the change in mesh quality and influence on J-integral values around the crack circumference. J-integral results from the baseline mesh were compared to a refined mesh. To limit the scope of the study, only HCRACK3 results were examined for the new wheel with a 1.5-inch-thick rim, and WS2 loads were used.

The effect of normal contact loads at position 1 (furthest from the crack) and position 4 (centered over the crack) were considered. Two additional crack contact types were included. Type 1 assumes that the entire surface area of the crack faces is in contact up to and including the crack front. Type 2 uses a reduced contact area, with a buffer zone between the edge of the contact area and the crack front. J-integral results show that type 2 contact is preferred and it was therefore used in all final analysis simulations.

Examination of baseline versus refined mesh results show mixed results. The conclusion is that the baseline mesh is adequate for all final analysis simulations, especially given the current large RAM and disk space requirements. See Figures 71–77.

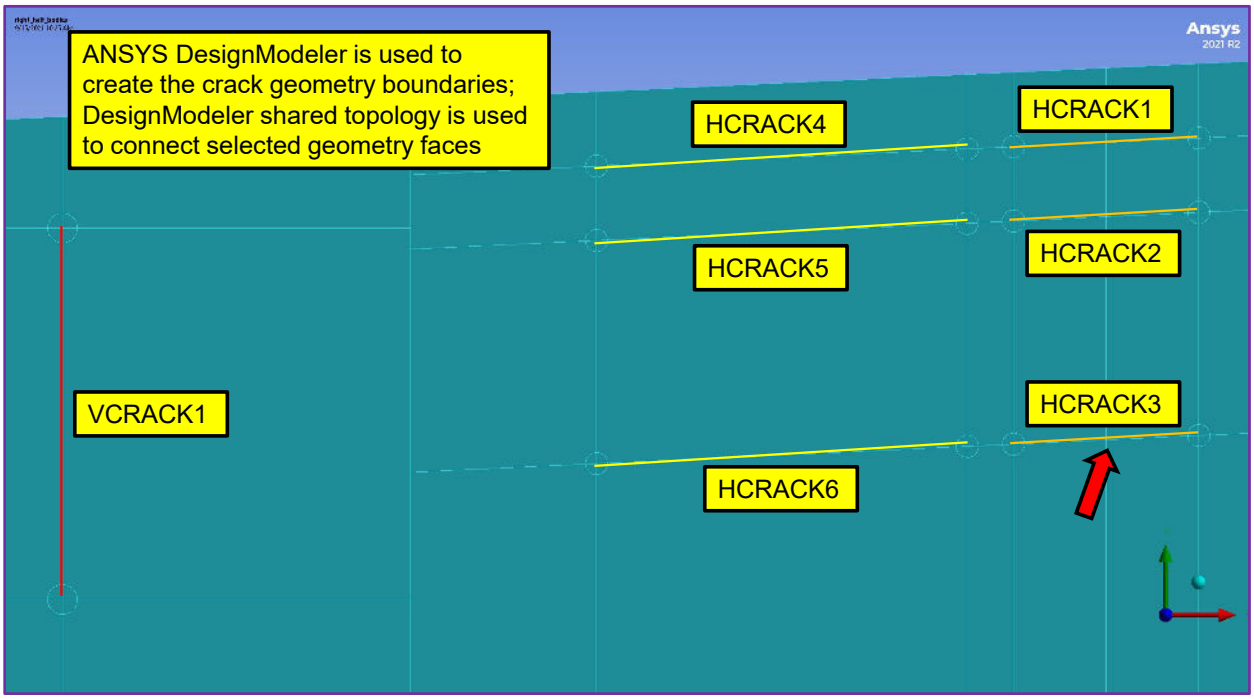

Figure 71. HCRACK3 Subsurface Location

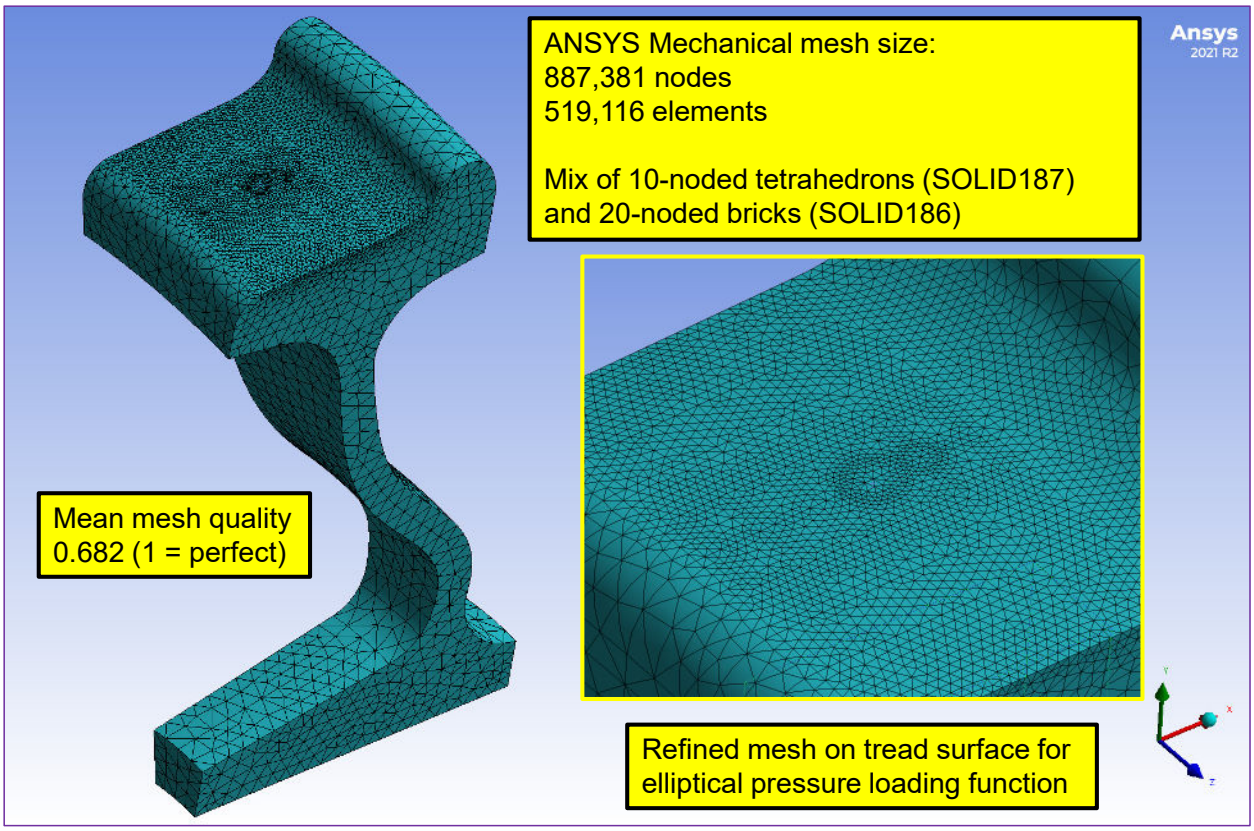

Figure 72. Baseline Computational Mesh

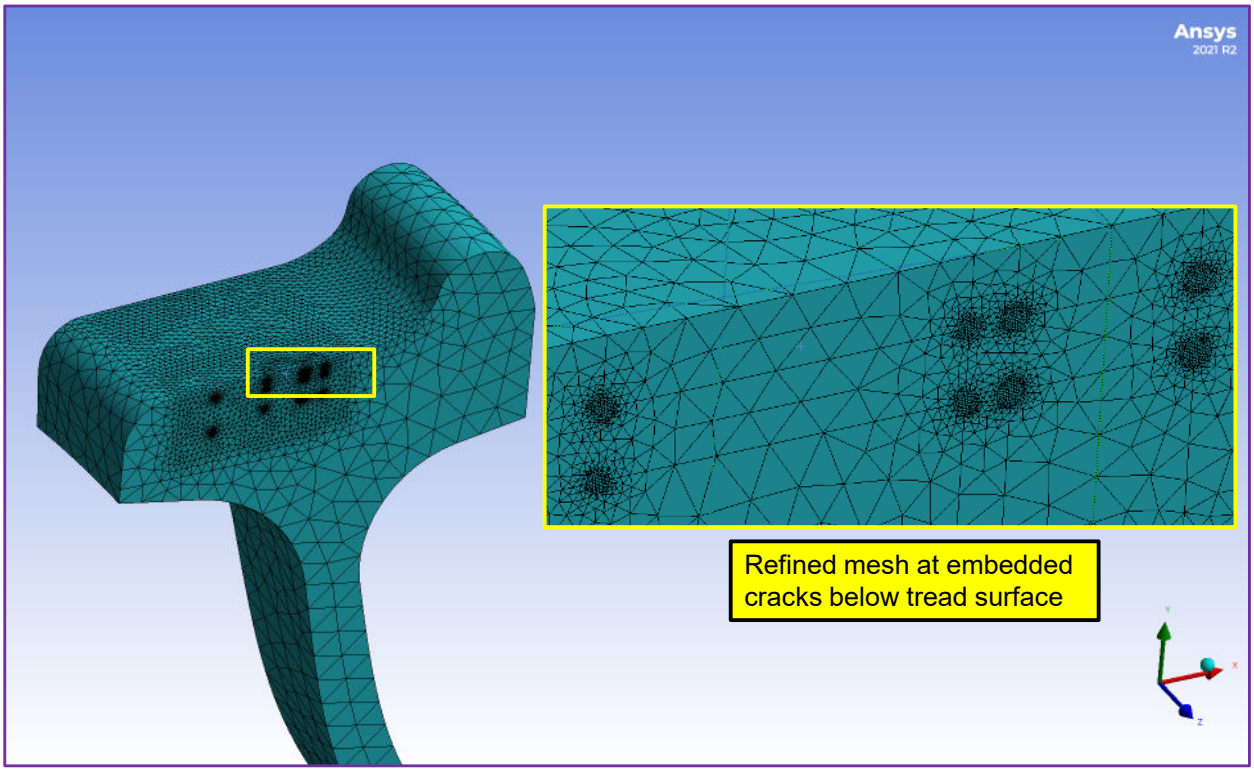

Figure 73. Baseline Computational Mesh: Subsurface Cracks

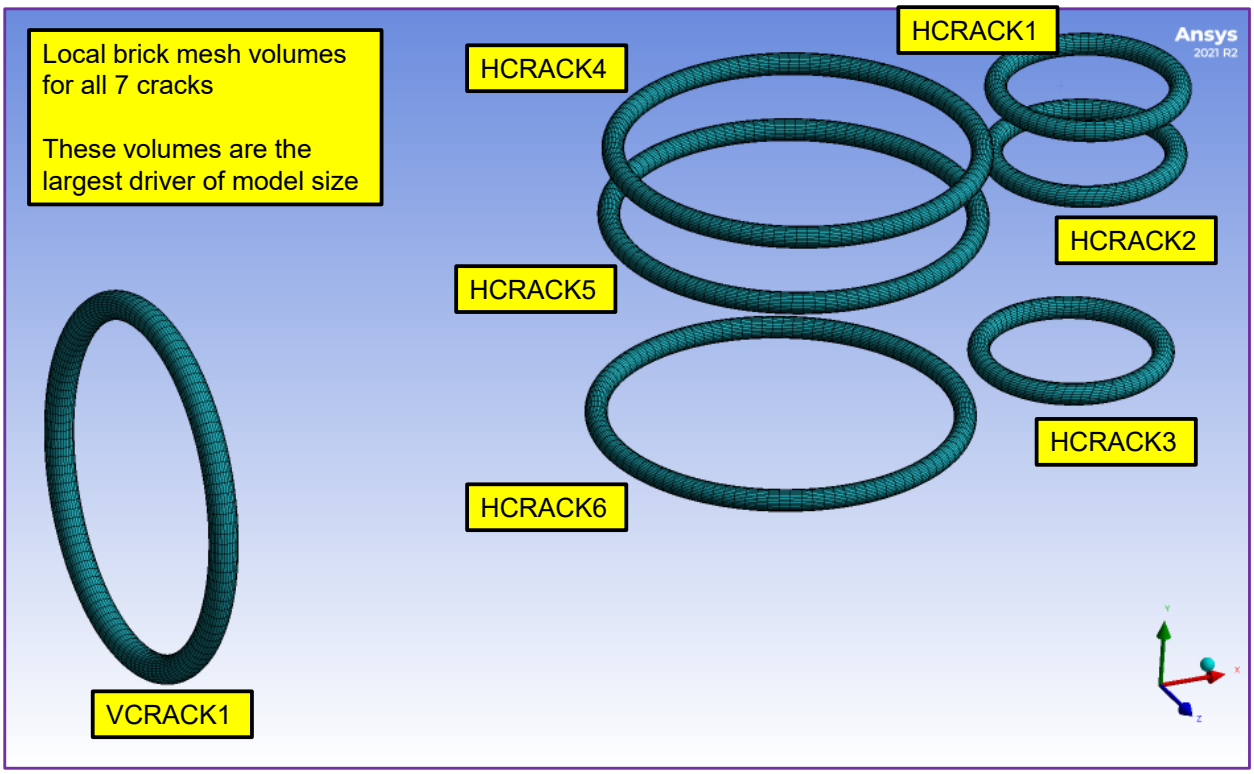

Figure 74. Baseline Computational Mesh: Subsurface Crack Volumes

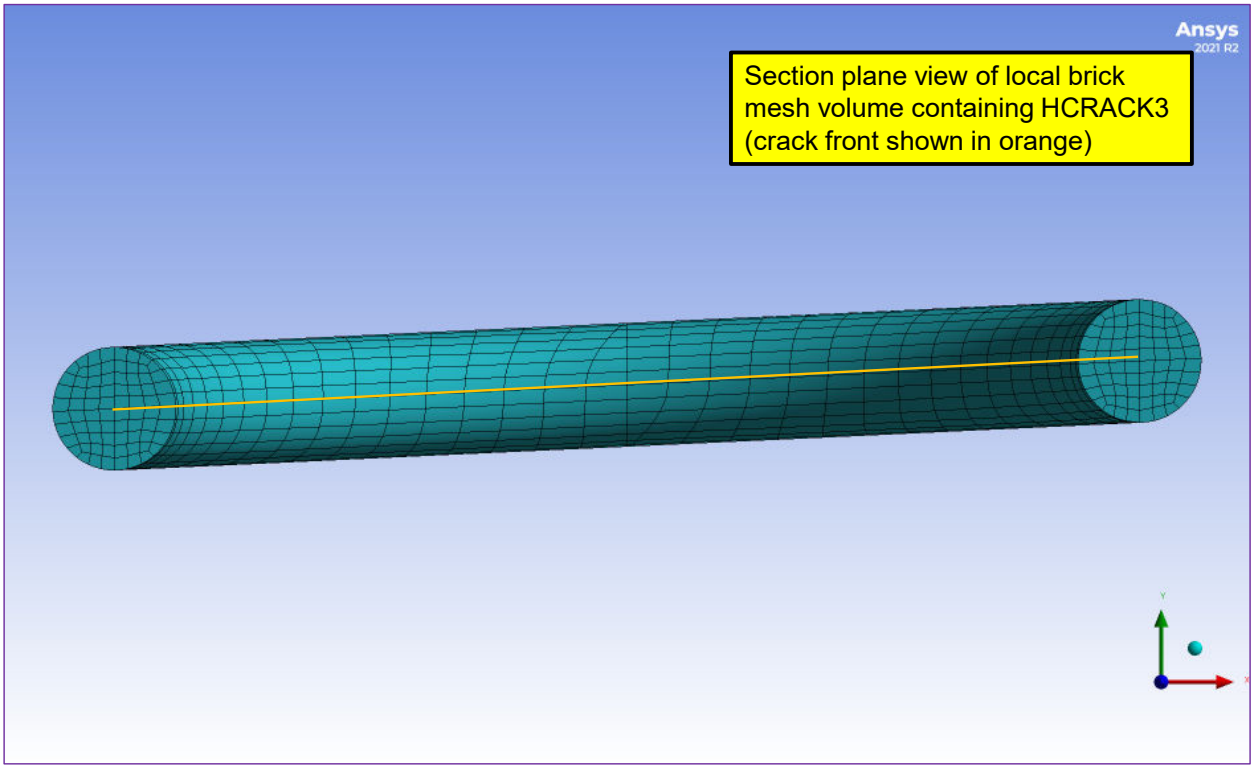

Figure 75. Baseline Computational Mesh: Local HCRACK3 Hexahedral Mesh

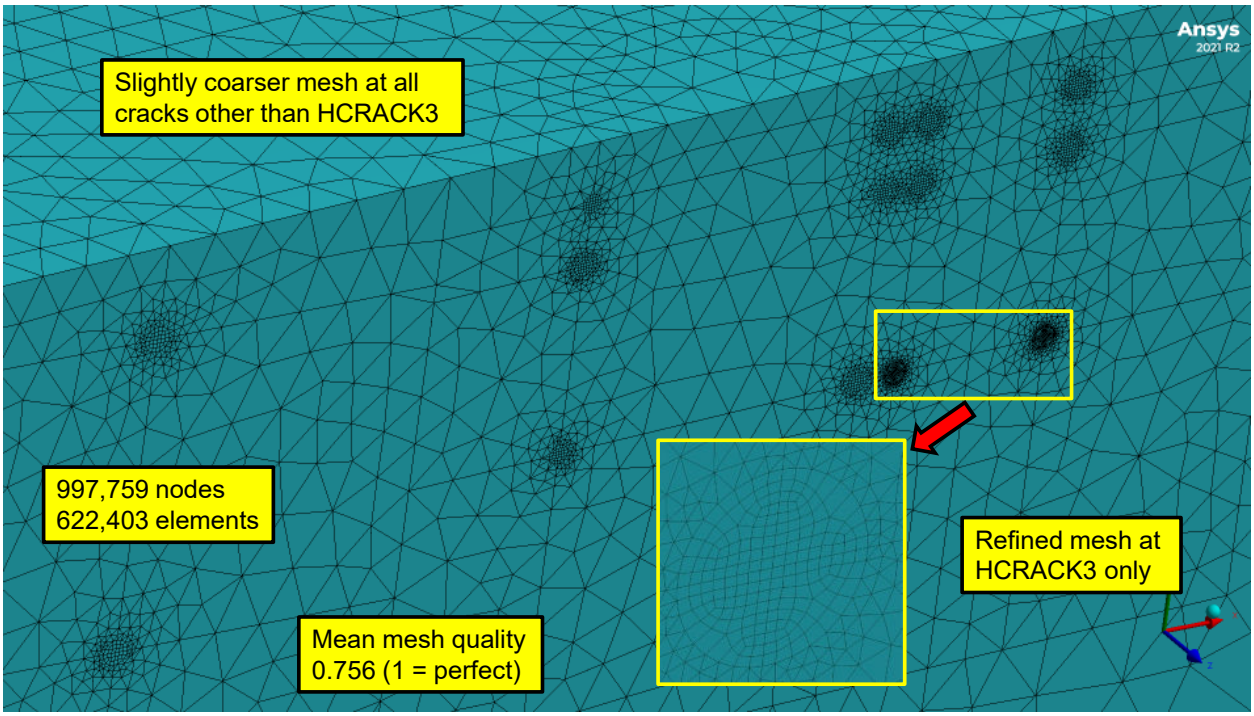

Figure 76. Refined Computational Mesh: Subsurface Cracks

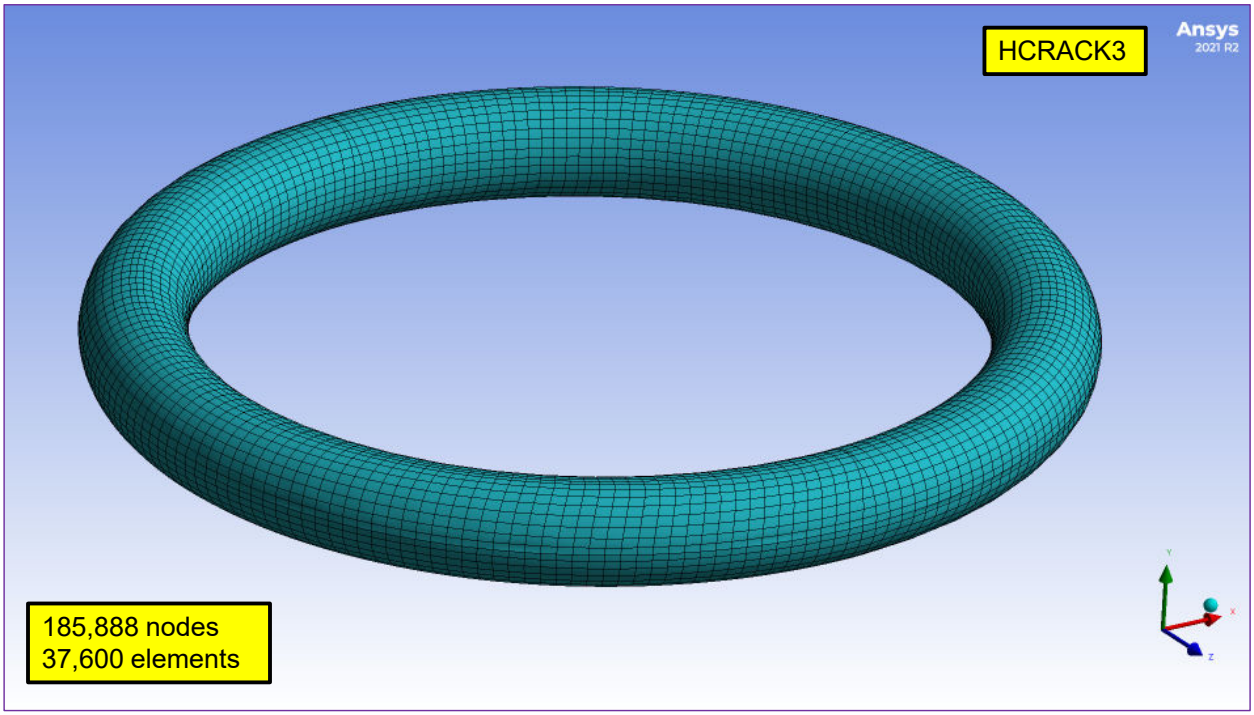

Figure 77. Refined Computational Mesh: Local HCRACK3 Hexahedral Mesh

Table 10. HCRACK3 J-Integral Results: Contact Force Position 1

HCRACK3 J-integral Results: Baseline vs. Refined Mesh (psi-in) Contact Force Position 1								
Crack Angle (deg)	WS2 Baseline Mesh		WS2 Baseline Mesh w/Reduced Contact		WS2 Refined Mesh		WS2 Refined Mesh w/Reduced Contact	
	Min	Max	Min	Max	Min	Max	Min	Max
0	0.21	0.77	0.09	0.99	0.33	1.45	0.33	1.45
45	-0.84	0.58	-1.01	0.86	0.16	0.35	0.28	0.44
90	-0.10	0.81	0.10	1.05	0.37	0.40	0.44	0.57
135	-0.50	0.72	-0.58	0.90	0.09	0.52	0.18	0.50
180	0.19	2.24	0.11	1.69	0.87	3.16	0.22	3.10
225	-0.28	6.38	-0.41	7.66	-0.11	7.66	0	7.55
270	-0.10	1.67	-1.30	0.58	0.63	4.91	0.74	4.96
315	-1.15	1.12	-1.53	1.37	0.62	4.00	0.65	3.65

Table 11. HCRACK3 J-Integral Results: Contact Force Position 4

HCRACK3 J-integral Results: Baseline vs. Refined Mesh (psi-in) Contact Force Position 4								
Crack Angle (deg)	WS2 Baseline Mesh		WS2 Baseline Mesh w/Reduced Contact		WS2 Refined Mesh		WS2 Refined Mesh w/Reduced Contact	
	Min	Max	Min	Max	Min	Max	Min	Max
0	3.78	6.72	8.15	16.18	2.11	4.72	6.83	14.49
45	0.88	6.40	3.10	16.20	1.89	3.79	6.20	13.80
90	2.49	6.29	5.03	7.56	0.56	4.00	3.88	12.29
135	3.46	6.50	3.52	13.53	2.37	3.19	4.21	10.52
180	-1.08	7.26	5.61	10.29	2.96	6.78	4.41	14.14
225	5.30	13.41	6.49	19.44	3.29	13.92	6.34	18.02
270	3.19	5.83	8.55	14.34	1.82	12.47	8.56	15.79
315	1.91	8.06	3.50	14.75	0.53	11.83	4.30	16.07

Abbreviations and Acronyms

ACRONYMS	EXPLANATION
AAR	Association of American Railroads
FRA	Federal Railroad Administration
FEA	Finite Element Analysis
RRS	Office of Railroad Safety
SIF	Stress Intensity Factor
SWG	Stakeholder Working Group
VSR	Vertical Split Rims
WILD	Wheel Impact Load Detector
WS	Wheel Scenario